Geothermal Program on the CCGS NAHIDIK, cruises 1981–83, Canadian Beaufort Sea

Al Taylor and Vic Allen

Canada

EARTH PHYSICS · PHYSIQUE DU GLOBE

Internal Report 86–05

Gravity, Geothermics and Geodynamics Division
Earth Physics Branch
Energy, Mines and Resources Canada
1 Observatory Crescent
Ottawa, Ontario K1A 0Y3

March, 1986

SUMMARY

The Canadian Coast Guard has made the vessel "Nahidik" available since 1975 for a couple of weeks late each season to a group of EMR scientists for geotechnical work (Table 1.1). The Geothermal Group has had one or more personnel on the ship each year; this report describes the work carried out on the 1981, 1982 and 1983 cruises and presents the basic data and some preliminary interpretation.

The 1981-83 cruises covered a large area of the Beaufort Shelf (Fig. 1.1-1.3), extending from the central area north of Tuktoyaktuk to just east of Herschel Island in the west, adding to the regional coverage began in 1980. Generally, only that part of the Shelf and Canyon under 30 m or more water was surveyed. In these three cruises, 33 gradiometer casts with penetrations generally greater than 2 m were made, 363 conductivity measurements were made on core, and, as part of the field trial and proving of the time domain reflectometry method in saline sediments, 15 estimates of the unfrozen water content and 27 of the DC electrical conductivity were made using prototype equipment.

Permafrost temperatures (i.e. below 0°C) prevail in the sediments throughout the outer Beaufort Shelf, although not everywhere are they underlain by thick, relict, degrading ice-bonded sediments (e.g. Fig. 1.1 - 2.1). The average sediment temperature at the water interface is $-1.33 \pm .44$ °C, a value that is somewhat higher along the paleotopographic channels (-1.25 ± 0.5°C) and lower on the plains ($-1.50 \pm .14$ °C) (Fig. 3.10). Virtually all profiles exhibited a considerable thermal disturbance considered in most cases consistent with the seasonal variation in water temperatures or, in some areas, arising from a particular geomorphic feature. Temperature gradients (Fig. 3.3-3.7) varied from negative to near zero, with positive gradients occurring only in water deeper than 70 m; only one profile had a gradient similar to the expected geothermal gradient (50-70 mK/m) for the geologic province but the corrections necessary to yield a terrestrial heat flow would be impossible to estimate in this complex environment. A high, positive gradient observed on the continental slope may be the thermal signature of a recent mud slump exposing deeper strata (Fig. 3.7).

Sediment temperatures were noted to decrease along the channels in the offshore direction; in the Mackenzie Canyon, negative gradients near shore approach isothermal conditions as water deepens (Fig. 3.6). A three-profile transect was made across the diapir field at the northeastern shelf-break with the Canyon; there was evidence in the sediment temperatures consistent with a horizon at 2 m carrying a flow of cooler water downslope into the Canyon.

The average thermal conductivity, as determined by the needle probe method on the cores, is $1.33 \pm .2$ W/mK (Fig. 4.3). There seemed no difference between the mean of values taken in the Mackenzie Canyon and those taken elsewhere on the Shelf (Fig. 4.6). Individual profiles exhibited a somewhat lower conductivity in the upper few tens of centimeters of sediment (Fig. 4.8-4.11), indicative of higher water content, and consistent with other geotechnical measurements made on the cores (Hill et al., 1982).

Volumetric Water contents calculated from TDR traces on the core were within 20% of equivalent values determined by the Atlantic Geoscience Centre through weighing and drying adjacent samples in the cores (Tables 5.1, 5.2). There was a poor correlation between these water contents and needle probe conductivities (Fig. 5.5), according to the theory put forth by Ratcliffe (1960) and others, suggesting that the TDR method is unreliable in saline sediments in practice.

An evaluation of TDR-determined sediment electrical conductivity suggests that further refinement of the technique is required, as there was a lack of internal consistency among derived prosities, electrical conductivities and assumed pore water salinities. However, geologically reasonable values of electrical conductivity were obtained: the average of over two dozen determinations was 1.23 +/- .17 S/m (20°C), or 0.60 S/m (-1°C).

An analysis of the factor or factors giving rise to the prominent features in these profiles is left to a formal paper.

CONTENTS Page

Page

Appendices

Note: The Appendices consist of raw data tables and graphs.

TABLES

FIGURES

1.0 Introduction

Since the early 1970's, the Geothermal Group, Earth Physics Branch has been participating with other researchers in geophysical studies in the Beaufort Sea area. The field programs have included hydraulic jet drilling and thermistor cable installation from the sea ice during several Arctic springs, gradiometer casts from ships in the summer, thermal conductivity on retrieved core and temperature and salinity profiles through the water. A summary of these scientific investigations is given in Table 1.1.

While a variety of geophysical techniques had been used in the 1970's to study the thermal regime of the Beaufort Shelf, a multi-year program using a Bullard-type temperature gradiometer probe was initiated in 1980 to study the regional variation of sediment temperatures and temperature gradients. This was somewhat of a compromise among other techniques that were either not suitable in the deeper waters of the shelf (e.g. jet drilling/thermistor cable emplacement from sea ice) or too expensive (e.g. drilling cored holes from a ship with temperature probing ahead of the bit, as in the EBA Engineering method). A Bullard probe, measuring temperatures directly while inserted into the sediments, overcomes some of the demonstrated unreliability under field conditions of taking sediment temperature measurements in a gravity or piston core shortly after retrieval. The Bullard probe survey had the disadvantage, quickly and painfully learned, of its unsuitability in compacted sediments, a problem avoided to some extent by selecting sediment-fill channels or ponds from the excellent detailed bathymetry charts available by 1980 or from real-time sounder records.

The Bullard probe technique is a traditional deep sea method of determining the terrestrial heat flux (e.g. Langseth, 1965). It is important here to clarify its use in shallow, perhaps seasonally influenced coastal shelves underlain by thick degrading permafrost. The probe itself, less than 16 mm in diameter and containing a string of up to 9 thermistors spaced over its 2.4 to 3 metre length, measures the sediment temperatures to that depth on the date of measurement. A completely different profile might be measured a month or so earlier, or later. Burgess et al. (1977), for instance, compare sediment temperature in September with values obtained from cables in the spring and estimate a seasonal near-shore sediment temperature range of at least 2.5 K. As the three cruises reported here occurred in September of the three years, the profiles represent a snapshot of the near surface thermal regime, a result of probably the maximum summer seasonal disturbance. With the measured thermal conductivity on cores retrieved in the vicinity, one can calculate the heat flux into or out of the sediment at that time. It is not generally possible to derive a terrestrial heat flux, i.e., a flux typical of the deeper geologic environment, because of the large amplitude of the transient disturbance or of the thermal influence of the underlying degradational permafrost.

1.1 The Geology and Marine environment of the Beaufort Sea Shelf

1.1.1 The Mesozoic and Tertiary

An overview of the bedrock geology of the Mackenzie Delta-Beaufort Sea area is taken from Yorath and Norris (1975). The structural and stratigraphic framework developed in the northern Cordillera and adjacent Interior Platform continue through the Mackenzie Delta and seaward onto the Beaufort continental

shelf. An extension of the Kaltag fault of the Yukon crosses the area along with an array of Cretaceous right-lateral and extension faults, resulting in the development of a structural depression. The basin is filling with a northerly progadation of deltaic clastics which began in Late Cretaceous and is continuing today at the edge of the Beaufort shelf. A section through the present shelf would encounter Proterozoic and lower Paleozoic carbonate and clastic sediments overlain by Cretaceous and Tertiary clastics, and Quaternary deltaic sediments.

1.1.2 The Quaternary

The Beaufort Shelf attained its principal physiographic elements and bathymetric features in the Quaternary largely through the agents of deltaic formation, glaciation and deglaciation, sea-level changes and associated transgressions of the sea. Present studies of high resolution seismic profiles from the shelf indicate that most of the late Quaternary shelf area was created by deltaic deposition (Hill et al., 1982). The glacial history is still somewhat conjectural for the present Mackenzie Delta and less established for the Beaufort Shelf. Most of the present Shelf was unglaciated during the late Wisconsin (Prest et al., 1969). The late Wisconsin advance covered little of the Shelf except for a lobe in the Mackenzie Canyon, and had retreated out of this area by 16 to 14 ka BP (Mackay et al., 1972; Shearer, 1972; Forbes, 1980). The Mackenzie Canyon is the major northwest trending bathymetric feature and, on the basis of breaks in the lateral continuity of the sedimentary section, Shearer (1970, 1972) considers the Canyon to be a relict ice scour channel created in classical Wisconsin time by advances and retreats of an ice tongue, perhaps following a pre-Wisconsin fluvial channel. Through the dating of coastal icy beds and frozen sediments that appear to have experienced deformation due to a glacial load, Mackay et al. (1972) suggest that major loading occurred before 40,000 years ago.

Throughout the Quaternary, eustatic sea level changes resulted in large areas of the Shelf being sub-aerial. Mackay (1972) adapts a generalized sea level history to the area and suggests that the Shelf must have been sub-aerial for perhaps 50,000 years or more to account for the considerable thickness of permafrost below the seabed. Shearer (1972) suggests that sea level may have been as much as 90 m lower 14 to 16 ka BP when the ice lobe had retreated south of the Mackenzie Canyon. More recently, Forbes (1980) has synthesized available dates from the onshore to produce a hypothetical sea level history for the past 15 ka, noting that marine transgressions, rapid sedimentation in some areas and coastal erosion in others has severely limited the data in the Beaufort region. Very little transgression has apparently occurred in the past several thousand years; his curve suggests that sea level in the Beaufort may have been 60 m below present sea level as recently as 15 ka BP. Prior to this, sea level in the area may have been 100m lower than today around 20 ka BP. Hill et al. (1985) show evidence from the Beaufort Shelf of a fluctuation in sea level about 16,000 years ago.

O'Connor (1982b) has further subdivided the offshore region into nine physiographic area, based largely on a combination of bathymetry, paleotopography and sediment types. These are listed in Table 3.2, with their approximate boundaries shown on the maps, Figures 1.1-1.3.

1.1.3 The Holocene

Vilks et al. (1979) present a comprehensive picture of the Holocene marine environment as it effects the present study. The rapid sedimentation following deglaciation has arisen mainly from the outflow of the Mackenzie River through Shallow Bay into the Mackenzie Canyon, and from the East Channel. The visible sediment plume tends to move seaward 55 to 70 km while being deflected to the east by the Coriolis effect. In addition to this rapid sedimentation, ice scouring has been the other major influence on the seabed (see Fig. 2.3), in places being deep enough to bring glacial deposits to the seabed. Grooves 0.5m to 10m deep and several hundreds of metres long decrease in frequency of occurrence as water deepens from 10m to 50m (Pelletier and Shearer, 1972), with the few scours in deeper water thought to be mainly relicts (Lewis, 1975).

Hundreds of seabed samples and dozens of cores to several metres depths were obtained by Vilks et al. (1979) on the Hudson '70 cruise and through winter surveys. An examination of these samples showed that the sediments arise mainly from the Mackenzie River, decreasing in grain size in the direction of transport to the east. The post marine-transgressive sediments are 3 to 5 m thick on the Shelf northeast of the delta, and over 20m thick in the Mackenzie Canyon and overlying the denser glacio-fluvial sediments (Shearer, 1970). On the eastern Shelf, it appears that sedimentation and erosion are occurring side by side, and sediments are much thinner or absent. Hill et al. (1982) interpret high resolution seismic profiles along the continental slopes indicating a 50m thick sediment unit overlying an old erosion surface; the upper 6m to 10m may be post-glacial.

Vilks et al. (1979) have estimated Holocene sedimentation rates from dating done on the core. On the continental shelf, rates of 3 to 30 cm/1000 years are quoted, while 100 cm/1000 years is likely in the Mackenzie Canyon. Their figures 12 to 17 show the distribution of surficial sediments throughout the region. Clay and silty-clay predominate throughout our study area, with very little sand and gravel. Silty sediments predominate inshore in less than 10m water while clay covers most of the remaining Shelf, with clay being found in the Mackenzie Canyon and along the Kugmallit Channel. Much of the same data is presented in a recent atlas (Pelletier, 1985).

1.1.4 Permafrost and the frozen sediments of the Beaufort Shelf

Mackay (1972) records how the existence of permafrost below the Beaufort Sea was first confirmed in 1970 when frozen sediments and ice were encountered in some boreholes during industry drilling. Using a simple thermal model, Mackay developed several scenarios for the aggradation of Beaufort Shelf permafrost under sub-aerial conditions and its degradation under a transgressing sea. He showed how the sediment temperature profiles would reflect this history and predicted 300 to 400m of degradational permafrost to underly near-shore areas, with the depth to the top of the frozen material depending on the water temperature and influence of continental runoff.

Industry experience in petroleum exploration and geotechnical drilling throughout the Beaufort Sea has since substantiated these predictions (e.g. Weaver et al., 1982). Considerable further research has been undertaken to outline the distribution of ice-bonded sediments throughout the region. Judge (1974) uses thermal models and reasonable surface temperature histories for

the Beaufort Shelf to show that considerable thicknesses of ice-bonded sediments could be found under large areas of the Shelf. Hunter and Hobson (1974) describe the use of seismic refraction to detect sub-sea permafrost. Hunter et al. (1976; 1978), MacAulay et al. (1982) describe extensive seismic interpretation of in-house and industry data to delineate the occurrence of ice-bonded sediments on the basis of velocity contrasts. Generally, large areas of the Shelf north and east of the Mackenzie Delta (Fig. 1.1-1.3) are underlain by shallow high velocity zones that are interpreted as ice-bonded permafrost. The Mackenzie Canyon to the west appears not to be underlain by frozen sediments.

Where ice-bonded sediments have been interpreted through seismic analysis, the Shelf may be further subdivided into areas of shallow, discontinuous ice-bonded permafrost overlying a deeper, much thicker horizon (Hunter et al., 1978). Morack et al. (1983) have extended the coverage with detailed analysis along two long east-west trending lines; ice-bonded sediments at depths 5 to 50 m underly some of the more northern line across the Kringalik Plateau, little to none of the Ikit Trough, all of the Akpak Plateau, marginally the Kugmallit Channel, most of the Tingmiark Plain, and partly under the Niglik Channels. O'Connor and Assoc. (1982 a,b) have mapped the distribution of similarly shallow ice-bonding across the shelf by examining industry and government seismic sections for evidence of "acoustic permafrost" (see Fig. 2.1, for instance).

The geothermal investigations described in this report were designed to provide a regional coverage of the shallow thermal regime within the sediments, to assess the impact on it of the underlying permafrost regime and to detect variations in water temperatures across the Shelf relative to the major physiographic features. Physical measurements on the cores were meant to compliment other geotechnical investigations carried out on the samples.

2.0 C.C.G.S. Nahidik Cruises

2.1 The 1981 Cruise

Because of space limitations, the Geothermal Group had only one person (VSA) on this cruise, from August 31 to September 16. A satellite receiver was used for navigation. The region covered was the near-shelf area east of the Kringalik Plateau and successful gradiometer casts and coring was undertaken at 14 stations (Table 2.1; Figure 1.1). Measurements were attempted at several other stations but were unsuccessful in retrieving a reasonable length of core because of the hard bottom. Two gradiometer probes were used on the cruise: a 1.3 cm diameter, 2.4 long probe containing a precision calibrated thermistor string was used at stations 1 to 8; a similar probe of larger diameter (1.6 cm) was used at stations 9 to 17.

The former probe had been used on the 1980 Sohm Basin cruise (Burgess, 1983) and in the Beaufort Sea on this trip experienced frequent bends due to partial penetrations in the generally hard bottoms found in the survey area; this necessitated its replacement by the second probe.

With only one person on this cruise, there was no time in which to take needle probe thermal conductivity measurements on board. Upon retrieval, each core was saved in its plastic liner, capped and taped, to preserve its natural water content. These cores were shipped to Ottawa and thermal conductivity measurements were made the following year, using the automated needle probe measuring system developed on the 1982 cruise. In all, 60 conductivity determinations were made.

2.2 The 1982 Cruise

The authors participated in this cruise for its duration, from August 29 to September 18. Offshore Navigations (Canada) Ltd. provided the precision navigation for the cruise (ONCL report, 1982). In brief, however, we may note here that the ship, after being loaded in Inuvik, sailed for Tuktoyaktuk where final preparations were made. From August 31 to September 16 the ship was at sea, with the exception of the period September 6-9, when the ship returned to Tuktoyaktuk on account of weather. This year, the ship spent all of its time in the area generally to the west of Tuktoyaktuk as far as the Mackenzie Canyon, where ice conditions were abnormally good and where there was mutual interest amongst the investigators to accumulate data.

The 3m geothermal gradiometer probe was cast at 15 stations (Table 2.2, Figure 1.2). Casts were planned for several other stations but were aborted when the coring probes failed to penetrate or were unable to catch a reasonable length of core. Judging from the mud-line on the probe, penetrations of better than 2.3 m were achieved at 13 sites (Table 2.2). The apparent penetrations at two other sites were about 1.5 m with some evidence that the probe may have fallen over, perhaps pulling the probe partly out of the sea-bed. Each successful cast represents a sediment temperature profile with 5 to 7 points over the penetration interval; only these stations are plotted in Figure 1.2.

The only cores taken on the cruise were obtained by investigators from the Atlantic Geoscience Centre and these were made available to us for thermal conductivity and time domain reflectometry (TDR) measurements. Unlike

previous years, we did not attempt to take our own cores, as the AGC coring equipment was capable of taking much longer cores, similar in length to our gradiometer probe. Thermal conductivity determinations were made on all the cores at 10 to 15 cm intervals using a computerized data acquisition system. In all, 160 determinations of this property were made.

A single TDR plot, in most cases using two parallel transmission lines of different lengths, were taken for each core. This minimized the disturbance of the cores, which were destined for a suite of engineering property measurements later. The TDR was a field trial to test its suitability determine porosity and electrical conductivity for saline samples.

2.3 The 1983 Cruise

The authors boarded the ship on September 1 in Inuvik, departing the following day for Tuktoyaktuk. More equipment was boarded there, and the ship departed for the survey area late on September 3 (McElhanney Surv. Ltd., 1983). Three geothermal gradiometer casts were made across the shelf break forming the eastern boundary to the Mackenzie Trough (Table 2.3; Figure 1.3). A long, near-shore cruise was made westward in an attempt to get around the ice pack to the central Mackenzie Trough and to Herschel Basin. The close proximity of the ice to shore west of Shingle Point forced the abandonment of these priority areas at this time, and in fact, for the season. Stations 22 and 23 were taken in the Kugmallit Channel to fill in an area where gradiometer casts had not been taken in previous years. The ship then moved further east into the Niglik Channels north of McKinley Bay. An attempt to core brought up over a metre of sand, so a gradiometer cast was not attempted because of the demonstrated hardness of a sand bottom. Navigation problems forced the ship to return to Tuktoyaktuk, where Taylor left the cruise and P. Lanthier came on board. Several further days at sea yielded an additional gradiometer cast, stations 25, in deeper water on the continental slope.

As in 1982, sediment cores taken by the Atlantic Geoscience Centre were made available to us for thermal conductivity and time domain reflectometry measurements. Using a spacing of 10 cm, 118 conductivity measurements were made. Few successful TDR measurements were made because of an intermittent deterioration in signal-to-noise ratio that has since been traced to faults in the cable tester used for the measurement.

2.4 Available High Resolution Seismic Data

Over a number of years, the Resource Geophysics and Geochemistry Division and the Atlantic Geoscience Centre, Geological Survey of Canada, have run high resolution seismic lines across the Beaufort shelf as part of a regional survey to investigate the shallow sediment regime and the upper surface of the ice-bonded permafrost (Hunter et al., 1976; Hill et al., 1982; MacAulay et al., 1982; Morack et al., 1983; and cruise reports listed in Table 1.1). Most of the seismic sections were obtained by using an airgun source or a 3.5 kHz sub-bottom profiler.

The geothermal stations were located on master maps of the seismic coverage. Portions of all lines that passed within several kilometres of a geothermal stations were extracted (Table 2.4); several sections are reproduced here in Figures 2.1-2.4. The sub-bottom environment of each station was described, with particular note taken of ice-scour and sub-bottom

ice-bonding (Table 2.5). Since few geothermal stations lay directly on the lines, the seismic sections reflect the regionally-typical environment rather than the local situation at the station. Station 81-11, for instance, may lie above an island of shallow ice-bonding or above an area where ice-bonding is somewhat deeper (Fig. 2.1).

Station location overlays were made for the maps of shallow ice-bonding derived from an analysis of both Government and industry seismic records by O'Connor and Associates (1982). The scale of the latter maps is small and their author admits that the discontinuous nature of the shallow ice-bonding may be partly due to interpolation and inadequate coverage in many areas. The general conclusion from this review is that the geothermal stations east of the Mackenzie Trough may be underlain by ice-bonded permafrost at 5 to 50 m below the seabed (O'Connor and Assoc., 1982; Morack et al., 1983), although usually 20 m or more (Table 2.5).

3.0 Thermal Gradiometer Casts

Bullard-type gradiometer probes, designed by Applied Microsystems Limited largely to our specifications, were used on these trips.

Stations were selected to extend our regional coverage of the Beaufort Sea. A gradiometer cast required the ship to be anchored, so this restricted our operation to water less than about 100 m. Occasionally, a cast in deeper water was tried without anchoring, although this required station-keeping for the 20 minutes or so that the probe was in the bottom. The Nahidik is not designed for station-keeping, and there was some danger in abrading the Kevlar line on the ship's hull.

At a station, the customary procedures for oceanographic gradiometer work were followed. The electronics were activated and the unit was put over-board, and held for 10 minutes at 10 to 20 metres off the bottom. Following this settling time above the sea-bed, the probe was permitted to free-fall into the sediment, where it was left for 20 minutes. Finally, the probe was winched out of the bottom and brought on-board, de-activated and straightened as necessary. Several stations were occupied before the tape and batteries were changed.

3.1 Calibration of the Gradiometer

Three elements must be considered for the ultimate calibration of the Bullard probe: the calibration of the thermistors, in an absolute and in a relative or "zero gradient" sense, and the calibration of the digitizing electronic system.

The thermistors used in these probes were type YSI 44032, having a manufacturer's calibration with 0.1°C interchangeability.

In 1981, both probes used thermistor chains that had been further calibrated in our laboratory to an absolute accuracy of ±.03K. In 1982 and 1983, thermistors were not calibrated further than the manufacturer's values. This is the more common situation in oceanographic work, as the relative temperature gradient along the length of the probe is the prime quantity that is desired. Hence, it is most important to inter-calibrate the thermistors along the length of the probe in order to achieve the millidegree level resolution required to measure gradients with a 3m probe.

In deep oceanographic work, this relative calibration is done by holding the probe a few tens of metres off bottom, where isothermal conditions are assumed over the length of the probe. It was recognized that this assumption was not valid over most of the shallow Beaufort (see Burgess et al., 1977, for instance). Figure 3.1 shows the temperature profiles taken during the holding periods at the 1982 stations; the relative offsets from one thermistor to another are not consistent from station to station and are evidence for this lack of isothermal conditions. A solution is to suspend the probe horizontally but this was impractical at the time of the cruises reported here.

The intercomparison of the thermistors in the probes was achieved in several ways for these three cruises. For stations 1 to 8 in 1981 (1.3 cm probe), we relied entirely on the precise absolute calibration; for stations 9 to 13 (1.6 cm probe), we used bottom water holding data at two stations when

that probe was used on the Sohm Cruise (Burgess, 1983). In 1982, we used data obtained from near-bottom holds on the continental slope (stations 18 and 23, bold dashed traces, figure 3.1). In 1983, similar data was obtained at stations 25. It is unlikely that deep water on the continental slope is isothermal but this seemed the best compromise. This data is then used to obtain the relative "offset" of each thermistor relative to the deepest thermistor (Appendix A).

It was necessary as well to calibrate the digitizing electronics. The data acquisition system is contained in a pressure case, to which the probe is mounted. The processor scans the thermistor chain every 10 or 15 seconds, and digitally records the resistance of each thermistor on reel-to-reel magnetic tape. The internal conversion of resistance to "bits output" is calibrated before each cruise using a precision decade resistance box; values from 108 to 60 kohms are scanned at 1 kohm intervals and the processor "bits" are recorded. These resistances spanned the four-sector range (4 x 1024 bits) of the electronics, and, for the thermistors used, represented a temperature measuring capability from approximately -2.8 to 9.9°C.

A polynomial regression of temperature on bits over this entire range, as suggested by the manufacturer, was performed but found to be unsatisfactory for our application, as interpolated temperatures can be several tenths of a degree out. For best accuracy a separate degree-two polynomial fit of bits vs. temperature was made in each sector. The regression equations for each cruise are tabulated in Table 3.1.

In all cases, the coefficient of regression, R^2, is 0.999998. The mismatch between sectors is in the millidegree range, as is the goodness of fit within a sector to the original data. The regression is essentially linear to a few hundredths of a degree over each sector (note the magnitude of the coefficient of the quadratic term) and it would have been adequate to use the simpler linear formula. Note that the electronics used in 1982 and 1983 were identical and had a considerably higher sensitivity than the system used in 1981.

The dynamic temperature range of the electronics for these cruises is approximately 12K. The digital output divides this range into four sectors of 1024 bits each (Table 3.1). This, however, leads to an inherent ambiguity in the conversion of digital output "bits" to absolute temperature. Ideally, a separate probe should be deployed at each station to determine absolutely the temperature of the bottom water or the water/sediment interface. While this was not done on these cruises, there is ample evidence in the literature that bottom water and sub-bottom temperatures are negative over the Beaufort shelf for water depths greater than 30 m. (Mackay, 1972; Vilks et al., 1979). Hunter et al. (1976; and their Fig. 5-18) quote previously unpublished data that suggest the mean annual 0°C isotherm lies between the shoreline and the 20m isobath, such that most of the shelf experiences permafrost temperatures (less than 0°C) over which a small annual variation may be superimposed. Judge (1976c) suggests that at water depths greater than 15m, there is sufficient mixing with ocean water to maintain negative mean temperatures. Burgess et al. (1977) made absolute gradiometer and temperature casts in Kugmallit Bay and up to 30 km north of Pullen Island. They found that bottom water and sediment temperatures decreased away from the shoreline, reaching 0°C when depths of 13 to 18 m were reached (see their Figures 4 and 5). For the cruises reported here, all data were taken in water depths greater than

24m, usually in excess of 40m (Tables 2.1 - 2.3). All bottom water holding data and sediment temperatures (Appendix A) have been assumed to fall within the lowest temperature sector, i.e. -2.5° to + 0.6°C, and the appropriate "bits" to temperature conversion has been applied (Table 3.1).

3.2 Reduction of Gradiometer Data

The data was printed out in tabular form, of thermistor reading (in bits) versus time (at 10 or 15 s intervals). The temperatures for the thermistor at the bottom end of the probe are plotted in Figure 3.2. The rapid fall in temperatures from "on deck" values to the holding temperature is readily apparent, as is the frictional rise in temperature as the probe plunges into the seafloor. This frictional effect is larger for the deepest thermistor.

The 10 minute settling time was always sufficient for the probe to come to thermal equilibrium with the water (Figure 3.2); although not satisfactory as a relative calibration of the thermistors, this procedure did bring the temperature of the probe as close as possible to sediment temperatures. Figure 3.2 is typical of the cooling curve for the probe following sediment penetration.

Several procedures for deriving the sediment temperatures from the cooling curve may be used. Bullard (1954) suggests the use of an $F(\alpha, t)$ function to describe the frictional heat transient although the simpler asymptotic form of this function, i.e. a $1/t$ relation, is frequently satisfactory. Good equilibrium estimates can usually be achieved after a few minutes (e.g. Hyndman et al., 1979). Failure to properly extrapolate the measured time series can lead to non-linearities in the temperature profile (Noel, 1984), although the latter are much smaller than the presumed transient effects noted in this data.

Considering the difficulty in calibrating probes used in these cruises in the "zero gradient" sense, we simply took the measured temperature at 20 minutes after penetration as the equilibrium value. This time represents about 5 to 8 time constants for the probes used in these sediments (Von Herzen et al., 1982).

The sediment temperature profile at each station was determined by application of the conversion routine already described. The results for all stations are given in Appendix A, and in graphical form in Figures 3.3 to 3.7.

3.3 Gradiometer results

3.3.1 Sediment temperature profiles

Thirty-three gradiometer profiles were recorded during the 1981-83 cruises, generally during the first couple of weeks of September; dates and station locations and other details are given in tables 2.1-2.3 and figures 1.1-1.3. The distribution of gradiometer stations throughout O'Connor's (1982) physiographic regions is given in table 3.2. The temperature profiles measured at each station are listed in Appendix A, and are presented graphically in this section, as figures 3.3 to 3.7.

In traditional deep ocean measurements, a positive gradient arising from the terrestrial heat flow would be expected; this might amount to a temperature increase of about 0.2 K over the length of the 3 m probe. Without transitory conditions such as a variation in bottom water temperature, moisture movement in the sediments and rapid sedimentation, a positive gradient would be expected in the Mackenzie Canyon, and on the continental slope and beyond, both areas being known through other studies to be free of ice-bonded sediments. Near isothermal temperatures, linking freezing bottom water temperatures to the deeper degradational permafrost should occur in shallow sediments east of the Mackenzie Canyon. However, a considerable departure from such ideal profiles is observed and is evidence of other influences on the data.

Four general types of profiles are apparent: a) profiles with temperature decreasing with depth (negative temperature gradient); b) temperature profiles that are isothermal to within 0.1 K; c) profiles that exhibit a distinct temperature inversion, usually concave towards lower temperatures; and d) profiles showing temperatures increasing with depth (positive temperature gradient).

The variations exhibited by these shallow temperatures may be evidence of considerable disturbance such as seasonal or random changes in bottom water temperatures by several 0.1K or by water movement within the sediments. Both these phenomena are documented in other areas, ranging from the deep sea (e.g. Lachenbruch et al., 1968; Burgess, 1983) to less deep coastal areas (e.g. Lewis, 1983; Wright et al., 1984). The observation that many of the profiles, taken in September of each year, tend to higher temperatures nearer the sea-sediment interface suggests that the major cause is a seasonal increase in ocean temperatures. Some of the profiles were taken at stations where an anomalous geomorphic feature was being studied by other participants on the cruises; these profiles may, in addition, reflect a thermal effect of the feature.

1981 Profiles. Stations were occupied in the eastern Beaufort (Tingmiark Plain and Niglik Channels, Figures 1.1 and 3.3) and in the central region (the Akpak Plateau and the Ikit Trough, Figure 3.4). The area is underlain by ice-bonded permafrost, the upper surface of which is irregular and lies about 20 m below the seabed; Figure 2.1 is a typical seismic section. Station 1 is the most northerly of the group and has the lowest temperatures. Temperatures show a systematic decrease at stations progressively further down the channels, e.g. stations 17, 7 and 4 in the Niglik Channels (although 17 was measured a week after the others, Table 2.1) and stations 12 and 9 in the Ikit Trough. Profiles at all stations at some depth have a negative temperature

gradient (see also Appendix B); this may be evidence of higher seasonal bottom-water temperatures on the shelf.

Temperature inversions were the most common curve shape observed in 1981 and are evident at 2m at stations 2 and 6 on the Tingmiark Plain and at 5 stations to the west on the Akpak Plateau and Ikit Trough (Figure 3.4).

These latter profiles are very similar in shape and have a prominent inversion around 1.6m. At station 15, the inversion appears 0.3m deeper, suggesting that the probe penetration may have been over-estimated by 0.3m. This latter adjustment would make the profiles at stations 11 and 15 (20km apart) very similar, and cooler that station 13, further south on the Akpak Plateau. All stations were occupied within a three day period.

1982 Profiles. Sediments at six stations in the central area (Figures 1.2 and 3.5, Kringalik and Akpak Plateaus, Ikit Trough and the continental slope) are at least 0.2K lower in temperature than are the sediments in the Mackenzie Canyon (figure 3.6). Station 23 is on the continental slope in 125m of water (Figure 2.2) and exhibits one of the few positive temperature gradients (30mK/m, Appendix B); this value is somewhat lower than the range expected for this geological province and its use in estimating a terrestrial heat flux is treated in a separate paper (Taylor and Allen, 1986). A negative gradient, suggesting considerable seasonal heating, is observed at station 26 under 61m of water, about 5km from the edge of the shelf. Stations 5 and 6 are about 25km from the slope and show evidence of the seasonal variation; perhaps the greater range in temperatures at 5 and the similarity to profiles at stations 28 and 29 results from its position 'downstream' of the Ikit Trough. At depths around 3 m, most profiles seem to converge to -1.5°C, perhaps the upper temperature of the underlying degradational ice-bonded permafrost (Mackay, 1972; Judge, 1974).

In the Mackenzie Trough, there is a trend to lower temperatures at stations further downslope (Figure 3.6). High negative gradients (Appendix B) are recorded in sediments underlying 30m+ water off King Point (stations 11 and 12), and nearly isothermal temperatures further offshore under 80m water (stations 8 and 13). The Trough is not generally underlain by thick degradational permafrost as is other parts of the shelf (MacAulay et al., 1982). The trend in measured gradients in the Canyon to increase from negative near shore to approximately zero in deeper water may be considered a result of the gradual reduction in seasonal water temperature variations. Fully positive gradients would be expected further offshore (see station 5, 1983).

1983 Profiles. Stations 3, 4 and 5 straddle the northeastern edge of the Mackenzie Canyon (Figure 1.3 and 3.7), and traverse the north end of the area of diapir features depicted on the bathymetric charts. These are thought by some workers to represent sand casts of ice-cored morainic features associated with the ice lobe in glacial times (Gendzwill, 1983). A seismic line near station 3 (Figure 2.3) shows that the area is considerably ice-scoured, with a local relief of several metres. A weak reflector on the airgun record may arise from ice-bonded permafrost (Table 2.5) about 20 m below the seabed.

Temperature profiles exhibited a mild inversion on the Kringalik Plateau side, and a positive temperature gradient (73 mK/m) on the slope of the trough, at station 5. Again, the similarity of the profiles at stations 3 and

4 suggest that the estimate of penetration may be incorrect by 0.3m. Deepening the profile at station 3, for instance, would place the negative-going spikes around 2m in approximate depth coincidence at stations 3, 4 and 5. While the negative spikes might suggest a bad thermistor, it is not apparent at subsequent stations.

The coincidence of these spikes at the three stations could be attributed to a porous horizon common to the area and with a water flow through it into the deeper Canyon. The regional topographic slope at the three stations is 0.3, 3.8 and 0.7 degrees, respectively, in rough proportion to the magnitude of the negative-going spike in the temperatures. No temperature disturbance would be expected unless water was originating at a slightly lower temperature upstream. Without further information, it is impossible to estimate such a value and to calculate the flow rate that might lead to these anomalous negative spikes (Stallman, 1963; Lewis and Beck, 1977). Only short cores were recovered at stations 3 and 4, lending support to the argument because of the difficulty in coring a porous sand horizon. However, thermal conductivities on a longer core retrieved at station 5 (Appendix C, D) are uniform throughout without a tendency for an increase in conductivity as expected across the "sand" horizon.

Station 25 was taken in 150m of water on the continental slope and yields a gradient of 133 mK/m. This contrasts with the gradient of 30 mK/m observed at station 23 in 1982, on the slope about 30 km to the SW. The continental slope is an area where recent mud slumps are commonly seen on high resolution seismic records (Hill et al., 1982). A slump would result in a sub-seabottom horizon at a somewhat higher temperature being suddenly exposed to lower bottom-water temperatures. This step decrease in temperature would propagate downwards in time, yielding initially a high, near surface temperature gradient, perhaps as observed here, until equilibrium was re-established. We note that the seismic coverage of this station was done in 1982, at which time no evidence of a slump was apparent (Figure 2.4).

3.3.2 Bottom-water temperatures

Since the probe had no temperature sensor external to the recording head, temperatures measured by the tip thermistor during the holding period about 10 to 15m off the bottom are taken to be a measure of the deep, or bottom-water temperatures. These values are shown in figure 3.8. Temperatures appear to decrease offshore down the troughs and channels. Temperatures of water in the Mackenzie Canyon tend to be higher than elsewhere on the shelf. Figure 3.9 shows the low correlation of these temperatures to total depth.

3.3.3 Sea/sediment interface temperatures

The upper section of each gradiometer profile discussed above (figures 3.3-3.7) has been extrapolated to z=0 to give a sea/sediment interface temperature (figure 3.10; Appendix B). The correlation between this sediment temperature and the bottom-water (i.e. holding depth) temperature is illustrated in figure 3.11. The scatter is considerable, attributable to the assumption of the holding temperature reflecting actual bottom water values; however, the calculated correlation coefficient is .7 and the average temperatures are surprisingly close for a data set of 32 values (-1.30+-0.49°C for holding water and -1.33+-.44°C for sediments). Figure 3.12 plots the sediment temperatures versus water depth and year of observation. Because the

area surveyed was different each year (Figures 1.1-1.3), the apparent partitioning of sediment temperatures by year is probably not totally a reflection of different seasons. No stations were reoccupied in subsequent years.

In the channels, there is little correlation between sediment temperature and water depth (coefficient 0.2) while on the plateaus the correlation is somewhat better (0.4). The higher sediment temperatures occur under the channels with an average of -1.25+-0.5°C, compared to the average under the plateaus, -1.50+-0.14°C. In this data set, the average water depths in the channel and plateau areas are 48 and 42m, respectively.

3.3.4 Apparent sediment temperature ranges

As noted earlier, sediment temperatures vary over a considerable range at a station, apparently on account of a similar, recent variation in bottom-water temperatures. Figure 3.13 depicts this range of temperatures over the depth interval measured at each station. This shouldn't be compared with the mean annual range, although had similar measurements been made at other times of the year an estimate of that value might be made, as done by Burgess et al. (1977). The largest ranges occur in the near-shore Mackenzie Canyon. Figure 3.14 examines the correlations more closely. The greatest ranges occur in the channels or troughs, with an average slightly higher (0.30K) than in the plateau regions (0.25K). With a larger data set, this contrast might be used in modelling the current regime of the Beaufort Sea.

4.0 Thermal Conductivity Measurements on Core

In the 1982 and 1983 cruises, at least one piston-core and occasionally a gravity core, each up to 3 m long, were obtained at all stations by personnel from the Atlantic Geoscience Centre. The cores were waxed, labelled and stored upright in the ship's hold. In 1981, Allen obtained shorter gravity cores at each station.

The thermal conductivity lab was set up in one of the cabins on board in 1982 and 1983. The primary requirements were for a clean area where temperatures did not fluctuate rapidly and where the computerized measuring system could be set up. A few core that were too long for the cabin were measured in the hold at the end of the trip when that area could be isolated, kept clean and reasonably stable in temperature.

A two-metre long wooden box, insulated with 5 cm of polystyrene, was used to hold a core vertically and to provide some thermal isolation. Holes were drilled in the plastic core liners at 10 cm or 15 cm intervals to accommodate the Fenwall Needle probes. Up to 10 probes were inserted in a core at once, one simply to monitor the ambient core temperature. A constant current source in series with the the needle probe heaters provided approximately 100 ma (measured to 0.1ma) for 6 minutes. The measuring system was programmed to scan the needle probes every 10 seconds for 12 minutes, recording the data on magnetic disc for later processing. For each scan, the system measured the thermistor resistance and voltage across each heater. The results at 10 cm at stations 5, 1982 were studied in detail to assess the operation of the acquisition system; Figure 4.1 and 4.2 are plots of needle probe temperature versus the logarithm of the elapsed time (during heating phase, 0 to 355 s) and versus a modified function of time for the following cooling phase.

Thermal conductivity may be calculated from needle probe temperatures recorded during the heating phase, (Von Herzen et al., 1959):

$$T = \frac{VI}{4\pi k \ell} \ln t \ (°C)$$

where t = elapsed time (s)
T = axial temperature (°C)
V = voltage across heater (volts)
I = current (amps)
k = thermal conductivity ($Wm^{-1}K^{-1}$)
ℓ = length of heater in medium (m)

Conductivity may be written in terms of the slope of the log-linear plot, i.e.

$$k = \frac{VI}{4\pi \ell b} \quad \text{where } b = \frac{d}{dT}(\ln t) = \text{slope}$$

The following are the results of the regression at 10 cm, station 5 (Figure 4.2):

16 points from 205 s to 355 s
$k = 1.14\ Wm^{-1}K^{-1}$ with $R^2 = 0.99999$

23 points from 135 s to 355 s
$k = 1.15\ Wm^{-1}K^{-1}$ with $R^2 = 0.9999$

30 points from 65 s to 355 s
$k = 1.48\ Wm^{-1}\ K^{-1}$ with $R^2 = 0.895$

It is generally found by other experimenters that the calculation of the thermal conductivity from the cooling curve is less reliable, partly because of the uncertainty in the form of the time function. Lachenbruch (1957) suggests replacing t by t/(t-s), where s is the heating period (Figure 4.1). Using the last 16 points in the cooling curve, from 565 s to 715 s in the above example, yields

$k = 1.49\ Wm^{-1}K^{-1}$ with $R^2 = 0.999$.

These calculations assume the ambient temperature of the core does not change. In the above run, the temperature of the core was found to increase by 0.0105K in the interval 205 - 355 s due to an increase in room temperature. This ambient temperature increase is equivalent to 0.25K/hour. If the 16 temperature points (205-355s) are adjusted to eliminate this variation,

$k = 1.17\ Wm^{-1}K^{-1}$ with $R^2 = 0.9998$.

This is 2.6% higher than the uncorrected value, as might be expected from the formula by comparing the ratio of the ambient increase (0.0105K) to the measured heated temperature rise (0.33K) of the needle probe itself (Appendix C).

This emphasized the importance of allowing core to come essentially to equilibrium before calculating a needle probe conductivity. Otherwise, a simple correction for the rise/fall in ambient temperature, if sufficiently well-known, would need to be applied. For low power levels used here, this adjustment may easily become a large fraction of the temperature rise due to the heater. The above example is the worst case and no attempt was made to correct for such small ambient variations.

With the above considerations and following some repeatability trials, we believe the conductivity measurement error is about ±0.05W/mK.

4.1 Thermal Conductivity Results

Using the needle probe technique in the sides of sediment cores retrieved by EPB in 1981 and by the Atlantic Geoscience Centre in 1982-83, 363 conductivity determinations were made. These are tabulated in Appendix C.

4.1.1 Histograms

Figure 4.3 shows the distribution of all the measured conductivities. Values are considerably higher than usually found for deep ocean sediments (.8 to 1 W/mK) and are evidence for lower water contents in these generally compacted sandy-silts. The small tail to higher values comes largely from the 1981 results. A normal distribution was fitted to the observations; it yields a mean of 1.33+-.2 W/mK.

The distribution for the 1981 values is shown in figure 4.4. Conductivities were not measured on these cores on the ship; rather, they were brought to Ottawa, where they were measured the following year when some dessication was apparent. The mean of the normal distribution, 1.40 W/mK, is slightly higher, reflecting this situation. In 1982, 185 conductivities were measured (figure 4.5), approximately half from the Mackenzie Canyon. Figure 4.6 compares the fitted normal curves to these two sub-groups; the Mackenzie Canyon data shows a somewhat narrower distribution, and a slightly higher mean, than the remaining data. The results for 1983 are given in figure 4.7, with a normal mean of 1.32 W/mK.

4.1.2 Conductivity-depth distributions

There is a general tendency for somewhat lower thermal conductivity values in the upper few tens of centimeters (Figure 4.8 is typical), in distinct contrast to the CESAR results. Without having a a lithologic description, this is consistent with a slight increase in compaction with depth i.e. a higher water content in the upper layer; effects of the core recovery may be involved as well. This observation is borne out by the scattergrams in Figures 4.9 to 4.11 for each year. The 1981 values are unusually badly scattered, undoubtedly a result of the delay in measuring them.

5.0 Time Domain Reflectometry Measurements on Core

5.1 Volumetric Moisture Contents

The dielectric constant for water is greater than the dielectric constant of the solid component of soils by a factor of 20 or more, and of ice by a similar amount. These contrasts in the dielectric constant have been applied in agriculture to determine soil moisture (e.g. Fletcher, 1939; Topp et al., 1984); recently, some theoretical and experimental studies have developed its usefulness to determine the water fraction that may remain as liquid in frozen soils (Patterson, 1980; Smith and Patterson, 1981a, 1984b; Patterson and Smith, 1981). An empirical relation is used:

$$K_a = 3.01 + 10.1\theta_v + 143\theta_v^2 - 75\theta_v^3$$

where θ_v = unfrozen water fraction. K_a, the dielectric constant, may be measured by inserting a transmission line in the medium and measuring the travel time of the electromagnetic wave ("A" point to "B" point, Fig. 5.1):

$$K_a = \left[\frac{c\Delta t}{\ell} \right]^2$$

where c = speed of light in vacuum (ms^{-1})
t = travel time (s)
ℓ = line length (m)

Note that a 20% error in selecting the "B" point (t) results in only a 15% error in the θ_v determination.

Some work has also been done to show the viability of the method in saline sediments (Smith and Patterson, 1984a). These laboratory experiments usually have used coaxial transmission lines rather than the parallel lines that are more practical in the field. In the latter case, they show that the overlay of traces resulting from lines of different lengths is the only practical way to locate the B reflection point, and hence the moisture content, using the TDR in saline sediments. Figure 5.1 shows how the relection point for a shorter probe can be determined by overlaying its trace with that from an identical, but longer probe. The gradual separation of these traces at the B point for the shorter transmission line suggests a greater uncertainly in its "pick" than experienced in non-saline materials. Note that the B point for the longer transmission line lies further down the trace and cannot be used with confidence.

To facilitate this overlay procedure, Smith and Patterson (1984a) developed a dual length probe incorporating two parallel transmission lines of different lengths. This eliminates the disturbance created in the sample using separate probes when the short probe is removed and the long one inserted. It has the disadvantage that the curvature of the sides of the core tube prevent its use along the length of the core; it must be inserted axially at the ends.

The Nahidik cruises provided an opportunity to test the practicality of TDR in a field situation on saline cores. A few TDR measurements were done on the 1981 cores at the same time the thermal conductivities were done, i.e. about a year after the cores were retrieved. In 1982 and 1983, measurements were made on board the ship; however, as the TDR probe causes much more disturbance to the core than the needle probes, TDR was attempted at fewer selected intervals, generally only once per core section.

5.2 DC Electrical Conductivities

The DC electrical conductivity of the sediment may be determined from the relative impedence match with the probe in the sediment (Smith et al., 1981a). This is determined on the trace from the relative values of the incident pulse height and the reflected pulse height measured at "infinite" time (Figure 5.2), and does not suffer the same difficulties as does the TDR determination of volumetric water content in saline sediments.

$$\sigma_{DC} = \left[\frac{1 - \rho_\infty}{1 + \rho_\infty}\right] \cdot \frac{c\varepsilon_o}{\ell} \cdot \frac{Z_1}{Z_2}$$

where ρ_∞ = TDR reflection coefficient at long time
ε_o = permittivity of free space
Z_o, Z_1 = impedence coefficients for unmatched lines
(1983: probe # 2, Z_o = 200, Z_1= 330)

5.3 Results from TDR

5.3.1 Volumetric water contents

Results are summarized in Tables 5.1, 5.2. The volumetric moisture contents determined by TDR are somewhat lower than the average of volumetric values (68%) determined by a weighing and drying technique on the cores from the 1975 Nahidik cruise (Hunter et al., 1976; p. 48).

Densities and gravimetric water contents were measured on the 1982 and 1983 cruises as part of the geotechnical investigations undertaken by the Atlantic Geoscience Centre. Unpublished values were provided by K. Moran (pers. comm. 1984) so that an independent check might be made of values determined here. The gravimetric water contents (percent dry weight) were converted to volumetric water contents using

$$\theta_v = \frac{\rho_B}{\left(1 + \frac{1}{w}\right)} \quad (m^3/m^3)$$

where ρ_B = bulk wet density (Mg/m^3)
w = gravimetric water content,
fraction dry weight

$$= \frac{\text{mass of water}}{\text{mass of dry sediment}}$$

$$= \frac{\rho_L \theta_v}{\rho_s(1-\theta_v)} \quad (kg/kg)$$

ρ_L = density of water (=1)
ρ_s = density of solid constituents
(dry bulk density)

The converted values nearest in depth to these determinations made by the TDR are given for comparison in Table 5.1 and 5.2 and Figure 5.3. Agreement appears better in 1983 when the trace overlay method was used. The 1982 values are consistently below the absolutely determined values, perhaps a result of picking the B point too early in the trace; a 20% error in travel time results in a 15% error in the water content. Note that the TDR-derived values are scattered over double the range of the absolute determinations; this is evidence of lack of precision in the TDR method in saline sediments.

Figure 5.4 compares the TDR-derived volumetric water contents with the profiles determined by absolute measurements for 1983 stations 4, 5 and 22. The TDR values are within 10% of the absolute values, a variation that may reflect simply that the same samples or depth intervals are not being measured. The absolute profile for station 4 suggests an enhanced water content near the seabed, and this is reflected in the higher TDR value at Z=0.

5.3.3. Comparison of thermal conductivity and water content data

The thermal conductivity of water (~0.59 $Wm^{-1}K^{-1}$) is about one-quarter the conductivity of the solid component in ocean sediments, hence, bulk thermal conductivities depend more on the water content than on their solid constituents.

Ratcliffe (1960) demonstrated the relationship between thermal conductivity and water content by wet weight for sediments from various oceans. Bullard and Day (1961) and Lachenbruch and Marshall (1966) undertook similar regressions with their data. A similar analysis was performed on the Nahidik data for 1982 and 1983 to attempt to demonstrate the reliability of the TDR - determined water contents (we assume the conductivities are more precise, probably $\pm$ 0.05 W/mK).

Ratcliffe used a grain density, ρ_s = 2.35 Mg/m^3; we use the average value of 2.68 Mg/m^3 determined from holes drilled in Kugmallit Bay (Hunter et al., 1976; their figure 5-14 and Table G-4). This higher value reflects the generally higher sand and silt content of Beaufort Shelf sediments compared to the deep oceans.

Bulk densities were calculated from the densities of water and the sediment solid component:

$$\rho_B = \theta_v + \rho_S (1-\theta_v)$$

and water contents by wet weight were obtained using

$$\frac{\text{mass of water in sample}}{\text{wet mass of sample}} = W = \frac{\theta_v}{\rho_B}$$

where ρ_B = bulk density (kg/m^3)
ρ_S = solid phase density (bulk dry density)
θ_v = volumetric water content (from TDR) (m^3/m^3)
W = water content by wet weight (kg/kg)

Table 5.3 and Figure 5.5 summarizes this data for the 1982 and 1983 cruises; Figure 5.5 illustrates the regression for this data and compares the similar curves obtained by Bullard and Day (1961) and Lachenbruch and Marshall (1966), whose regression equations are given in Table 5.4.

With only 15 points, the test is not terribly conclusive. The regression on the Nahidik needle probe data appears much less sensitive to water contents than found for the literature data. Clearly, further field studies are needed using the new dual length probe in the ends of core and taking needle probe conductivities at the same location.

5.3.2 DC electrical conductivity

Over two dozen determinations of the DC electrical conductivity of the sediment cores were made using the TDR. Electrical properties are temperature dependent to a considerable degree, and various formulas or nomograms exist to convert rock or sediment electrical resistivity from one temperature to another (e.g. Dresser Atlas Chart book, Table 1-4):

$$\theta_1 = \theta_2 \cdot \frac{(T_1 + 21.5)}{(T_2 + 21.5)}$$

where θ_1, θ_2 = electrical conductivity at temperature T_1 and T_2 (siemans/metre)
T_1, T_2 = sediment temperature (°C)

Hilchie (1984) gives a refined equation but the result is the same for the conversion required here from lab temperature to in situ sediment temperatures of -1°C.

Sediment electrical conductivity values are given in Tables 5.1 and 5.2, at the temperature of measurement on board (about 20°C) and at the in situ temperature of about -1°C. Omitting the single, high value gives an average

of 1.23 S/m (20°C) or 0.60 (-1°C). For reference, the electrical conductivity of seawater is about 5 S/m at 20°C and 2.9 S/m at -1°C. Boyce (1968) reports similar values in the range 2 to 3.3 S/m for sediments from the deeper Bering Sea. There is insufficient data to plot depth profiles for individual cores, but the entire data set is shown in Figure 5.6. A slight tendency for lower values at greater depths is consistent with an increase in compaction and a lowering of the porosity. The scatter in Figure 5.6 may arise from the technique; however, sediment conductivities taken with a conventional technique on the shallow Florida Shelf vary up to 60% over 5 m at particular stations (Bennett et al., 1983).

Figures 5.1 and 5.2 suggest that the derivation of the electrical conductivity should be easier than the calculation of porosity in saline sediments. Archies equation:

$$\frac{\sigma_w}{\sigma_f} = a\,\theta_v^m$$

σ_f = electrical conductivity of the saturated sediment (s/m)
σ_w = electrical conductivity of the interstitial water (s/m)
(where a and m are parameters depending on the soil type) was used to predict the porosity (e.g. Becker et al., 1982) from the electrical conductivity to compare with the values directly measured by TDR and to those converted from the gravimetric values (K. Moran, pers. comm. 1984; Tables 5.1, 5.2). The predicted values were both higher and lower than the corresponding TDR determinations, but about 20% lower than the Moran's values. This casts further doubt on the present ability of the TDR to recover porosity values; further, it would suggest either a considerable underestimation of the conductivity and/or an inappropriate value of parameters m and a in Archie's equation (m = -2, a = 1, Jackson et al., 1978).

Refinement of the TDR method of determining the electrical conductivity should be pursued. Boyce (1968) notes the importance of conductivity in estimating other physical properties of the sediment. The salinity of the pore fluid can be calculated from the electrical conductivity if the porosity is known; this would be advantageous in the near-shore Beaufort Shelf, where considerable fresh water overlies the sediment for much of the year. Alternatively, the salinity of the pore fluids might be measured independently, and the relationship between thermal and electrical conductivities might be investigated for Beaufort sediments (Hutt and Bug, 1968). Harrison et al. (1978, 1982) and Swift et al. (1983) emphasize the importance of determining the electrical conductivity as a measure of salt content of interstitial water in studying moisture migration and the evolution of subsea permafrost.

6.0 Implications for heat transport

An objective of this three year study was to demonstrate the utility of a traditional deep ocean geothermal technique in a continental shelf area. This section discusses briefly the implication to heat transport processes of the study across the Beaufort Shelf.

6.1 Terrestrial heat flow

The terrestrial heat flow generally cannot be determined from the gradiometer profiles obtained on these cruises. In areas of thick, degrading ice-bonded permafrost, heat flow from depth is consumed in supplying heat of melting at the base of the partially frozen zone. In the remaining, non ice-bonded areas, the seasonal variation in the observed temperature profile is so great, and supporting information on the causative seasonal variation so lacking, as to make the normal adjustment for these transient effects not possible. In addition, the Holocene history of deltaic sedimentation and sea level change will have a substantial, and poorly known, effect on the deeper thermal regime.

However, calculations normally undertaken in connection with traditional heat flow studies (e.g. Jaeger, 1965; Noel, 1984) may be used to analyse the sediment temperature profiles observed here. Such analysis can suggest mechanisms for the transient and local effects that are evident in this data. In particular, it can be shown that reasonable models of bottom water temperature changes over periods of weeks to several years can explain all the variation noted in these profiles. This modelling is left to a formal paper (Taylor and Allen, 1986).

6.2. Heat transport by pore water motion within the sediments

Non-linearities in deep sea temperature profiles may arise due to heat transferred through the motion of pore water within the sediments (Noel, 1984). In an area of a normal (positive) geothermal gradient, a vertical upwards movement of water carries heat to a shallower depth within the sediments than expected for a purely conductive regime, and a concave down temperature profile is observed; a vertical, downwards movement results in a concave up temperature profile. The effect has been observed in sediments flanking young oceanic ridges and is attributed to forced cellular convection (e.g. Anderson et al., 1979) although elsewhere this interpretation has implications hard to reconcile with the mechanisms required to drive such water motion (e.g. Langseth et al., 1981). Similarly, a transverse flow of water through the sediments may distort temperature profiles in some sediment sequences, given an appropriate source and driving mechanism (Bullard and Niblett, 1951; Stallman, 1963; Lewis and Beck, 1977). Water flow within a well, as sometimes observed on land, distorts the ground thermal regime but is physically, and mathematically, an unrelated problem.

The one-dimensional problem of simultaneous conductive heat flow and fluid flow has been solved by Bredehoeft and Papadopulos (1965):

$$T(z) = (T_2 - T_1)\,[\exp(\beta z/L) - 1]/[\exp(\beta) - 1] + T_1$$

$$(\beta) = \frac{c\rho v L}{k}$$

where T is the temperature at depth z, v the fluid flux occuring over depth interval L across the temperature difference $T_2 - T_1$. β is the Peclet number, a measure of the ratio of convected to conducted thermal transport, ρ and c are the density and specific heat, respectively of the convecting fluid, and K is the thermal conductivity of the bulk porous medium. Non-linear temperature profiles may be fitted to the above equation to obtain β, and hence the velocity of the fluid flow. Alternatively, differentiating the equation with respect to z shows that the variation between temperature gradient and temperature in a region of uniform vertical flow is linear; β may be calculated from the slope (e.g. Mansure and Reiter, 1979).

The equation implies a monotonic change of temperature with depth, the departure from a linear gradient being attributed to vertical water movement. Hence, a vertical fluid flux could not explain the temperature inversions depicted in Figure 3.4 and the negative gradients observed in the Mackenzie Trough (Fig. 3.6).

The effects of pore water flow have been considered for data from Station 82-23. The linear section of the interval temperature plot (Figure 6.1) is consistent with an upwards migration of water between 1.6 m and .75 m at a rate of about 3×10^{-7} m/s. It is unlikely flow would be restricted to such a narrow interval. In addition, such analysis does little to change the conductive gradient and heat flow (about 40 mW/m^2) to values more typical of the geologic environment (Judge, 1974). It is unlikely, hence, that the curvature in the temperature profile at this station is a result solely of pore water migration.

7.0 Recommendations

7.1 Further work on the existing data

a) The inclusion of data from the 1980 Nahidik cruise would approximately double the data set analysed here (Table 1.1; Figure 7.1). They would greatly increase the number of stations and their distribution in some of the physiographic regions (Table 3.2) and increase the value of the correlations made here. In particular, any variation in the uniformity of the thermal conductivity amongst the physiographic regions (e.g. Figure 4.6) could be assessed with some statistical significance.

b) Other types of analyses might be attempted. A trend-surface analysis with mapping algorithm (e.g. Agterberg and Chung, 1975) should yield most of the correlations noted casually here and may better quantify the degree of agreement between the borders of the physiographic regions and geophysically measureable parameters, greatly strengthening O'Connor's (1982) original definitions.

c) Geothermal modelling may be done to test the hypothesis, for instance, of the genesis of the temperature inversions. At some stations (e.g. 1981 stations 1, 2 and 6) an assumption of reasonable time-simultaneity of measurements may be valid. This might make a valuable contribution to the understanding of the current regime on the Shelf (see Lachenbruch et al., 1968; Lewis, 1983).

d) The data obtained on these cruises and arising from the subsequent analyses should be useful in further modelling studies of the Beaufort Shelf, in view of the paucity of other thermal data. In particular, this data would add to the environmental parameters used by Vigdorchik (1980) in his modelling of subsea permafrost in the U.S. Beaufort; he used a factor analysis method to predict areas having the highest potential, in a statistical sense, for ice-bonding.

7.2 Future cruises

a) The regional coverage of this type of survey could be extended west of the Mackenzie Canyon (Natsek Plain) and east into the Kaglulik Plain and beyond to Amundsen Gulf. With the large data set now available in the central area, principal correlations can be established and considerably few stations would characterize the remaining Shelf areas. An effort might be made to more closely locate geothermal stations on seismic lines, although often softer sediment ponds must be located to ensure probe penetration.

b) An opportunity was missed in not deploying data loggers to record bottom water temperatures; one might be left in a central, generally ice-free area at the beginning of the cruise and retrieved a couple of weeks later. No bottom water temperature time series longer than this exist in the public literature. A larger record might be obtained by deploying a recorder with an acoustic release in the spring through the sea ice - positioning may be a problem when returning to recover by ship; or by deploying by ship and retrieving a subsequent summer.

c) A valuable insight into the year-to-year variation in sediment temperatures might be obtained by reoccupying an easily accessible station each year. The ARGO navigation system used for several years now has an accuracy of a few metres and would make this relatively straightforward.

d) A water temperature profile should be taken at each gradiometer station. No further time need be expended, since a probe could be lowered in increments through the water column while the gradiometer probe was equilibriating in the bottom (note: a prototype automatic recording probe was used for this purpose in the 1982 cruise but was found to be unreliable).

e) With a ship capable of station-keeping without anchoring, data should be extended onto the continental slope and further north into the deeper basin. A transect starting north of the area underlain by ice-bonded permafrost and extending across the continental slope should add to the knowledge of the Holocene glacial history of the Shelf. Further down the slope, quality terrestrial heat flow measurements would extend other data taken in the Canada Basin.

f) The limitations to such shallow data in this area are apparent. Interest should now focus on obtaining deeper temperature data perhaps as add-on's to industry geotechnical programs. Several drillholes to a few tens of metres would provide the opportunity to take in-situ temperatures, complementary to data from thermistor cables installed further inshore in earlier studies on the Shelf (Table 1.1). Many of the geotechnical holes drilled by industry have no reliable temperature information.

g) The project to date has focussed on a regional coverage of the Beaufort Shelf. While some stations have been taken deliberately in anomalous areas in cooperation with other cruise scientists, future cruises might well realign their focus to examine such features in greater detail.

8.0 Conclusions

The essential results are given in the Summary, at the beginning of the paper. In this section, an attempt is made to assess the success of the geothermal program and the significance of the data.

A principal objective was to demonstrate the use of deep ocean geothermal techniques to a continental shelf underlain by degrading permafrost. Hyndman (1976), Lewis (1983) and Wright et al. (1984) have derived terrestrial heat flow estimates and other geothermal information by extending the method to the shelves and fiords off the coasts of southern Canada. To do so required corrections arising from bottom water temperature changes, sedimentation, and other effects known to influence such shallow geothermal measurements (Jaeger, 1965; Noel, 1984).

While we were cognizant from the outset that heat flow values could not be obtained in such a complex thermal environment, an attempt has been made to examine the data in considerable detail to ascertain what information can be derived from it. In studies conducted much closer to shore, Osterkamp et al. (1982) and Swift et al. (1983) have examined somewhat longer temperature profiles in the U.S. Beaufort to investigate heat and mass transport processes, particularly the movement of pore water and salt near a freezing boundary.

Our regional survey across the shelf suggests that periodic and aperiodic changes in bottom water temperature of a few tenths of a degree are the overwhelming influence on sediment temperatures to 3m depth. Considering the unusually low thermal diffusivity of sediments compared to rock, the theoretical skin depth (attenuation by 1/10) of a variation in water temperatures of period 1 month is 1.1 m; of period 2 months, 1.6 m; of 1 year, 3.9 m and of 2 years is 5.5 m. Aperiodic changes will be decremented in a similar fashion. Our data (Fig. 3.6, for instance) suggests that the dominant effects are restricted to the upper 3 m. Beyond the simple correlations noted in this work, somewhat deeper temperature measurement would be needed to reflect the regime of underlying permafrost or to map the thermal signature of its discontinuous, upper surface.

In a classic paper, Lachenbruch et al. (1968) show that mud acts as a long term memory of temperature changes at its surface; they derive valuable insight into the changes in bottom water conditions over time. Similar modelling has been undertaken but is left to a formal paper (Taylor and Allen, 1986).

The subsurface temperature effects of changes in bottom water temperature are difficult to differentiate from the effects of other processes such as pore water motion and other effects, a point noted by Noel (1984) and Osterkamp et al. (1982). It would seem prudent not to attempt to derive other process-related information from data that appear so heavily influenced by realistic variations in bottom water temperature.

Several geotechnical properties were measured on the sediments. The thermal conductivity values present in this work are the first made available from the outer shelf, complementing a similar but smaller data set from the inner shelf (Hunter et al., 1976). The Beaufort shelf derives virtually all of its unique features that set it apart from many other world shelf deltas

through the temperature history of this arctic area. Sediment thermal conductivities are crucial for further modelling or characterizing of the dynamic behaviour of the degrational ice-bounded permafrost. We note that thermal conductivity closely reflects the lithology of sediments, although a description of the latter was not available in the detail needed to see this (Fig. 4.8).

The cruises gave an opportunity to assess the TDR method as a useful field technique. Poor agreement of TDR-determined water contents with absolute values suggests that the technique requires further refinement before it can be considered truly a field technique; better agreement may have been attained had the TDR measurement been made in a proper ship lab, but then there would be little need for a simple, portable technique. Porosity is a crucial parameter because of the important role played by water in many seabed properties and in freezing processes.

We feel the TDR fared much beeter in its determination of sediment electrical conductivities, although no measurements of this parameter by other means have been made. Boyce (1968) notes the importance of electrical conductivity of sediments in the determination of other properties, although we were limited in further application by the lack of precision in the porosity values. Harrison et al. (1982) note the complementary relations between heat flow, moisture and salt transport through the interstitial pores around freezing fronts, underlying the potential for electrical conductivity data.

We feel this program has made a modest, but further contribution to knowledge of this complex thermal environment and has added to the understanding of the oceanography of the Beaufort Sea (Taylor and Allen, 1986).

9.0 Acknowlegements

We thank the Canadian Coast Guard for making the C.C.G.S. NAHIDIK available for our use for these and previous cruises through arrangements made with the Atlantic Geoscience Centre (S. Blasco), Resource Geophysics and Geochemistry Div., GSC (J. Hunter) and the Earth Physics Branch (A. Judge). Assistance with the coring operations and the gradiometer deployment was freely given by the ship's crew. We thank Fred Jodrey (AGC), Ron Good and Hugh MacAulay (GSC) for assistance often when it was most needed. Kate Moran (AGC) made the cores available to us for thermal conductivity measurements and for the TDR tests, and supplied some unpublished geotechnical data. Bob Harmes (AGC) was able to ferret out various cruise records, seismic sections and unpublished reports that were used in this study. Mike O'Connor and colleagues at O'Connor and Associates provided occasional office space and assistance in extracting appropriate seismic sections. Considerable logistic support, storage and laboratory facilities were provided by the Western Arctic Scientific Resource Centre at Inuvik. The Polar Continental Shelf Project assisted in Tuktoyaktuk. This work was funded partly through the Office of Energy Research and Development, EMR Canada.

In the Earth Physics Branch, we thank Micheline Whissell, Kathy Magladry and Cathy Johnson for typing the manuscript, Ruth Decosse for drafting most of the figures and Richard Delaunais for making prints.

Bibliography

Agterberg, F.P. and Chung, C.F., 1975. A computer program for polynomial trend-surface analysis. G.S.C. paper 75-21, 51 pp.

Anderson, R.N., Hobart, M.A. and Langseth, M.A. 1979. Geothermal convection through oceanic crust and sediments in the Indian Ocean. Science 204, 828-832.

Becker, K. et al., 1982. In situ electrical resistivity and bulk porosity of the oceanic crust Costa Rica rift. Nature 300, 594-598.

Bennett, R.H., Lambert, D.N., Hulbert, M.H., Burns, J.T., Sawyer, W.B., and Freeland, G.L., 1983. Electrical resistivity /conductivity in seabed sediments. In, Geyer, R.A., ed. CRC Handbook of Geophysical Exploration at Sea. CRC Press, Boca Rouge, Fla. p. 333-375.

Boyce, R.E. 1968. Electrical resistivity of modern marine sediments from the Bering Sea. J. Geophys. Res. 73, 4759-4766.

Bredehoeft, J.D. and Papadopulos, I.S., 1965. Rates of vertical groundwater movement estimated from the earth's thermal profile. Water Resources Res. 1, 325-328.

Bullard, E.C., 1954. The flow of heat through the floor of the Atlantic Ocean. Proc. R. Soc. A. 222, 408-429.

Burgess, M. and Judge, A.S., 1977. Thermal Observations Conducted as Part of Beaufort Delta Oil Project Limited's Sampling Cruise on the M.S. Norweta. Beaufort Sea, September 1976. Geothermal Service of Canada, Internal Report 77-1, pp.

Burgess, M.M., 1983. Summary of Heat Flow Studies in the Sohm Abyssal Plain: C.S.S. Hudson cruise 80-016. Atomic Energy of Canada Ltd., Technical Records TR-22, Pinawa, Manitoba

Fletcher, J.E., 1939. A dielectric method of measuring soil moisture. Soil Sci. Soc. Am. Proc. 4, 84-88.

Forbes, D.L., 1980. Late quaternary Sea levels in the southern Beaufort Sea GSC paper 80-1B, 75-87.

Gagné, R.M., 1980. Cruise report, CCGS Nahidik, Beaufort Sea. Unpublished manuscript of Geological Survey of Canada.

Gendzwill, D.J., 1983. Underwater pingos of the Beaufort Sea: a review Musk-ox 32, 1-9.

Good, R.L., 1978. Cruise report: CCGS Nahidik, Beaufort Sea. Unpublished manuscript of Geological Survey of Canada.

Harrison, W.D. and Osterkamp, T.E., 1982. Measurements of the electrical conductivity of interstitial water in subsea permafrost. in, H.M. French, ed. Proc. Fourth Can. Permafrost Conf., Ottawa, P. 229-237.

Hilchie, D.W., 1984. A new water resistivity versus temperature equation. The log analyst 25, n. 4, 20-21.

Hill, P.R., Moran, K.M., and Blasco, S.M., 1982. Deep deformation of sediments in the Canadian Beaufort Sea. Geo-Marine lett., 2, 163-170.

Hill, P.R., Mudie, P.J., Moran, K. and Blasco, S., 1985. A Sea-level curve for the Beaufort Shelf. Can. J. Earth Sci. 22, 1383-1393.

Hunter, J.A., 1977. Cruise Report: Southern Beaufort Sea, 1977. Unpublished manuscript of Geol. Survey of Canada.

Hunter, J.A., Judge, A.S., MacAulay, H.A., Good, R.L. and Burns, R.A., 1976. Permafrost and Frozen Sub-Seabottom Materials in the Southern Beaufort Sea. Beaufort Sea Proj. Tech. Rept. No. 22, D.O.E. 174 pp.

Hunter, J.S. and Judge, A.S., 1977. Geophysical Investigations of Sub-Sea Permafrost in the Canadian Beaufort Sea. Proc. 3rd. Int. Conf. on Port and Ocean Engineering, Univ. Alaska, Fairbanks, 1025-1058.

Hunter, J.A. and Hobson, G.D., 1974. A seismic refraction method of detecting sub-seabottom permafrost in, J.C. Reed and J.E. Sater, ed. The Coast and Shelf of the Beaufort Sea., A.I.N.A., p. 401-416.

Hunter, J.A., Neave, K.G. MacAulay, H.A. and Hobson, G.D., 1978. Interpretation of sub-seabottom permafrost in the Beaufort Sea by seismic methods, in Proc. Third Intl. Permafrost Conf., 1, 521-526.

Hutt, J.R., and Berg, J.W., 1968. Thermal and electrical conductivities of sandstone rocks and ocean sediments. Geophysics 33, 489-500.

Hyndman, R.D., 1976. Heat flow measurements in the inlets of southwestern British Columbia. J. Geophys. Res. 81, 337-349.

Hyndman, R.D., Davis, E.E. and Wright, J.A., 1979. The measurement of marine heat flow by a multipenetration probe with digital acoustic telemetry and in situ thermal conductivity. Mar. Geophys. Res., 4, 181-205.

Jackson, P.D., Taylor-Smith, D. and Stanford, P.N. 1978. Resistivity - porosity - particle shape relationships for marine sands. Geophysics 43, 1250-1268.

Jaeger, J.C., 1965. Application of the theory of heat conduction to geothermal measurements. Chap. 2, in W.H.K. Lee, ed. Terrestrial heat flow. Geophysical monograph series no. 8, Am. Geophys. Union.

Judge, A.S., 1974. Occurrence of offshore permafrost in Northern Canada. Proc. Symp. Beaufort Sea, Arctic Inst. N. Am. Spec. Vol., 427-437.

Judge, A.S., 1976a. Permafrost, Hydrates and the Offshore Thermal Regime. Tech. Memo., 119, Assoc. Com. Geotech. Res., NRC, 99-113.

Judge, A.S., 1976b. The thermal character of the sediments beneath the Beaufort Sea and the Implications for Offshore Drilling. Geothermal Service of Canada, Internal Report 76-3, 9 pp.

Judge, A.S., 1976c. Permafrost, hydrates and the offshore thermal regime. Geothermal Service of Canada, Internal Report 76-7, 19 pp.

Judge, A.S., MacAulay, H.A. and Hunter, J.A., 1975. Anomalous Seismic Refraction Velocities in Mackenzie Bay, N.W.T., Geol. Surv. Can. Report of Activities 76-1A.

Judge, A.S., MacAulay, H.A. and Hunter, J.A., 1976. An Application of Hydraulic Jet Drilling Techniques to Mapping on Sub-Seabottom Permafrost. Geol. Sur. Can. Report of Activities 76-1C, 75-78.

Lachenbruch, A.H., 1957. A probe for measurement of thermal conductivity of frozen soils in place, Trans. AGU 38, 691-697.

Lachenbruch, A.H. and Marshall, B.V., 1968. Heat flow and water temperature fluctuations in the Denmark Strait. J. Geophys. Res. 73, 5829-5842.

Langseth, M.G., 1965. Techniques of measuring heat flow through the ocean floor. Chap. 4, in W.H.K. Lee, ed. Terrestrial heat flow. Geophysical monograph sen. no. 8, Am. Geophys. Union, Washington.

Langseth, M.G. and Herman, B.M., 1981. Heat transfer in the oceanic crust of the Brazil Basin. J. geophys. res. 86, 10805-10819.

Lewis, C.F.M. 1975. Bottom scour by sea ice in southern beaufort Sea; Beaufort Sea Project Technical Report No. 23, Dept. of Environment, Victoria, B.C.

Lewis, Trevor, 1983. Bottom water temperature variations as observed, and as recorded in the bottom sediments, Alice Arm and Douglas channel, British Columbia. Can. Tech. Rep. Hydrogr. Ocean Sci. 18, 138-161.

Lewis, T.J. and Beck, A.E., 1977. Analysis of heat-flow data: detailed observations in many holes in a small area. Tectonophysics 41, 41-59.

MacAulay, H.A. and Hunter, J.A., 1982. Detailed seismic refraction analysis of ice-bonded permafrost layering in the Canadian Beaufort Sea. In French, H.M., ed. Proc. 4th Can. Permafrost conf., Nat. Res. Counc. of Canada, Ottawa p. 256-266.

MacAulay, H.A., Judge, A.S., Hunter, J.A., Burgess, M.M., Gagné, R.M., Allen, V.S. and Burns, R.A., 1979. A Study of Sub-Seabottom Permafrost in the Beaufort Sea-Mackenzie Delta by Hydraulic Drilling Methods. Earth Phys. Br., Open File 79-11, 42pp.

MacAulay, H.A., Judge, A.S., Hunter, J.A., Allen, V.S., Gagné, R.M., Burgess, M. M., Neave, R.G. and Collier, J., 1977. A Study of Sea-bottom Permafrost in the Beaufort Sea Mackenzie Delta by Hydraulic Drilling Methods. Earth Phys. Br., Open File 77-16, Geol. Surv. Can., Open File 472, 83 pp.

Mackay, J. Ross, Rampton, V.N. and Fyles, J.G., 1972. Relict pleistocene permafrost, western Arctic Canada. Science 176, 1321-1323.

Mackay, J. Ross, 1972. Offshore permafrost and ground ice, southern Beaufort Sea, Canada. Can. J. Earth Sci. 9, 1550-1561.

McElhanney Surveying and Engineering Ltd., 1983. Navigation and Positioning for C.C.G. Nahidik, Beaufort Sea. Job no. 083708, Nov. 1983.

Mansure, A.J. and Reiter, M., 1979. A vertical groundwater movement correction for heat flow. J. geophys. res. 84, 3490-3496.

Morak, J.L., MacAulay, H.A., and Hunter, J.A., 1983. Geophysical measurements of sub-bottom permafrost in the Canadian Beaufort Sea. In Proceedings, Permafrost, Fourth International Conference. National Academy Press, Washington, p. 866-876.

Morton, C.J., 1979. A study of the environment necessary for aggradation of sub-sea permafrost under the Beaufort Sea, Canada. BSc. thesis, Faculty of Arts and Science, Queen's University, Kingston. 40 pp. and maps.

Neave, R.G., Judge, A.S. and Hunter, J.A., 1978. Offshore permafrost distribution in the Beaufort Sea as Determined from Temperature and Seismic Observations. Geol. Surv. Can. Paper 78-18, 13-18.

Neave, R.G. and Judge, A.S., Hunter, J.A., 1979. Offshore Permafrost Distribution in the Beaufort Sea as Determined from Temperature and Seismic Observations. Assoc. Comm. Geotech. Sci. Tech. Memo., 124.

Noel, M., 1984. Origins and significance of non-linear temperature profiles in deep-sea sediments. Geophys. J.R. astr. Soc. 76, 673-690.

O'Connor, M.J. and Associates Ltd., 1982a. A review of the distribution and occurrence of shallow acoustic permafrost in the southern Beaufort Sea. A report prepared for the Geological Survey of Canada, Job no. 10-116, March, 1982. 144 pages and appendix.

O'Connor, M.J. and Associates Ltd., 1982. An evaluation of the Regional geology of the southern Beaufort Sea. A report prepared for the Geological Survey of Canada, Job no. 10-127, March, 1982. 188 pages and appendix.

Offshore Navigation (Canada) Ltd., 1982. Navigation and Positioning report, C.C.G.S. Nahidik, Beaufort Sea, 1982. Project 1369.

Osterkamp, T.E. and Harrison, W.D., 1982. Temperature measurements in subsea permafrost off the coast of Alaska. in, H.M. French, ed. Proceedings, Fourth Canadian Permafrost Conference, Nat. Res. counc. of Canada. 238-248.

Patterson, D.E., 1980. The measurement of unfrozen water content in freezing soils by Time Domain Reflectometry. MSc. Thesis, Geography Dept., Carleton University, Ottawa, 69 pp.

Patterson, D.E. and Smith, M.W., 1981. The measurement of the unfrozen water content by time domain reflectometry: results from laboratory tests. Can. Geotech. J. 18, 131-144.

Pelletier, B.R., 1985, ed. Marine Science Atlas of the Beaufort Sea, Sediments. Geol. Surv. of Canada. Miscell. Rep. 38.

Pelletier, B.R. and Shearer, J.M. 1972. Sea bottom scouring in the Beaufort Sea of the Arctic Ocean; Proc 24th International Geological Congress, Section 8, p. 251-261.

Poley, Denise F., 1982. A detailed study of a submerged pingo-like feature in the Canadian Beaufort Sea, Arctic Canada. B.Sc. thesis, Dalhousie University, Halifax, N.S.

Prest, V.K. 1969. Retreat of Wisconsin and Recent ice in North America; Geol. Surv. Can., Map 1257A.

Ratcliffe, E.H., 1960. The thermal conductivites of ocean sediments. J. geophys. res. 65, 1535-1541.

Shearer, J.M. 1970. Thickness of Recent (post-glacial?) mud in Beaufort Sea. Geol. Surv. Can., Open File 126.

Shearer, J.M. 1972. Geological structure of the Mackenzie Canyon area of the Beaufort Sea. GSC paper 72-1A, 179-180.

Smith, M.W. and Patterson, D.E., 1981a. Investigation of freezing soils using time domain reflectometry. Earth Physics Br., Open File 81-6, 54 pp.

Smith, M.W. and Patterson, D.F., 1981b. Investigations of Freezing soils using Time Domain Reflectometry. Progress Report, Sept. 30, 1981 to EMR re contract 23235-1-0699.

Smith, M.W. and Patterson, D.E., 1984a. The use of Time Domain Reflectometry in determining the phase composition of saline permafrost. Final Report, May 1984 to EMR re contract 23235-3-0902.

Smith, M.W. and Patterson, D.E. 1984b. Determining the unfrozen water content in soils by Time-Domain Reflectometry. Atmos. - Ocean 22, 261-263.

Stallman, R.W., 1963. Computation of ground water velocity from temperature data. USGS water Supply paper 1544-H, p.36-46.

Swift, D.W., Harrison, W.D. and Osterkamp, T.E., 1983. Heat and salt transport processes in thawing subsea permafrost at Prudhoe Bay, Alaska. In Proceeding, Permafrost, Fourth International Conference. National Academy Press, Washington, p. 1221-1226.

Taylor, A.E. and Allen, V.S., 1986. Shallow sediment temperature variations and thermal properties, Canadian Beaufort Shelf. submitted to Can. J. Earth Sciences.

Topp, G.C., Davis, J.L., Bailey, W.G., and Zebchuk, W.D., 1984. The measurement of soil water content using a portable TDR hand probe. Can. J. Soil Sci. 64, 313-321.

Vigdorchik, Michael E., 1980. Submarine permafrost on the Alaskan Continental Shelf. Westview Press, Boulder, Colo. 118 pp.

Vilks, G., Wagner, F.J.E. and Pelletier, B., 1979. The Holocene marine environment of the Beaufort Shelf. GSC bulletin 303.

Von Herzen, R.P., Detrick, R.S., Crough, T., and Epp, D. and Fehn, U., 1982. The thermal origin of the Hawaiian swell: heat flow evidence and thermal models. J. Geophys. Res. 87, 6711-6723.

Von Herzen, R. and Maxwell, A.E., 1959. The measurement of thermal conductivity of deep-sea sediments by a needle probe method. J. Geophys. Res. 64, 1557-63.

Weaver, J.S. and Stewart, J.M., 1982. In-situ hydrates under the Beaufort Sea shelf. in, H.M. French, ed. Proc. Fourth Can. Permafrost conf., Nat. Res. Counc. of Canada. p. 320-328.

Wright, J.A., Keen, C.E., and Keen, M.J., 1984. Marine heat flow along the northeast coast of Newfoundland. in, Current Research, Part B, Geol. Surv. of Canada, Paper 84-1B, 93-100.

Yorath, C.J. and Norris, D.K., 1975. The Tectonic development of the southern Beaufort Sea and its relationship to the origin of the Arctic Ocean basins.

TABLE 1.1

Summary of Scientific Investigations carried out by Geothermal Group, EMR, in Beaufort Sea.

Date	Mode	Principal Work	Reference
1975/08	Cruise "Nahidik"	94 conductivity measurements	Judge, 1976b; Hunter, et al., 1976
1976/03	Sea ice		
1976/09	Cruise "Norweta"	21 gradiometer casts, 42 water temperature and salinity profiles	Burgess et al., 1977
1977/03	sea ice	21 thermistor cables emplaced by jet drilling	MacAulay et al., 1977
1977/09	Cruise "Nahidik"	53 water temperature profiles; bottom temperatures; 62 short cores for thermal conductivity measurements	Hunter, 1977
1978/03	sea ice	12 Thermistor cables emplaced by jet drilling	MacAulay et al., 1979
1978/09	Cruise "Nahidik"	Water temperature and salinity profiles; bottom temperatures	Good, 1978; Morton, 1979
1980/09	Cruise "Nahidik"	29 gradiometer casts; 35 cores for thermal conductivity measurements	
1981/09	Cruise "Nahidik"	14 Gradiometer casts; 54 thermal conductivity measurements; some TDR	this report; Taylor and Allen, 1986
1982/09	Cruise "Nahidik"	13 gradiometer; casts; 160 thermal conductivity measurements on core; some TDR	this report; Taylor and Allen, 1986
1983/09	Cruise "Nahidik"	6 gradiometer; casts; 118 thermal conductivity measurements; some TDR	this report; Taylor and Allen, 1986

TABLE 2.1

NAHIDIK/81 Geothermal Stations

Station Number (Date)	LAT/LONG	Water depth (m)	Gradiometer Penetration (m)	Number of Conductivity Measurements
1 (1981/09/03)	70°50'05" 132°52'10"	75	1.3	3
2 (1981/09/04)	70°19' 59" 132°42'33"	38	2.7	5
3 (1981/09/04)	70°07'50" 132°36'42"	28	2.4	5
4 (1981/09/05)	70°45'43" 131°29'49"	48	1.0	2
6 (1981/09/05)	70°17'27" 132°11'50"	36	2.7	3
7 (1981/09/06)	70°26'43" 131°30'33"	32	2.4	5
8 (1981/09/06)	70°32'52" 131°10'51"	31	?	
9 (1981/09/10)	70°09'24" 135°21'09"	47	2.4	5
11 (1981/09/11)	70°19'31" 134°31'58"	45	2.4	5
12 (1981/09/11)	70°04'31" 134°55'36"	32	2.4	3
13 (1981/09/11)	70°09'38" 134°31'55"	33	2.3	5
15 (1981/09/12)	70°25'01" 134°06'04"	42	2.7	2
16 (1981/09/12)	70°08'30" 132°31'05"	28	1.9	5
17 (1981/09/13)	70°14'47" 131°32'51"	24	1.0	4

TABLE 2.2

NAHIDIK/82 Geothermal Stations

Station Number (Date)	LAT/LONG	Water depth (m)	Gradiometer Penetration (m)	Number of Conductivity Measurements	Core Number (litho-logy)	T D R
5 (1982/09/03)	70°24'11" 135°38'58"	65	3.9	15	PC03	1
6 (1982/09/03)	70°32'03" 135°00'08"	59	3.0		GC07	1
8 (1982/09/05)	69°38'00" 137°54'07"	78	3.5	15	PC04	1
9 (1982/09/05	69°30'51" 137°49'20"	44	3.5	15	PC05	1
10 (1982/09/05)	69°22'01" 138°05'30"	45	3.5	20	PC06	1
11 (1982/09/05)	69°11'18" 137°49'28"	30	3.5	20	PC07	1
12 (1982/09/05)	69°19'02" 137°29'07"	35	3.5	19	PC08	1
13 (1982/09/05)	69°41'58" 137°50'28"	80	3.0?	5	PC09	
15 (1982/09/09)	69°44'10" 137°01'11"	32	2.3+	20	PC12	1
18 (1982/09/12)	70° 43' 49" 135° 21' 56"	150	none	(holding depth profile at 125m only)		
23 (1982/09/14)	70°32'44" 136°10'01"	125	2.3	15	PC21 (clay)	1
26 (1982/09/15)	70°22'58" 136°42'37	61	2.3	6	PC-24	
28 (1982/09/15)	70°06'02" 135°50'12"	40	3.0	6	GC-11	
29 (1982/09/15)	70°15'31" 136°03'05"	53	3.5	6	PC-26	

TABLE 2.3

NAHIDIK/83 Geothermal Stations

Station Number (Date)	LAT/LONG	Water depth (m)	Gradiometer Penetration (m)	Number of Conductivity Measurements	Core Number	T D R
3 (1983/09/06)	70°04'14" 137°06'05"	42	2.7	3	PC-01	
4 (1983/09/06)	70°02'04" 137°20'52"	50	3.1	18	PC-02	
5 (1983/09/06)	70°00'05" 137°30'43"	71	3.2	22	PC-03	3
22 (1983/09/10)	70°14'59" 133°33'54"	53	3.5	20	PC-09	3
23 (1983/09/10)	70°23'59" 133°40'01"	64	3.2	19	PC-10	
25 (1983/09/)	70°42'39" 135°25'03"	150	?	36		

TABLE 2.4

High Resolution Seismic Lines Adjacent to Geothermal Stations

Station	Line	Fix (Time)	Distance From Line Fix to Station
81-11	F82 09 1216 (B99 S#1)	531 (19:15)	0.923 km SW
81-11	83-06	875	0.878 km NE (Fig. 2.1)
81-13	83-06	3250	2.969 km W
82-13	F82 09 0604 (DENNY)	(04:12)	0.127 km W
82-13	F82 09 0423 (CORGAS)	412 (07:05)	0.525 km NW
82-15	F82 09 0604 (DENNY)	(09:30)	0.090 km E
82-23	Grid Site #2 AB	8 (14:50)	0.010 km E (Fig. 2.2)
82-29	F82 09 0315 (B99 KUD)	244 (22.20)	0.090 km E
83-3	F82 09 0315 (KUD 044)	308 (03:45)	2.581 km S (Fig. 2.3)
83-22	F82 09 1603 (IRKTIM)	628 (07:40)	2.343 km SW
83-25	Grid Site #1 line AB	15 (18:50)	0.220 km S
83-25	83 - 13.05	209	0.982 km SW (Fig. 2.4)

TABLE 2.5

Permafrost Environment Near Geothermal Stations (from Seismic Data)

Station	Line	Fix (Time)	Distance From Line Fix to Station
81-11	F82 09 1216 (B99 S#1)	531 (19:15)	0.923 km SW

Seismic line runs north westerly to east of station. Area of 1 - 2 m amplitude ice scour on Akpak plateau. Hummocky acoustic permafrost occurs throughout record, about 20 m below seafloor in vicinity of geothermal station. (Compare Fig. 2.5.6 in O'Connor, 1982b). The seabed topography is gentle in the area and these features are unlikely to be side echos.

81-11	83-06	875	0.878 km NE

Seismic line runs northerly to west of station. Strong reflections on airgun record from hummocky acoustic permafrost. Note small horizontal scale, Figure 2.1.

Ice scour up to 3 m amplitude covers seafloor in area, showing up best on the 3.5 kHz record. Scour does not penetrate a flat-lying unconformity just below, which itself contains several deeper scour channels in vicinity of station.

81-13	83-06	3250	2.969 km W

This station lies south of 81-13 on the Akpak plateau. Strong reflection from hummocky acoustic permafrost across record and in vicinity of station is about 30 m below seafloor.

82-13	F82 09 0604 (DENNY)	(04:12)	0.127 km W

Station lies in 90 m of water in the Mackenzie Trough, well to the west of the thick, ice-bonded shelf. The airgun record shows strong reflectors conformable with the seabed to several metres depth and some regions of acoustic voids (gassy sediments?)

The 3.5 kHz sub-bottom profiler record shows a prominent reflector about 10m below the seabed. Signal fade-out, perhaps indicating gassy sediments, appear at 15 to 40 m below the seabed.

82-13	F82 09 0423 (CORGAS)	412 (07:05)	0.525 km NW

Line runs north westerly through the Mackenzie Trough passing to the east of the geothermal station. The records are somewhat better than for line 0604 and show the same features in the vicinity of the station. Note that a suspected gas anomaly was being profiled in the area of fix 413 (ONCL, 1982).

82-15	F82 09 0604 (DENNY)		(09:30)	0.090 km E

The 3.5 kHz record shows little stratification especially in vicinity of the gas anormany, thought to be about 200 m east of the station. The general featureless nature of the record may arise from gaseous sediments.

82-23	Grid Site #2 AB	8	(14:50)	0.010 km E

This line trends northwesterly, essentially across the shelf break, over the geothermal station on the slope and and into deeper water (Fig. 2.2). The station lies near the top of a chaotic region that may a slump feature with a mud diapir near its terminus. The station appears in the middle of a depression filled with stratified sediments. Diapirs seem to have accumulated further sediment. See Hill et al. (1982).

82-29	F82 09 0315 (B99 KUD)	244	(22.20)	0.090 km E

This station lies along the Kringalik Plateau/Ikit Trough boundary, on the above line. The 3.5 kHz record shows a diminishing frequency of ice scour. An uncomformity lies perhaps 10 m below the seabed.

83-3	F82 09 0315 (KUD 044)	308	(03:45)	2.581 km S (Fig. 2.3)

This station lies to the east of the diapir field occurring along the NE margin of the Mackenzie Trough. The line lies north of the site and runs in a north easterly direction. Area has considerable ice scour (Fig. 2.3) and is underlain by two paleosurfaces also showing paleo-scour, seen on the 3.5 kHz record. A weak reflector appearing at several areas across the airgun record may be acoustic permafrost (compare Fig. 2.2.3 in O'Connor, 1982a).

83-22	F82 09 1603 (IRKTIM)	628	(07:40)	2.343 km SW

This station lies near the centre of the Kugmallit Channel; the line trends NW. On the airgun record, a distinct unconformity lies about 3 m below the seabed; the section shows a prominant paleochannel on this surface. (Compare Fig. 2.6.3 and 2.6.4 in O'Connor, 1982b). A sparse distribution of ice scour are observed on the 3.5 kHz record.

83-25	Grid Site #1 line AB	15	(18:50)	0.220 km S

This line trends north westerly across the outer shelf break onto the slope. The geothermal station lies within a long span of undisturbed sediments just upslope of an increase in the bathymetry gradient, Figure 2.4. There is no indication of a slump feature in the vicinity of the station on this line.

83-25	83 - 13.05	209	0.982 km SW (Fig. 2.4)

This line trends in an E-W direction in a slightly downslope sense. The sediment stratigraphy in the vicinity of the geothermal station appears generally undisturbed.

TABLE 3.1

MICROPROCESSOR CALIBRATIONS

Temperature Range (per 1024 bit section)	Regression Coefficients[1]			Correlation
	a	b	c	R^2
-2.8 to + 0.4°C				
1981	(2)			
1982	-2.773	0.00316	-4.28×10^{-8}	0.99999
1983	-2.819	0.00307	$+3.24 \times 10^{-8}$	0.99986
0.4 to 3.5°C				
1981	(2)			
1982	0.4215	0.00307	-2.38×10^{-8}	0.99999
1983	0.3573	0.00311	-6.55×10^{-8}	0.99973
3.5 to 6.6°C				
1981	(2)			
1982	3.543	0.00303	-1.17×10^{-8}	0.99999
1983	3.505	0.00306	-5.11×10^{-8}	0.99994
6.6 to 9,9°C				
1981	(2)			
1982	6.634	0.00300	$+1.93 \times 10^{-8}$	0.99999
1983	6.579	0.00311	-6.89×10^{-8}	0.99991

Notes:

(1) Regression equation:
$T = a+b\ (BITS) + c\ (BITS)^2$, °C

(2) These values differ for each thermistor because of the individual calibrations.

TABLE 3.2

Distribution of Gradiometer stations
Beaufort Sea

PHYSIOGRAPHIC PROVINCE (1)	GRADIOMETER STATIONS
Natsek Plain	none
Mackenzie Trough	82-8, 9, 10, 11, 12, 13, 15 83-5
Kringalik Plateau	82-28 83-3, 4
Ikit Trough	81-9, 12 82-5, 29
Akpak Plateau	80-13, 14, 15, (12) 81-11, 13, 15 82-6
Kugmallit Channel	80-2, 3, (5), 6, 7, 8, 9, 11 83-22, 23
Tingmiark Plain	80-5, 12, 19, 21, 22, 23, 24, 26 -35, 36, 37, 38, 39, 42, 44 81-1, 2, 3, 6, 16
Niglik Channels	80-1, 28, 29, 30, 33, 34 81-4, 7, 8, 17
Kaglulik Plain	80-32
Shelf Edge or Slope	82-18, 23, 26 83-25

Notes:

(1) These nine physiographic regions are proposed by O'Connor and Associates, and are largely based on a combination of bathymetry, sediment types and paleotopography. Their approximate boundaries are shown in maps, figures 1.1 - 1.3.

TABLE 5.1

NAHIDIK/82 Volumetric water content and Electrical Conductivity of Core from TDR

Station Number	Core Number	Depth (cm)	Line Length (cm)	K_a	Volumetric water content (m^3/m^3) meas.	(drying)	DC electrical conductivity (siemens/m) 20°C	-1°C
5	PC03	59	2.54	26	0.40	(N/A)	1.86	0.94
5		59	4.76				1.44	0.73
6	GC07		4.60				1.49	0.79
6			9.52				1.23	0.65
8	PC04	144	2.38	31	0.46	(0.65)	1.29	0.67
8		144	4.76				1.22	0.63
9	PC05	101	2.54	23	0.37	(0.64)	1.47	0.76
9		101	4.76				1.13	0.59
10	PC06	126	2.54	31	0.47	(0.60)	1.40	0.73
10		126	4.76				1.32	0.69
11	PC07	181	2.22	30	0.45	(N/A)	1.45	0.75
12	PC08	149	2.38				1.42	0.74
12		149	4.76				1.13	0.59
15	PC12	111	2.54	22	0.36	(0.45)	1.15	0.60
15		111	4.76				0.93	0.48
23	PC21	196	4.76				1.06	0.56

Note:

1) Volumetric water contents in brackets have been converted from gravimetric water contents obtained by weighing and drying of a nearby sample (K. Moran, pers. comm. 1984). See text, section 5.3.1 and Figures 5.3, 5.4.

2) The DC electrical conductivity of the sediment has been calculated from TDR measurements (section 5.2, 5.3.2). In comparison, seawater has an electrical conductivity of 5 S/m (20°C) and 2.9 (-1°C).

TABLE 5.2

NAHIDIK/83 Volumetric water content and Electrical Conductivity of Core from TDR

Station Number	Core Number	Depth (cm)	Line Length (cm)	K_a	Volumetric water content (m^3/m^3) meas.	(drying)	DC electrical conductivity (siemens/m) 20°C	-1°C
3	PC01	0	5.0	58	0.74	(0.57)		
4	PC02	0	5.1	60	0.75	(0.64)		
		100	5.1	36	0.52	(0.58)		
5	PC03	0	5.1	57	0.72	(0.62)		
		0	7.6				1.16	0.60
		120	5.1	57	0.72	(0.61)	1.24	0.64
		120	7.6				1.12	0.58
		240	5.1	45	0.61	(0.63)	1.20	0.62
		240	7.6				1.09	0.57
22	PC09	0	5.1	50	0.65	(0.68)	1.40	0.73
		0	7.6				1.31	0.68
		122	5.1	36	0.52	(0.63)	1.26	0.65
		122	7.6				1.15	0.60
		232	5.1	36	0.52	(0.67)	0.87	0.45
		232	7.6				1.03	0.53

Note:

1) Volumetric water contents in brackets have been concentrated from gravimetric water contents obtained by weighing and drying of nearby sample (K. Moran, pers. comm. 1984). See text, section 5.3.1, and figures 5.3 - 5.4.

2) The DC electrical conductivity of the sediment has been calculated from TDR measurements (section 5.2, 5.3.2). In comparison, seawater has an electrical conductivity of 5 S/m (20°C) and 2.9 (-1°C).

TABLE 5.3

Estimates of gravimetric water content and densities from TDR

Station	Depth (cm)	θ (m^3/m^3)	W (ρ_g=2.68) (kg/kg)	B (Mg/m^3)	k_{NP} (W/mK)
		meas.	Calc.	Calc. (Weighing)	
Nahidik/82					
5	59	0.40	0.20	1.01 (1.42)	1.19
8	144	0.46	0.24	1.91 (1.50)	1.30
9	101	0.37	0.18	2.06 (1.50)	1.26
10	126	0.47	0.25	1.89 (1.40)	1.34
11	181	0.45	0.23	1.92 (N/A)	1.44
15	111	0.36	0.17	2.07 (1.52)	1.39
Nahidik/83					
3	0	0.74	0.52	1.44 (1.33)	1.10
4	0	0.75	0.53	1.42 (1.40)	1.10
	100	0.52	0.29	1.81 (1.59)	1.25
5	0	0.72	0.49	1.47 (1.50)	1.15
	120	0.72	0.49	1.47 (1.52)	1.19
	240	0.61	0.37	1.66 (1.52)	1.24
22	0	0.65	0.41	1.59 (1.50)	1.04
	122	0.52	0.29	1.81 (1.50)	1.14
	232	0.52	0.29	1.81 (1.44)	1.33

Note:

Bulk density values in brackets have been obtained from direct measurements on nearby samples (K. Moran, pers. comm. 1984). See figures 5.3 - 5.5.

TABLE 5.4

Regression of thermal conductivities on water contents by weight

1. Nahidik/82 and /83

$$k = (0.684 + 0.417\ W)^{-1} \qquad (W/mK)$$

$$R^2 = 0.50$$

2. Bullard and Day, (1961), for several oceans

$$k = (0.385 + 1.56\ W)^{-1} \qquad (W/mK)$$

3. Lachenbruch and Marshall (1966) for Canada Basin and Alpha Rise

$$k = (0.227 + 1.77\ W)^{-1} \qquad (W/mK)$$

where W = gravimetric water content, fraction of wet sample weight
k = thermal conductivity (W/wK)

FIGURE CAPTIONS

Figure 1.1 Nahidik/81 geothermal stations, referred to in text as station 81-x. Base map and physiographic subdivisions from O'Connor and Assoc., 1982b. The approximate limit of ice-bonded permafrost (IBPF) is taken from Hunter et al. (1978) and Morack et al. (1983).

Figure 1.2 Nahidik/82 geothermal stations.

Figure 1.3 Nahidik/83 geothermal stations.

Figure 2.1 Airgun seismic section, from the Atlantic Geoscience Centre, typical of the Akpak Plateau near geothermal station 81-11. WS, water surface; SB, seabed; APF, acoustic permafrost (after O'Connor and Assoc. 1982 a,b.) Scales are approximate. Since station 81-11 is about 0.9 km northeast of fix 875, it may be, or may not be, underlain by an ice-bonded permafrost island, as shown (see Tables 2.4 and 2.5).

Figure 2.2 3.5 kHz sub-bottom profile (AGC) across the continental shelf break and over geothermal station 82-23. Scales are approximate.

Figure 2.3 3.5 kHz sub-bottom profile (AGC) typical of northwestern Kringalik Plateau and depicting ice scour. Geothermal station 83-3 is about 2.6 km south of fix 308. Scales are approximate.

Figure 2.4 Airgun seismic section from 1982 survey (AGC) on continental slope, close to geothermal station 83-25. Scales are approximate.

Figure 3.1 Water temperature profiles at holding depths at various stations, illustrating the variability in water temperatures 10-15 m above the bottom; this requires a different approach to obtain the relative calibration of thermistors in the probe than used in deep ocean studies (see section 3.1). The bold, dashed profiles were obtained in water over a hundred metres deep on the continental slope, and were used in the relative calibration of probe thermistors in 1982.

Figure 3.2 Example gradiometer temperature profiles versus time from three 1982 stations illustrating holding depth stabilization, penetration heating and decay, and pullout. In deep ocean work, the stabilizing temperature is closer to that of the seabed (see Fig. 3.11). Sediment temperatures were taken after 20 minutes in the bottom.

Figures 3.3-3.7 Sediment temperature profiles for all stations, as indicated.

Figure 3.8 Water temperatures 10-15 m above the seabed have a tendency to decrease in the offshore direction.

Figure 3.9 Water temperatures 10–15 m above the bottom have little correlation with total water depth.

Figure 3.10 Water/sediment interface temperatures determined from extrapolated sediment temperature profiles, showing a tendency for lower values in the offshore direction (see also Fig. 3.8). The troughs and channels appear to have slightly higher values than the plateaus.

Figure 3.11 Low correlation between sediment temperatures and water temperatures 10–15m above the bottom (see Fig. 3.2). Sediment temperatures are somewhat lower on the plateaus than in the channels.

Figure 3.12 Sediment temperatures versus water depth, showing the partitioning by year of measurement, and by implication, by general region. 1981 stations were on the central to eastern shelf (Fig. 1.1), where the lowest temperatures were recorded. Half the 1982 stations were in the Mackenzie Trough (Fig. 1.2), where higher temperatures were measured.

Figure 3.13 Ranges in sediment temperatures at time of measurement generally decrease in the offshore direction, suggesting a seasonal influence.

Figure 3.14 Ranges in sediment temperatures were slightly greater in the channels than on the plateaus; the largest ranges occur in the more shallow water.

Figure 4.1 Fitting needle probe temperature data to calculate the thermal conductivity k, (W/mK) at station 82–5. Upper, during constant heating (preferred); lower, during the cooling phase.

Figure 4.2 Detail of goodness of fit to the measured needle probe temperatures. Temperatures recorded shortly after the heater is turned on depart from linearity but an excellent fit is obtained after several minutes; the line is fitted to the last 16 points (from ln 5.3 to ln 5.9).

Figure 4.3 Histogram of 363 sediment thermal conductivity determinations across the Beaufort Shelf. The small tail at higher values originates with the measurements on the 1981 cores, which may have lost some moisture in the year between sampling and measurement.

Figure 4.4 Histogram of thermal conductivities measured on 1981 cores; some water loss may have occurred by the time the measurements were made.

Figure 4.5 Histogram of thermal conductivities of 1982 cores.

Figure 4.6 Histogram of thermal conductivities of 1982 cores, omitting the Mackenzie Canyon. The fitted normal distribution for these and for the Canyon are very similar, although the latter has a narrower distribution of thermal conductivity values.

Figure 4.7 Histogram of thermal conductivities for 1983 cores.

Figure 4.8 Typical thermal conductivity-depth profile showing a slight increase with depth that is generally consistent with observations of decreasing water contents (see Fig. 5.4) and increasing shear strengths with depth (Hill et al., 1982).

Figures 4.9-4.11 Thermal conductivity-depth scattergrams for 1981-82-83. The comparatively greater scatter seen in the 1981 results probably arises from the delay in measuring them.

Figure 5.1 Typical trace from the time-domain reflectometry method (TDR) to determine the unfrozen water content in saline sediments. The travel-time for an electrical signal down a parallel transmission line is measured by overlaying traces obtained with lines of different lengths and noting the time of departure of the traces (B point).

Figure 5.2 Typical TDR trace to illustrate the calculation of the DC electrical conductivity of the sediments. Voltage levels of the incident and reflected pulse denote the relative impedence match of probe in sediment.

Figure 5.3 Comparison of volumetric water contents derived by the TDR method and by gravimetric measurements. The latter data is from weighing and drying measurements done at AGC and is considered absolute. Most TDR-measured water contents are low, suggesting that the method is difficult to use in saline sediments. Note that the range of values determined by TDR is almost double that found by the absolute method.

Figure 5.4 Volumetric water contents calculated by TDR (small symbols) and by gravimetric means (large symbols) at three stations. Note the higher water contents indicated at the seabed (see Fig. 4.8-4.11).

Figure 5.5 Regression of needle probe thermal conductivity values with TDR-determined water contents, compared with similar regressions from the literature. There is no physical explanation for the flat slope to the Nahidik data; the wide spread of TDR water contents is probably not real (see Fig. 5.3) and compressing these points would cause them to lie closer to the envelope suggested by the literature.

Figure 5.6 Scattergram of sediment electrical conductivity, corrected to -1°C, with depth, as determined by the TDR method. The values obtained, and their range over a small depth interval, is typical of conductivities reported for the Bering Sea. (Seawater, 2.9 s/m at -1°C.)

Figure 6.1 Analysis of the temperature data at station 82-33 for evidence of pore water motion in the sediments. The linear section of the temperature gradient versus temperature profile is taken as possible evidence of heat transport by water movement (Mansure et al., 1979). Although it is unlikely in this small interval.

Figure 7.1 Locations of gradiometer stations for the 1980 Nahidik cruise (not reported here).

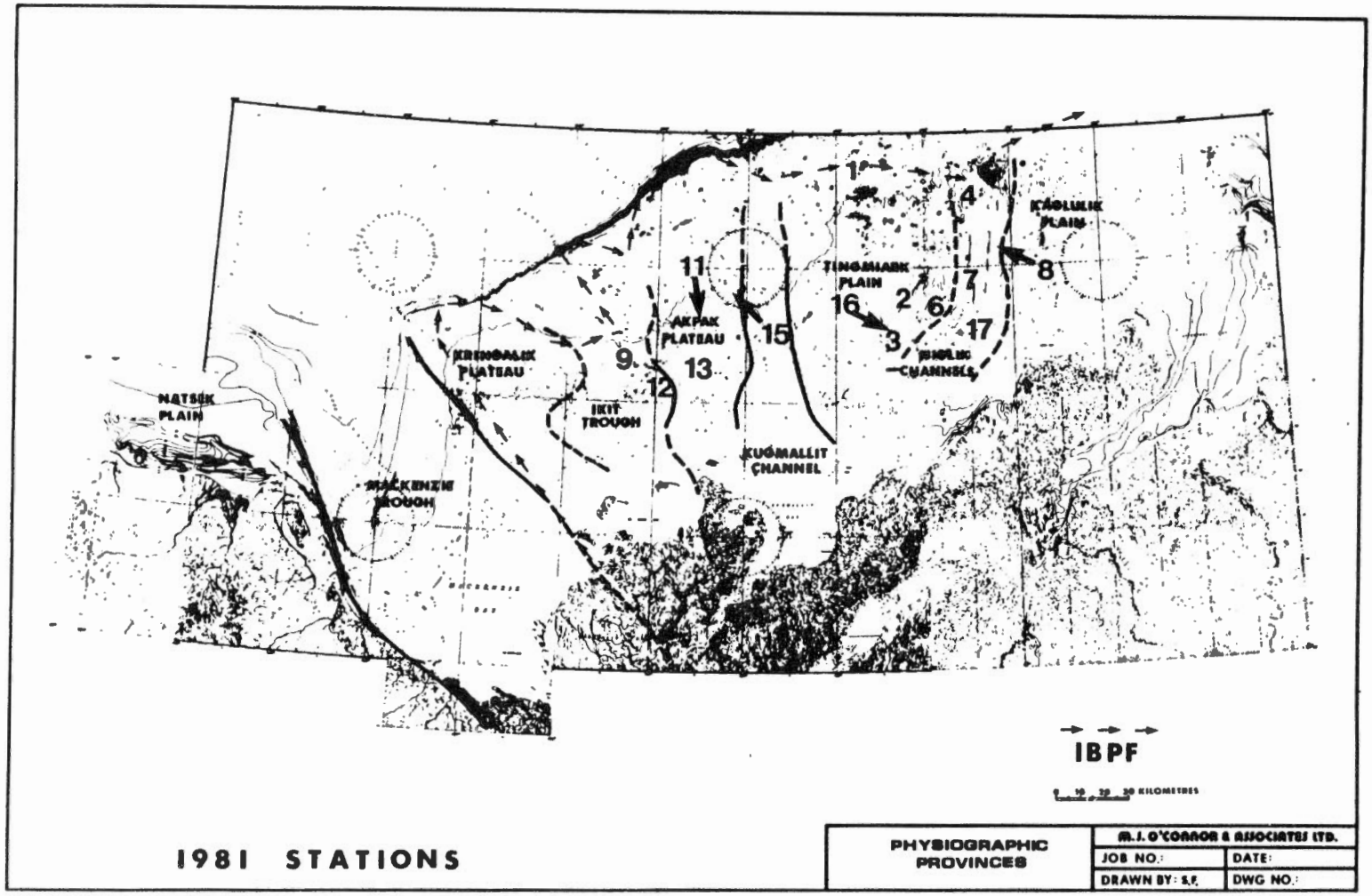
NATSIK PLAIN
MACKENZIE TROUGH
KRINGALIK PLATEAU
IKIT TROUGH
AKPAK PLATEAU
KUGMALLIT CHANNEL
TINGMIAK PLAIN
KADLULIK PLAIN
1
2
3
4
6
7
8
9
11
12
13
15
16
17
IBPF
1981 STATIONS
PHYSIOGRAPHIC PROVINCES
M. J. O'CONNOR & ASSOCIATES LTD.
JOB NO.:
DATE:
DRAWN BY: S.F.
DWG NO.:

FIGURE 1.1

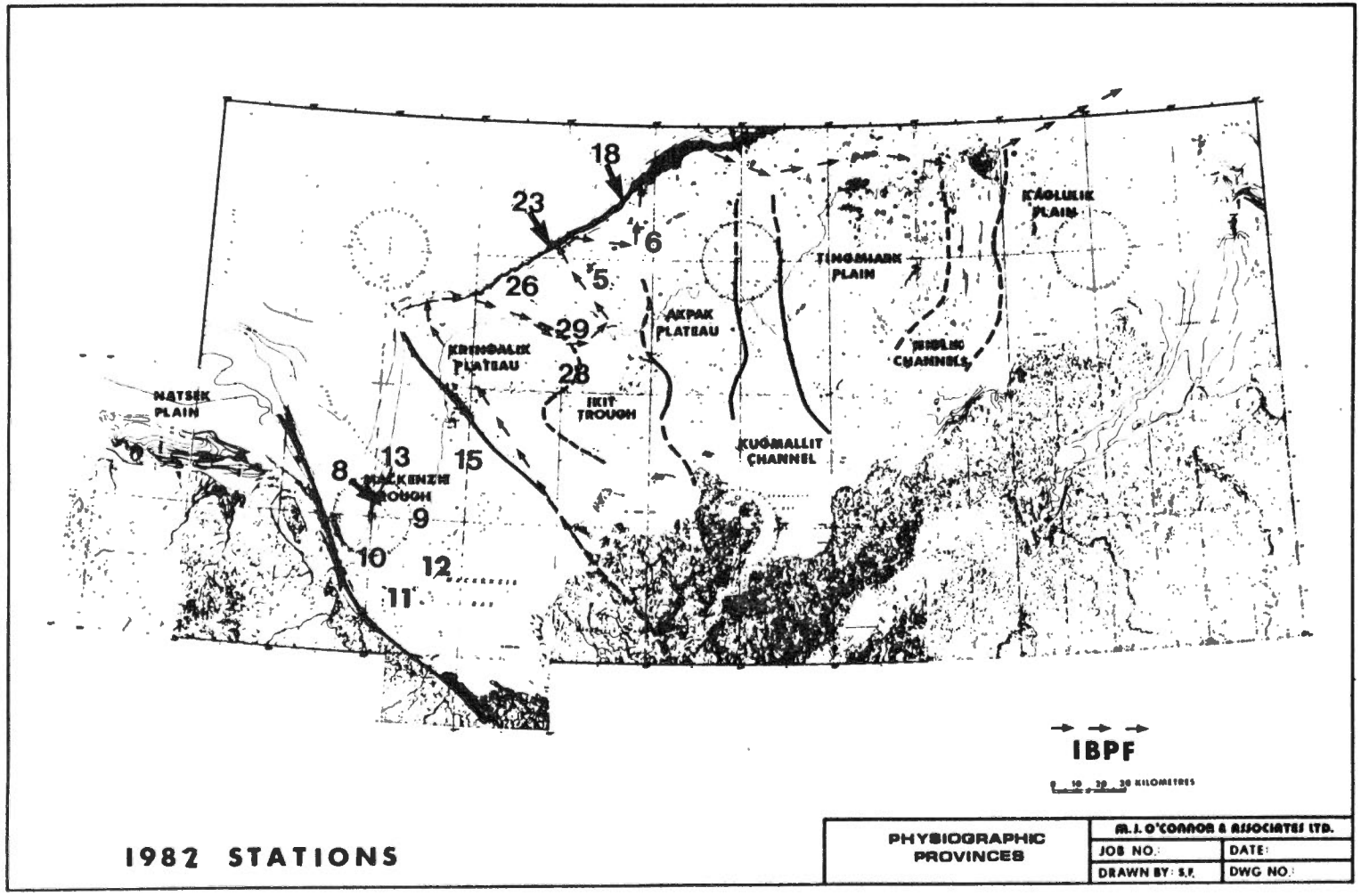
18
23
6
26
5
29
28
AKPAK PLATEAU
KRINGALIK PLATEAU
IKIT TROUGH
KUGMALLIT CHANNEL
TINGMIARK PLAIN
KAGLULIK PLAIN
NATSEK PLAIN
8
13
15
9
10
12
11
IBPF
1982 STATIONS
PHYSIOGRAPHIC PROVINCES
M. J. O'CONNOR & ASSOCIATES LTD.
JOB NO.:
DATE:
DRAWN BY: S.F.
DWG NO.:

FIGURE 1.2

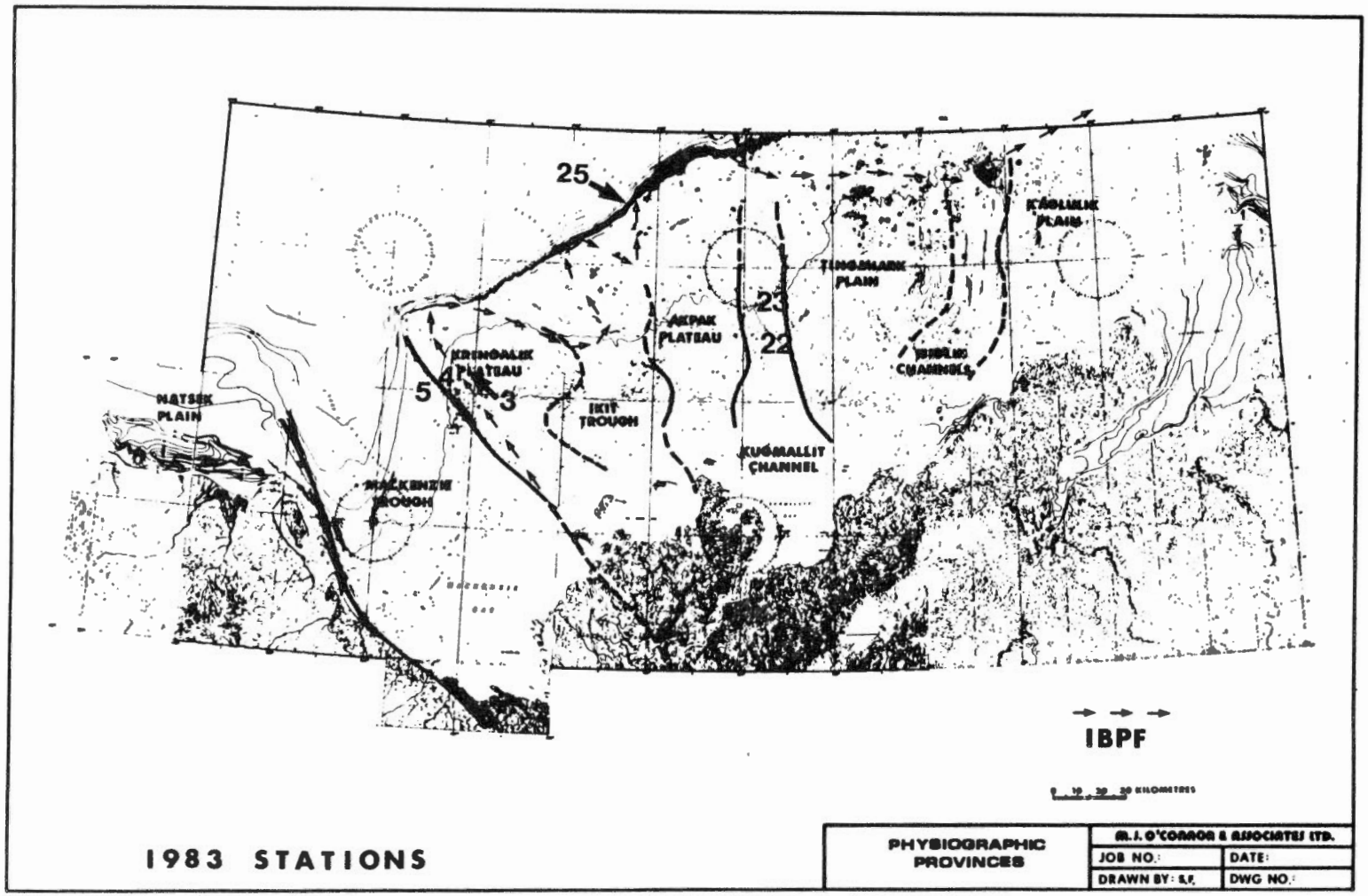
25
23
22
5
4
3
KRENDALK PLATEAU
AKPAK PLATEAU
IKIT TROUGH
KUGMALLIT CHANNEL
TESHEKPUK CHANNEL
TUKTOYAKTUK PLAIN
TUKTOYAKTUK PLAIN
MACKENZIE TROUGH
IBPF
1983 STATIONS
PHYSIOGRAPHIC PROVINCES
M. J. O'CONNOR & ASSOCIATES LTD.
JOB NO.:
DATE:
DRAWN BY: S.F.
DWG NO.:

FIGURE 1.3

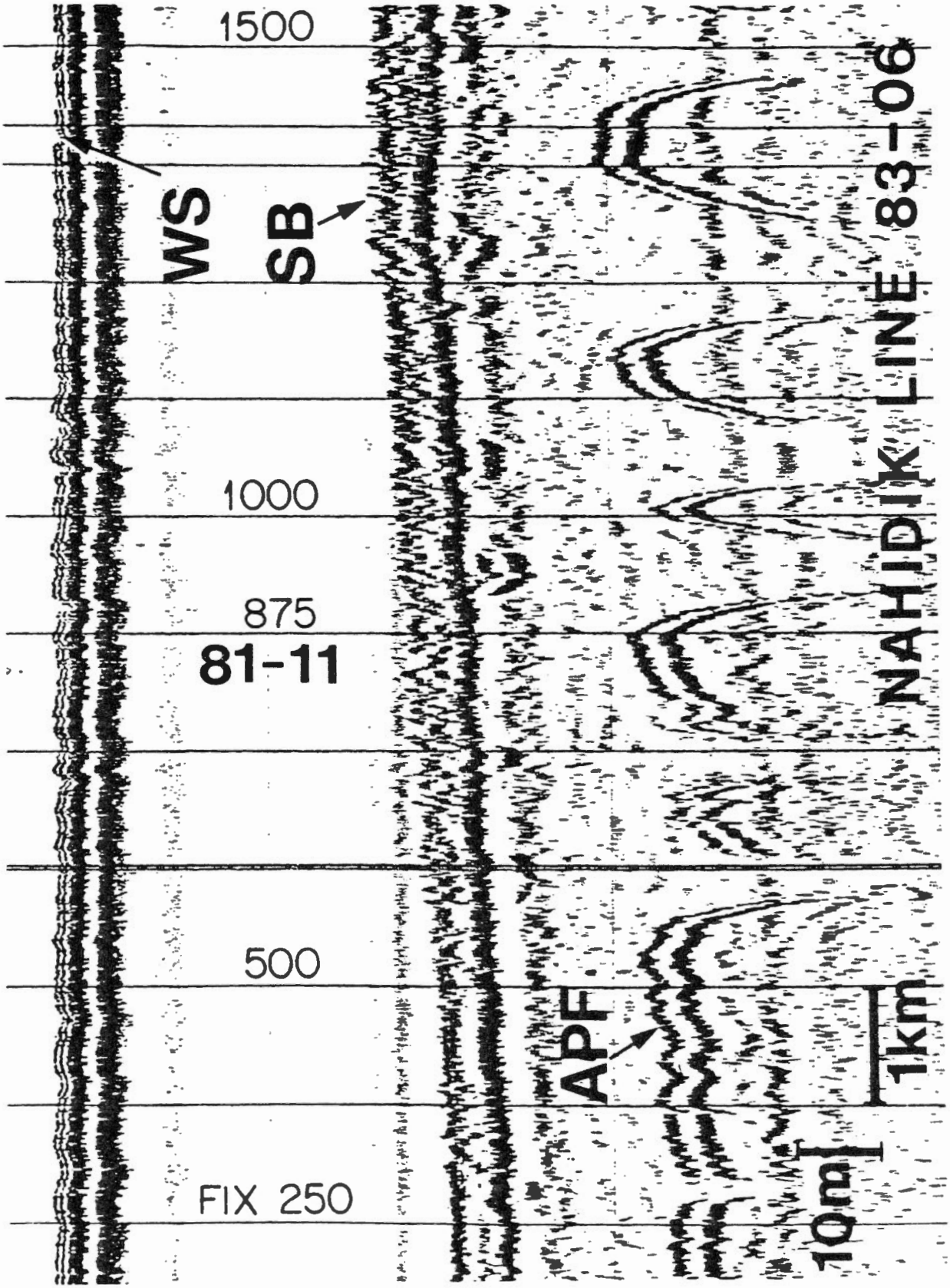
1500
1000
875
500
FIX 250
WS
SB
81-11
APF
1km
10m
NAHIDIK LINE 83-06

FIGURE 2.1

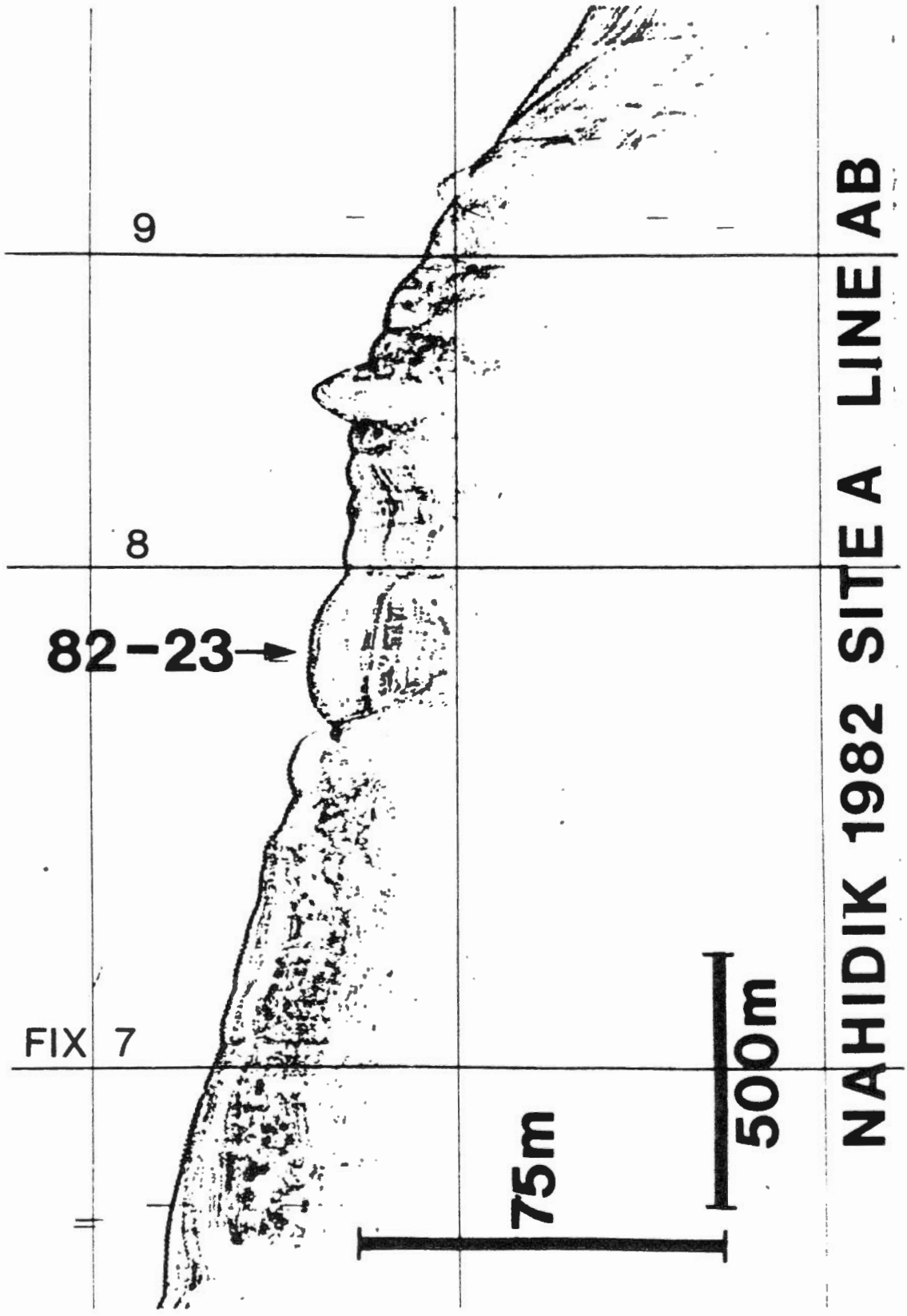

FIGURE 2.2

FIGURE 2.3

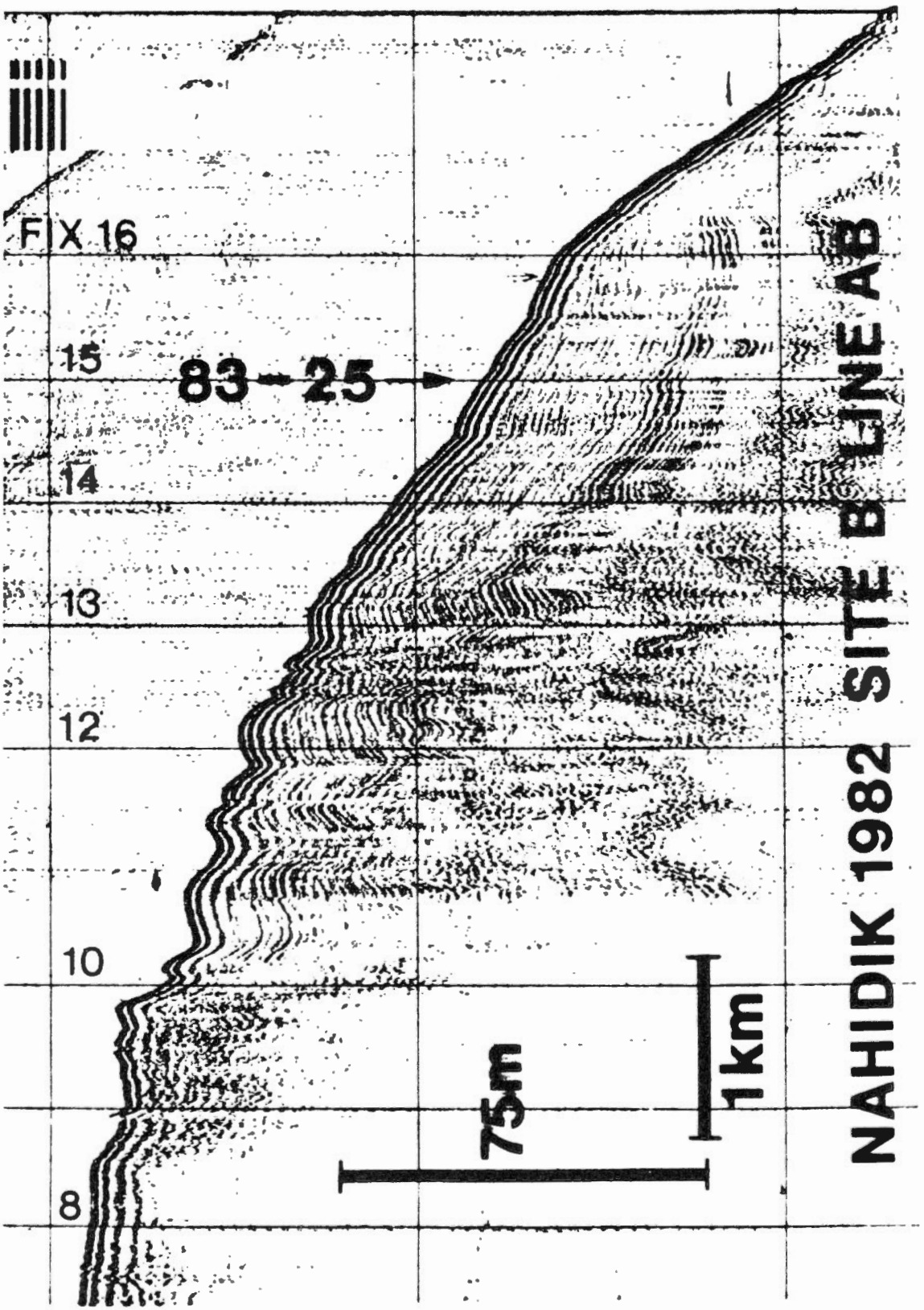

FIGURE 2.4

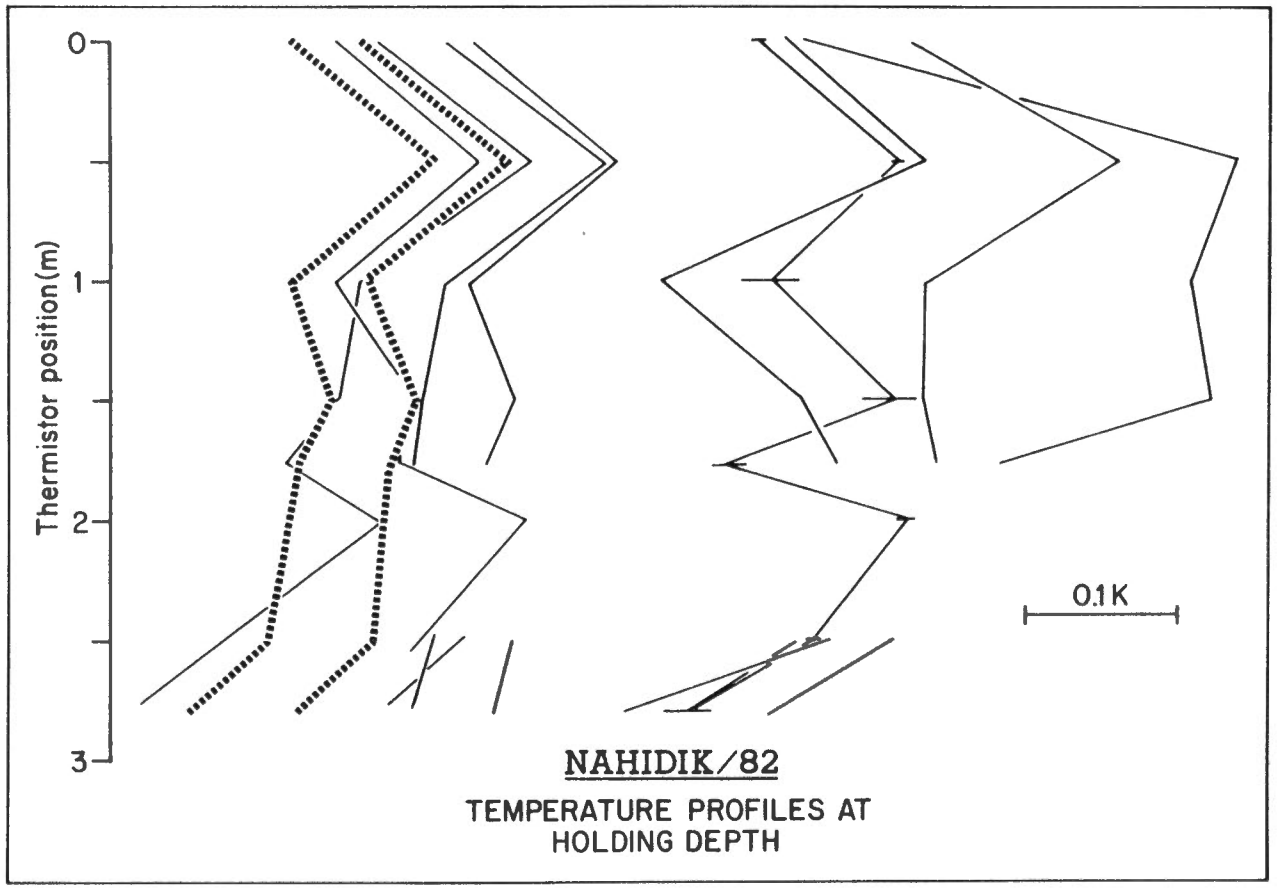
0
1
2
3
Thermistor position(m)
0.1K
NAHIDIK/82
TEMPERATURE PROFILES AT
HOLDING DEPTH

FIGURE 3.1

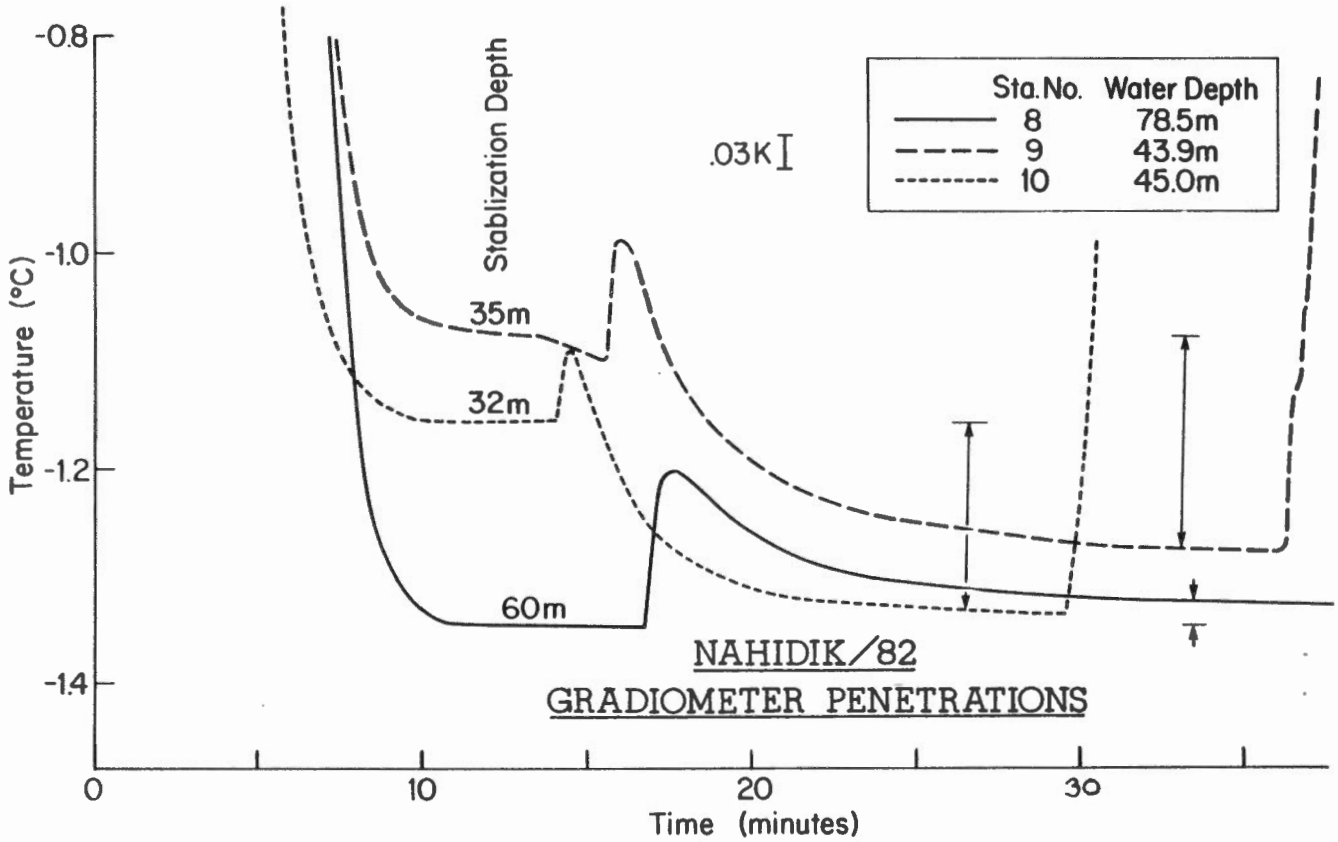
-0.8
-1.0
-1.2
-1.4
Temperature (°C)
0
10
20
30
Time (minutes)
Stablization Depth
.03K
35m
32m
60m
Sta.No. Water Depth
8 78.5m
9 43.9m
10 45.0m
NAHIDIK/82
GRADIOMETER PENETRATIONS

FIGURE 3.2

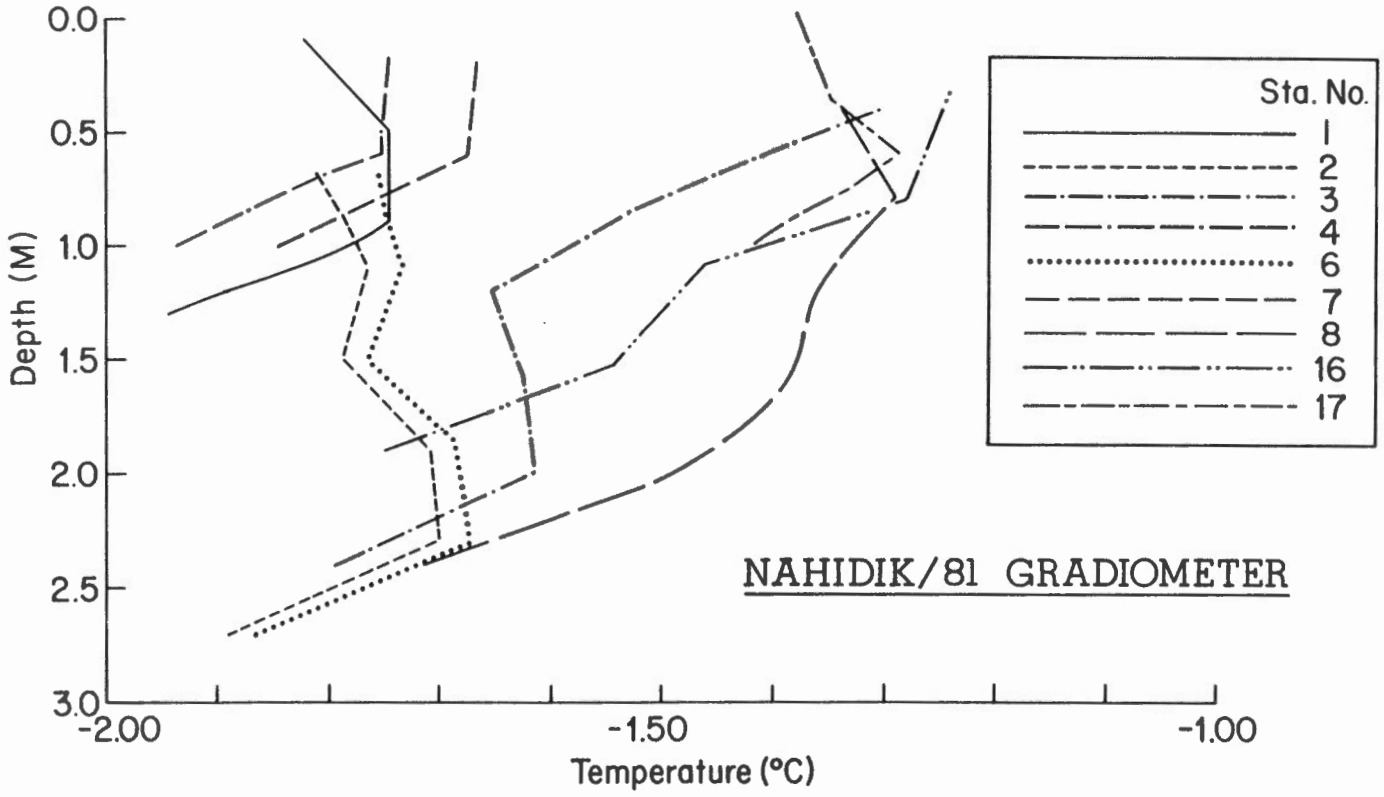
0.0
0.5
1.0
1.5
2.0
2.5
3.0
Depth (M)
-2.00
-1.50
-1.00
Temperature (°C)
Sta. No.
1
2
3
4
6
7
8
16
17
NAHIDIK/81 GRADIOMETER

FIGURE 3.3

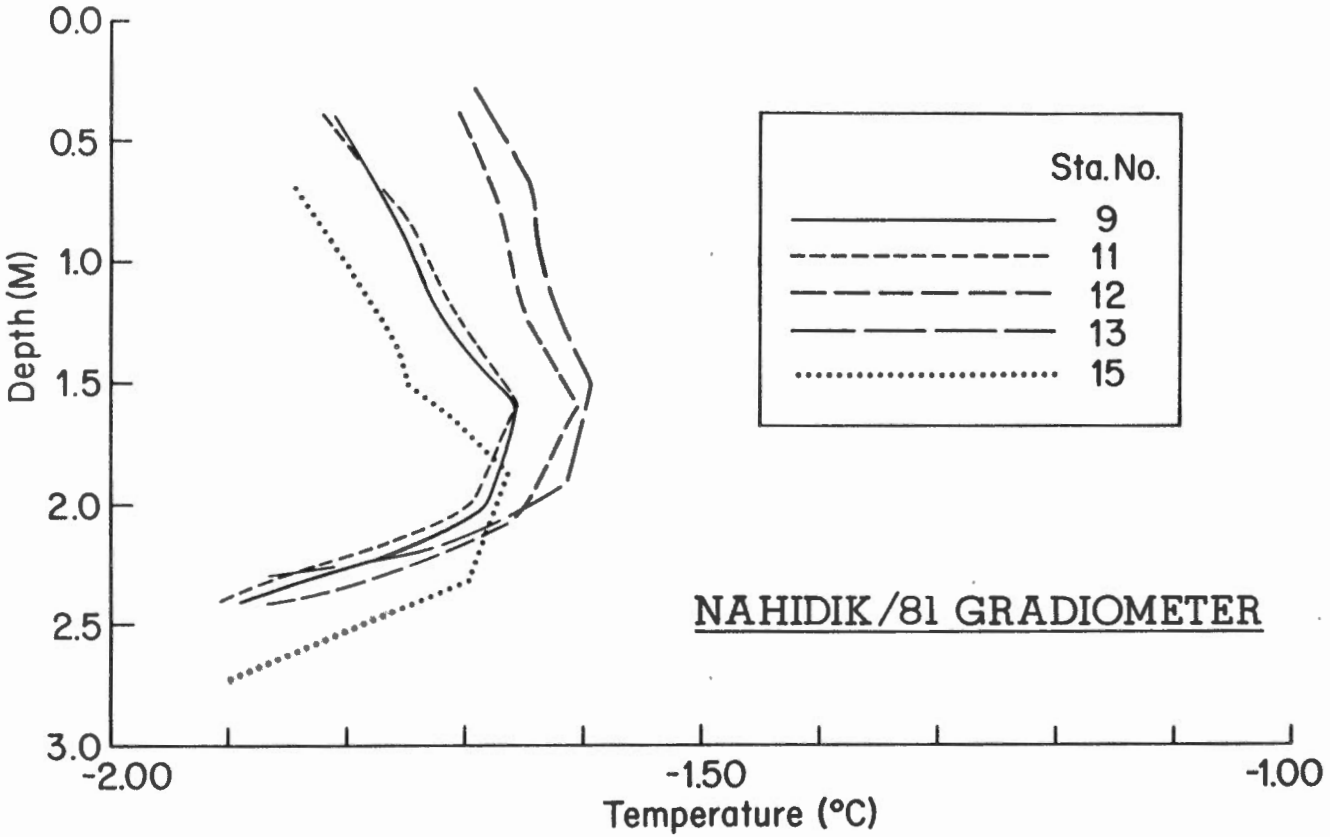
0.0
0.5
1.0
1.5
2.0
2.5
3.0
Depth (M)
-2.00
-1.50
-1.00
Temperature (°C)
Sta. No.
9
11
12
13
15
NAHIDIK/81 GRADIOMETER

FIGURE 3.4

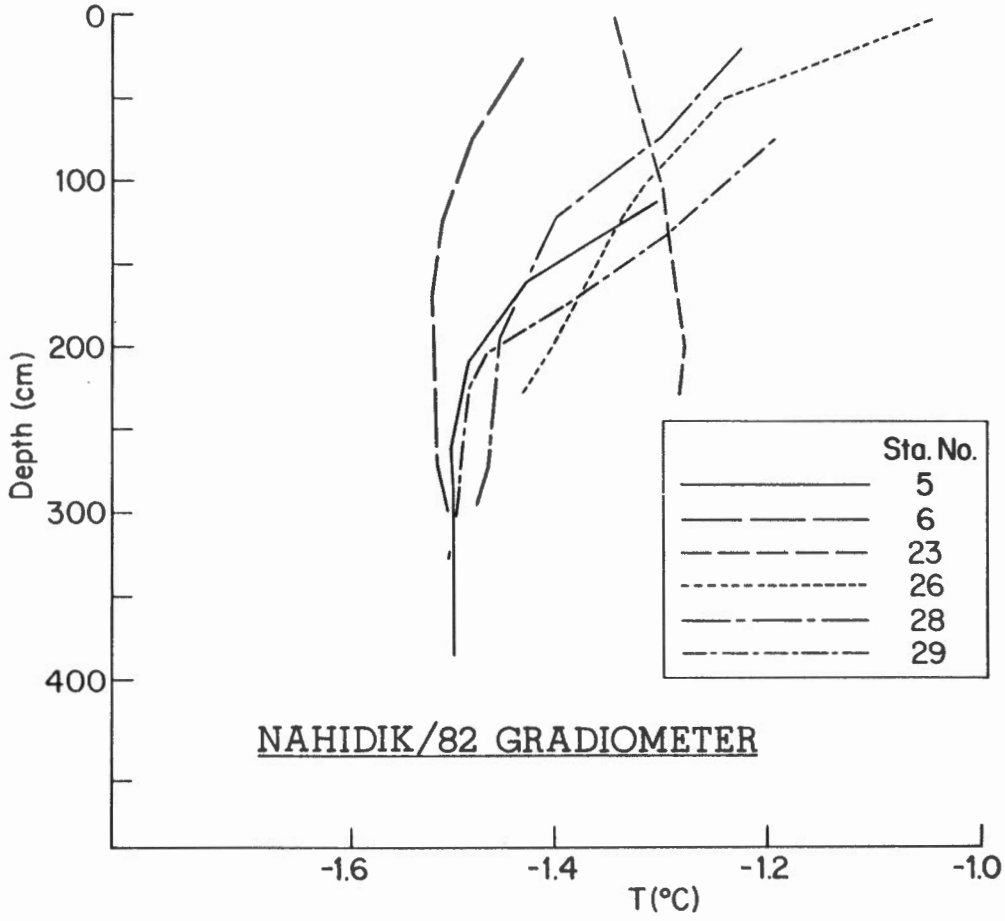
0
100
200
300
400
Depth (cm)
Sta. No.
5
6
23
26
28
29
NAHIDIK/82 GRADIOMETER
-1.6
-1.4
-1.2
-1.0
T(°C)

FIGURE 3.5

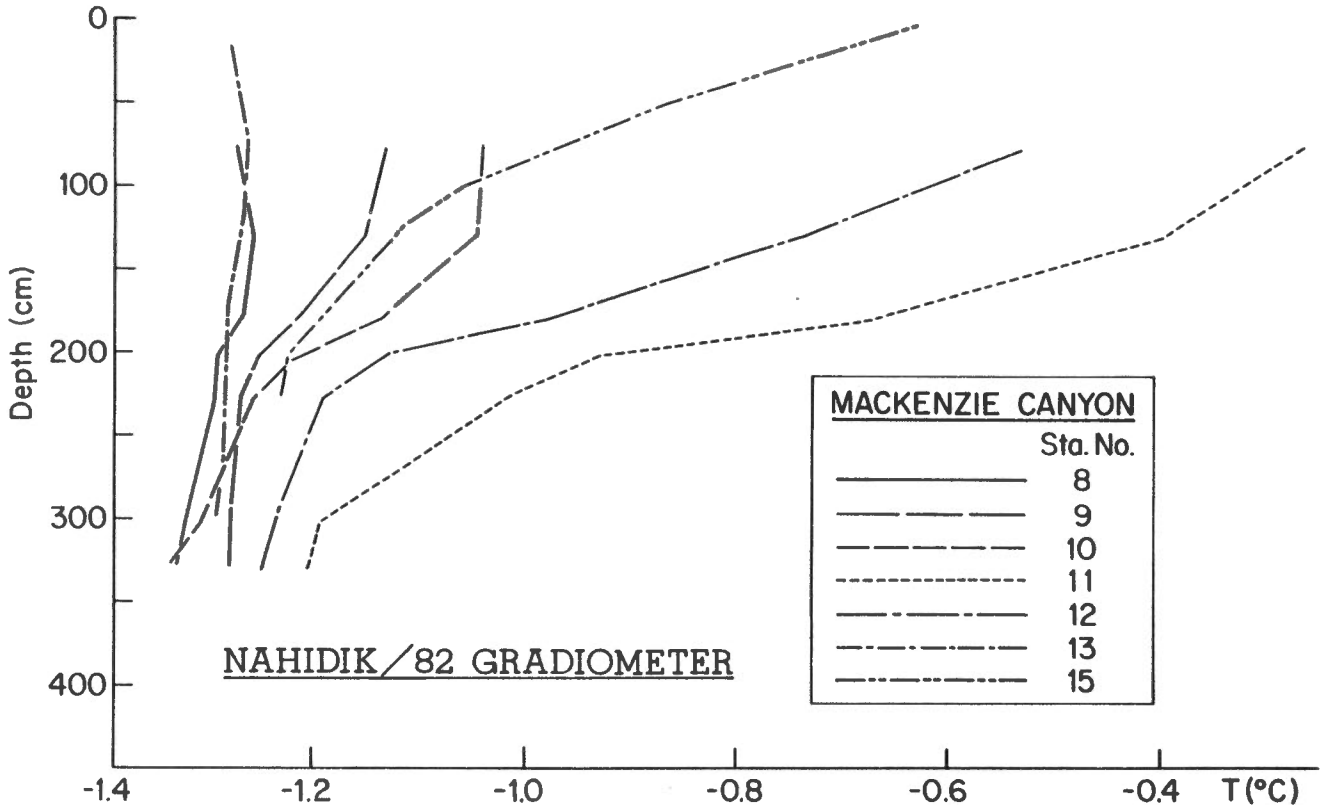
0
100
200
300
400
Depth (cm)
-1.4
-1.2
-1.0
-0.8
-0.6
-0.4
T(°C)
NAHIDIK/82 GRADIOMETER
MACKENZIE CANYON
Sta. No.
8
9
10
11
12
13
15

FIGURE 3.6

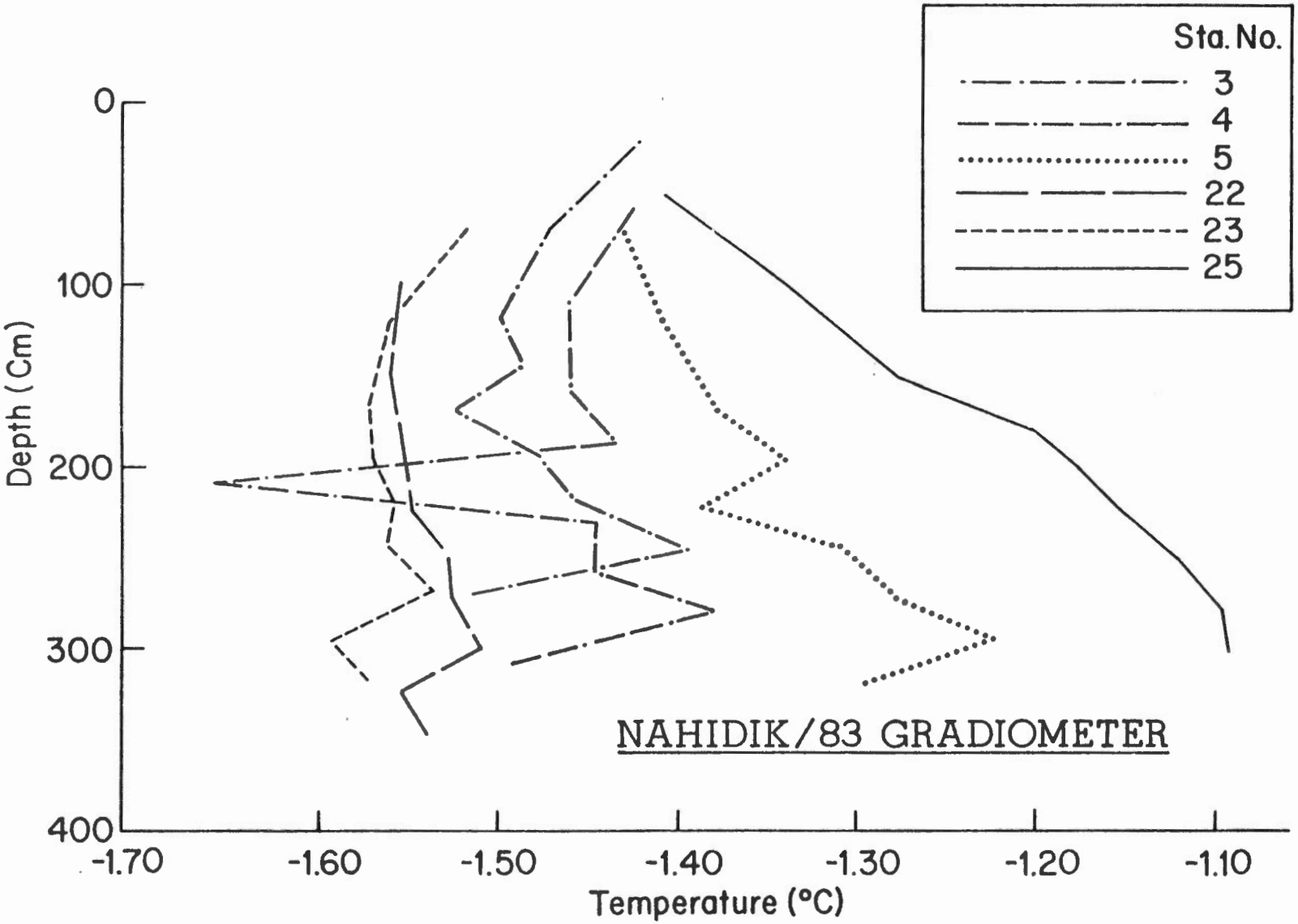
Sta. No.
3
4
5
22
23
25
0
100
200
300
400
Depth (Cm)
-1.70
-1.60
-1.50
-1.40
-1.30
-1.20
-1.10
Temperature (°C)
NAHIDIK/83 GRADIOMETER

FIGURE 3.7

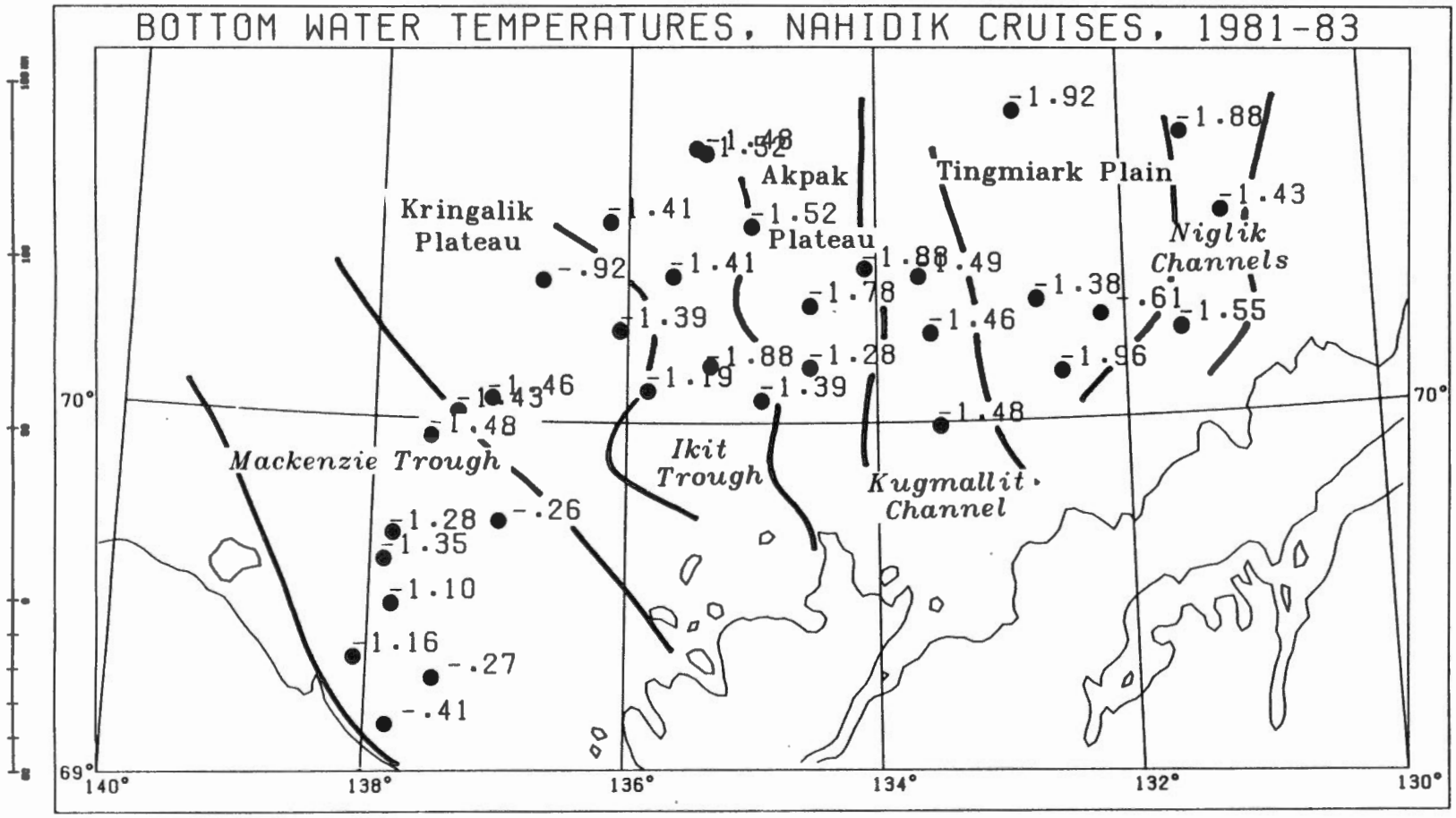

EARTH PHYSICS BRANCH
DIRECTION DE LA PHYSIQUE DU GLOBE EMR OTTAWA CANADA

FIGURE 3.8

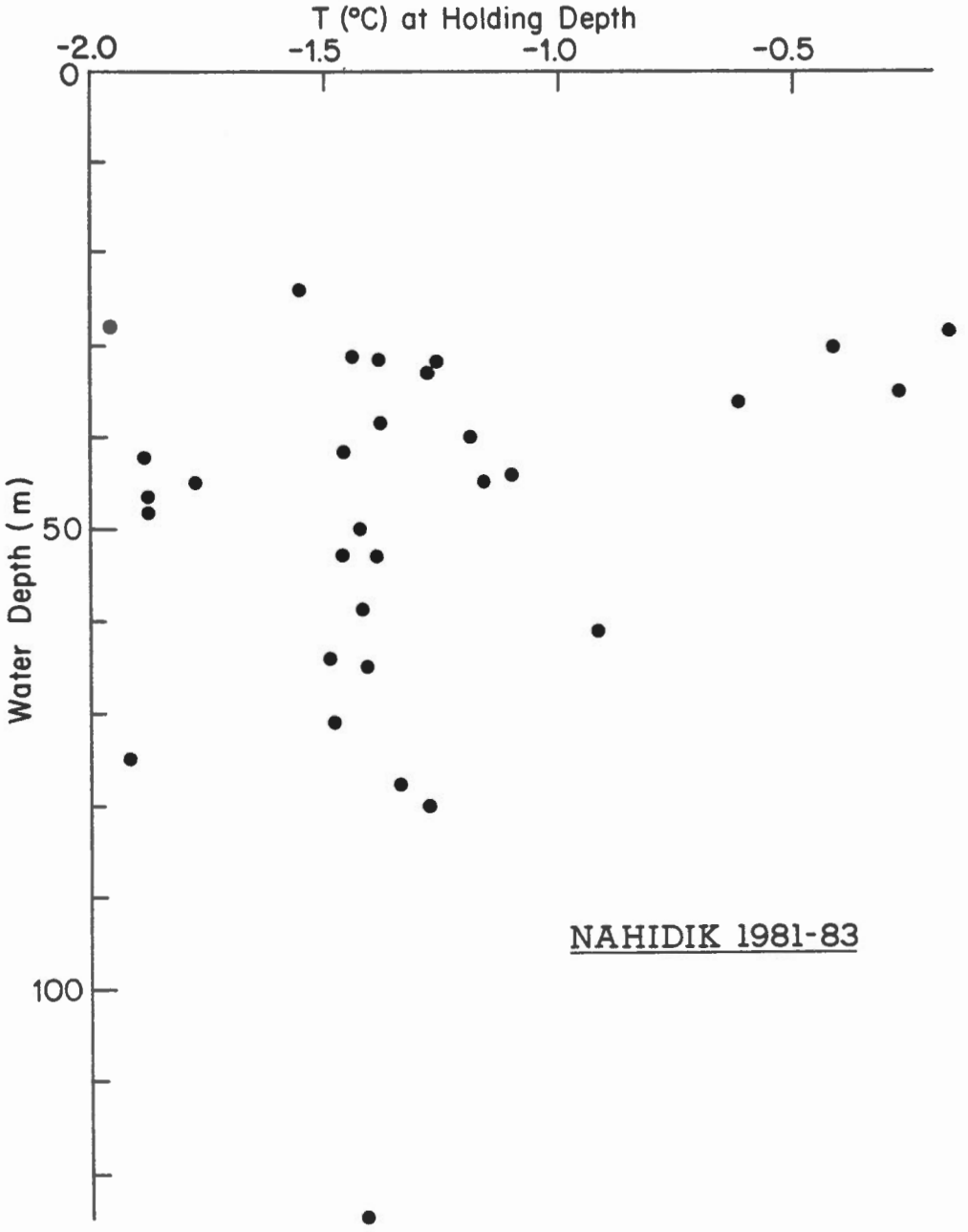
T (°C) at Holding Depth
-2.0
-1.5
-1.0
-0.5
0
50
100
Water Depth (m)
NAHIDIK 1981-83

FIGURE 3.9

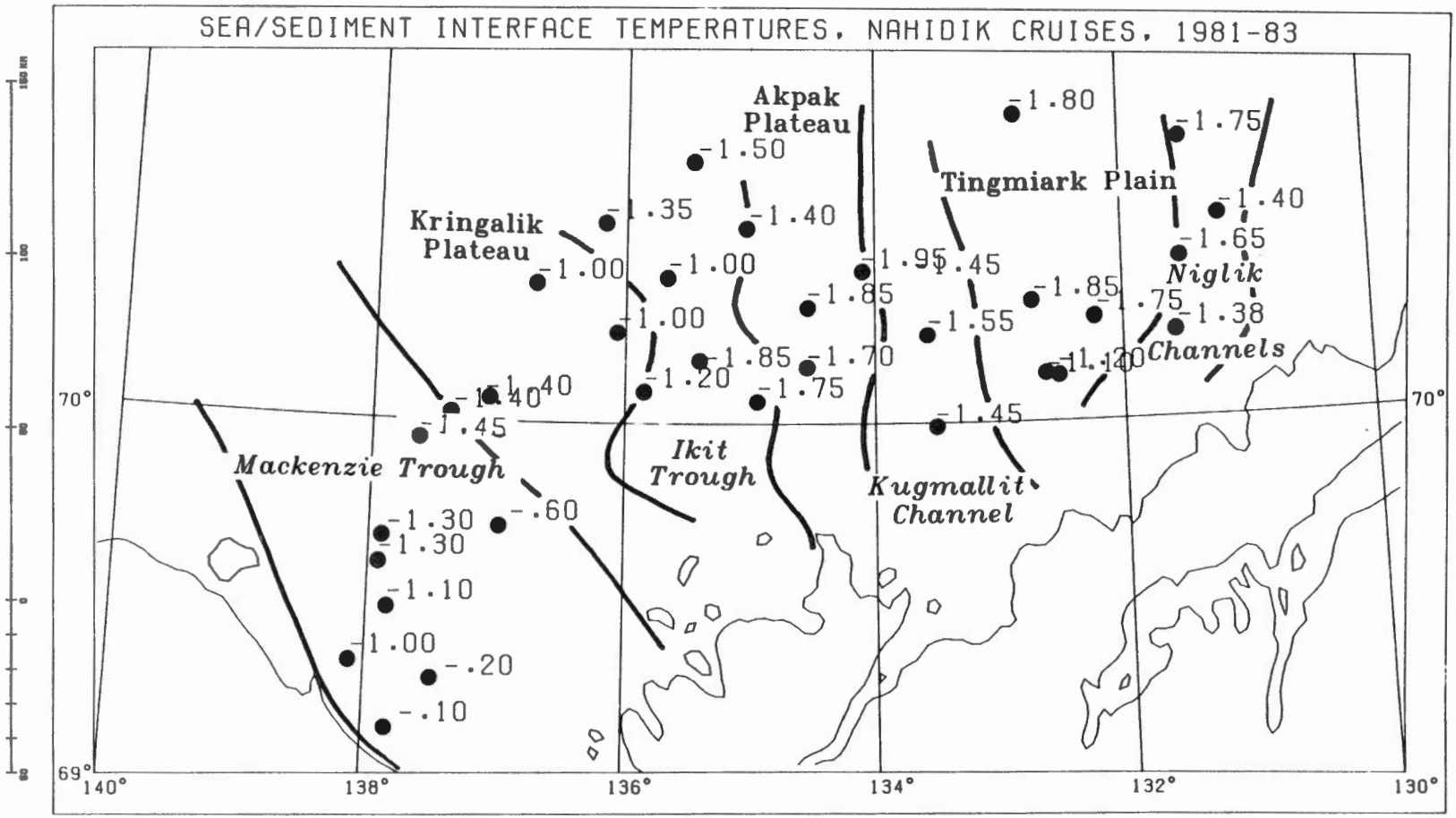

EARTH PHYSICS BRANCH
DIRECTION DE LA PHYSIQUE DU GLOBE EMR OTTAWA CANADA

FIGURE 3.10

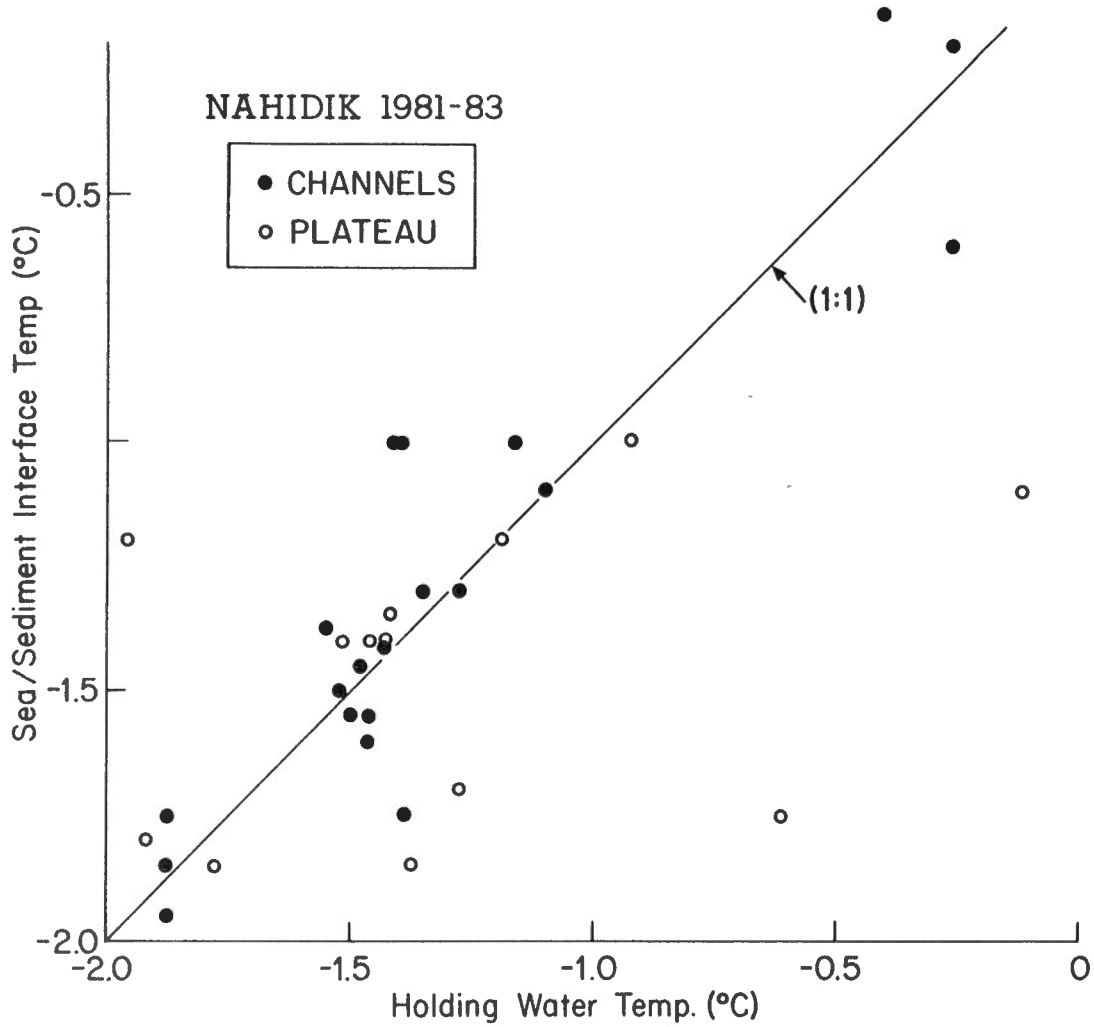
NAHIDIK 1981-83
CHANNELS
PLATEAU
(1:1)
Sea/Sediment Interface Temp (°C)
-0.5
-1.5
-2.0
-2.0
-1.5
-1.0
-0.5
0
Holding Water Temp. (°C)

FIGURE 3.11

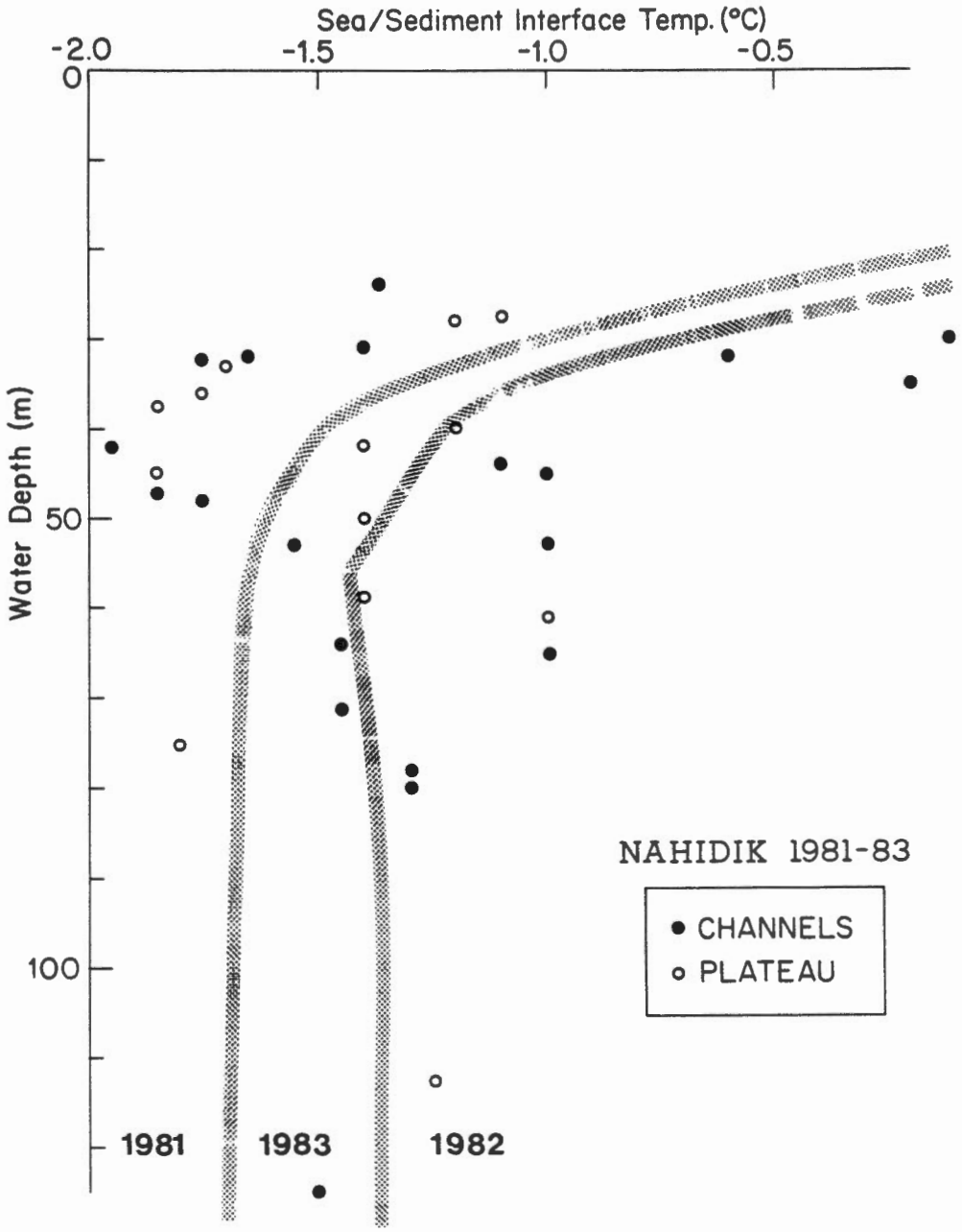
Sea/Sediment Interface Temp. (°C)
-2.0
-1.5
-1.0
-0.5
0
50
100
Water Depth (m)
1981
1983
1982
NAHIDIK 1981-83
• CHANNELS
o PLATEAU

FIGURE 3.12

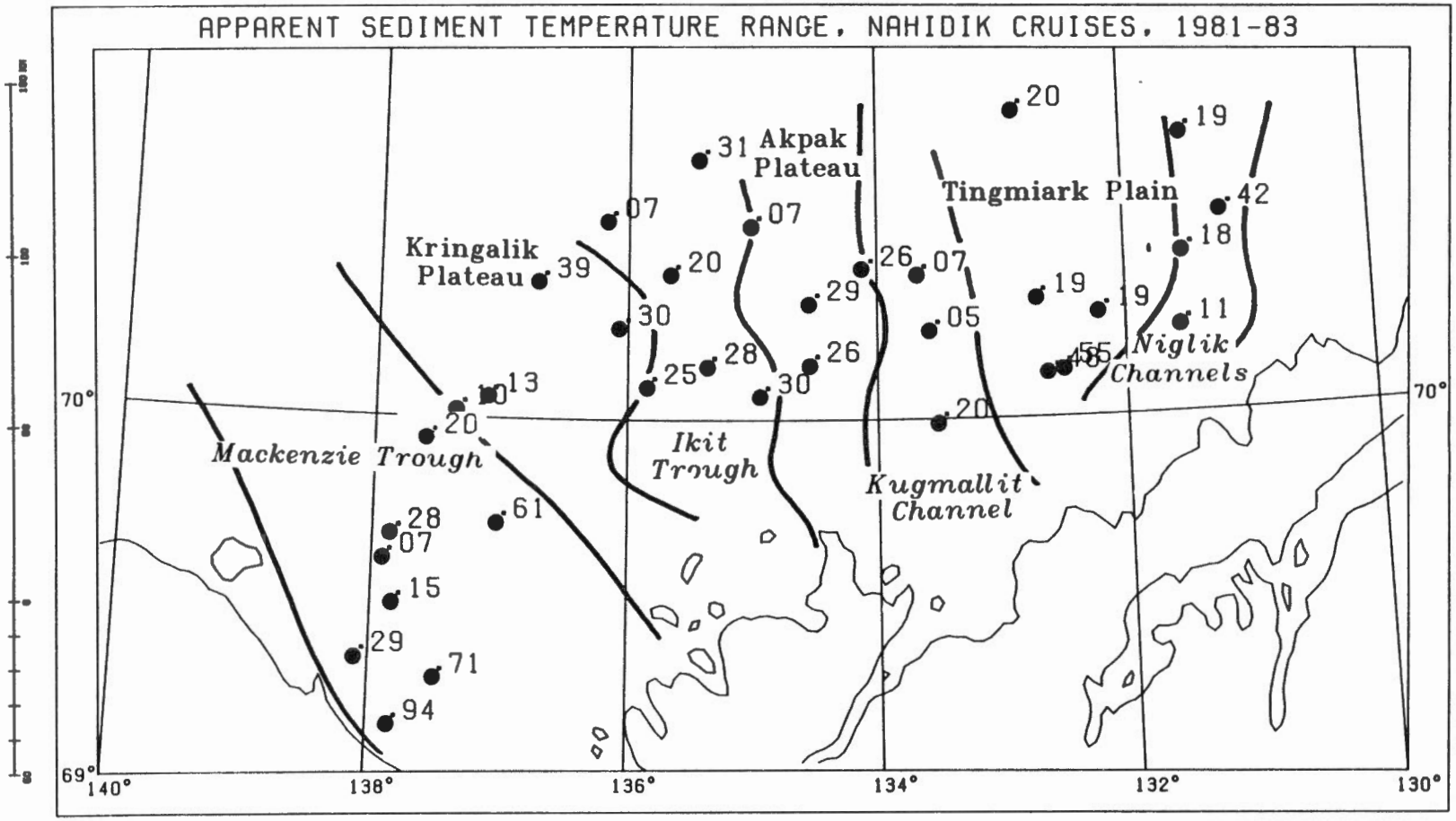
APPARENT SEDIMENT TEMPERATURE RANGE, NAHIDIK CRUISES, 1981-83
Akpak Plateau
Tingmiark Plain
Kringalik Plateau
Niglik Channels
Mackenzie Trough
Ikit Trough
Kugmallit Channel
70°
69°
140°
138°
136°
134°
132°
130°
EARTH PHYSICS BRANCH
DIRECTION DE LA PHYSIQUE DU GLOBE EMR OTTAWA CANADA

FIGURE 3.13

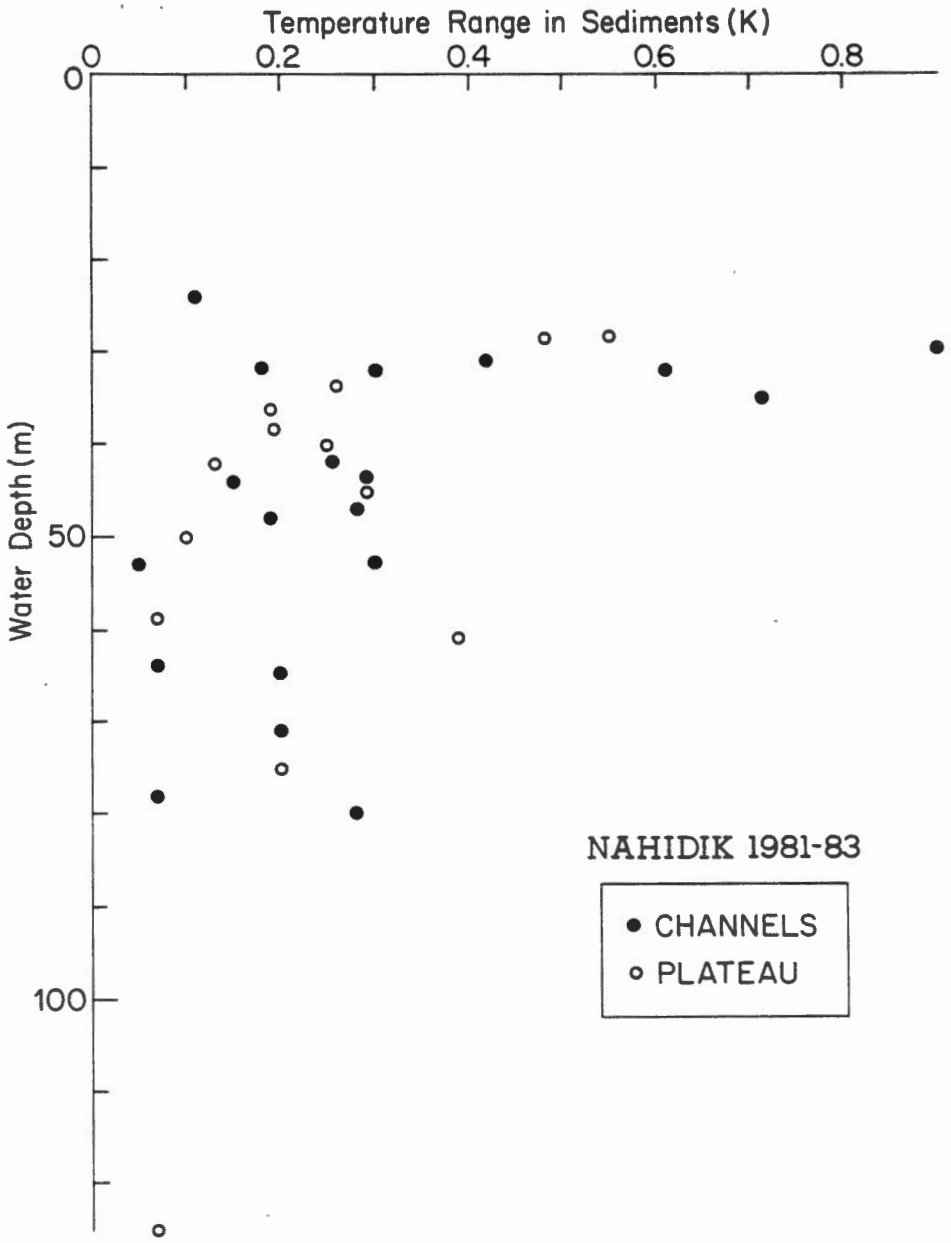
Temperature Range in Sediments (K)
0
0.2
0.4
0.6
0.8
Water Depth (m)
50
100
NAHIDIK 1981-83
• CHANNELS
o PLATEAU

FIGURE 3.14

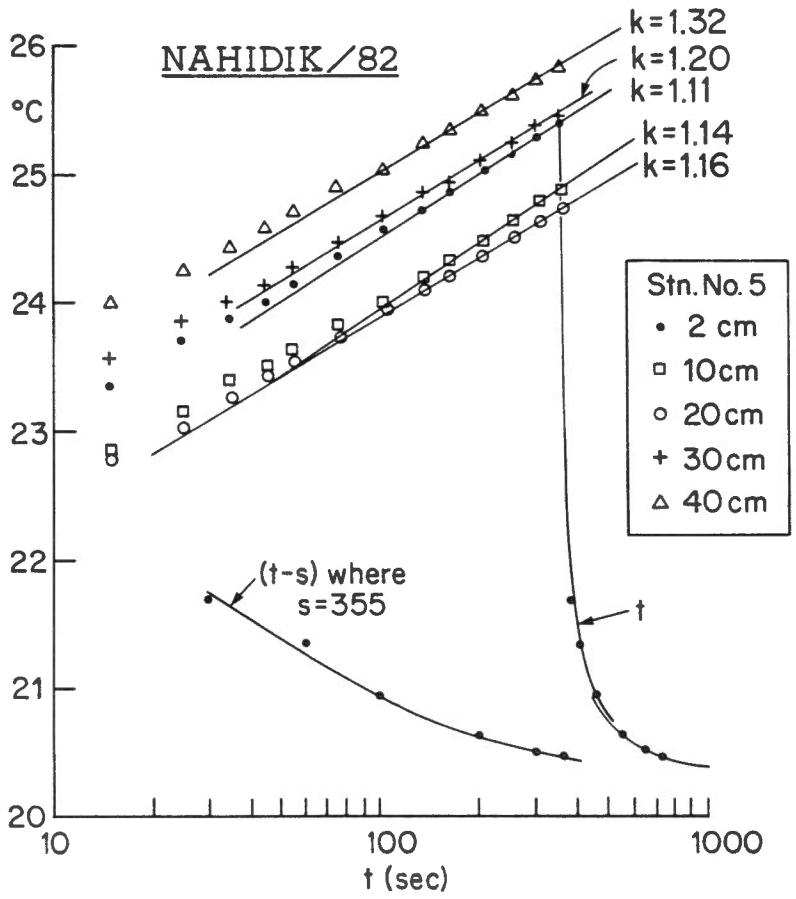
NAHIDIK/82
k=1.32
k=1.20
k=1.11
k=1.14
k=1.16
Stn. No. 5
• 2 cm
□ 10cm
○ 20cm
+ 30cm
△ 40cm
(t-s) where
s=355
t
26
°C
25
24
23
22
21
20
10
100
1000
t (sec)

FIGURE 4.1

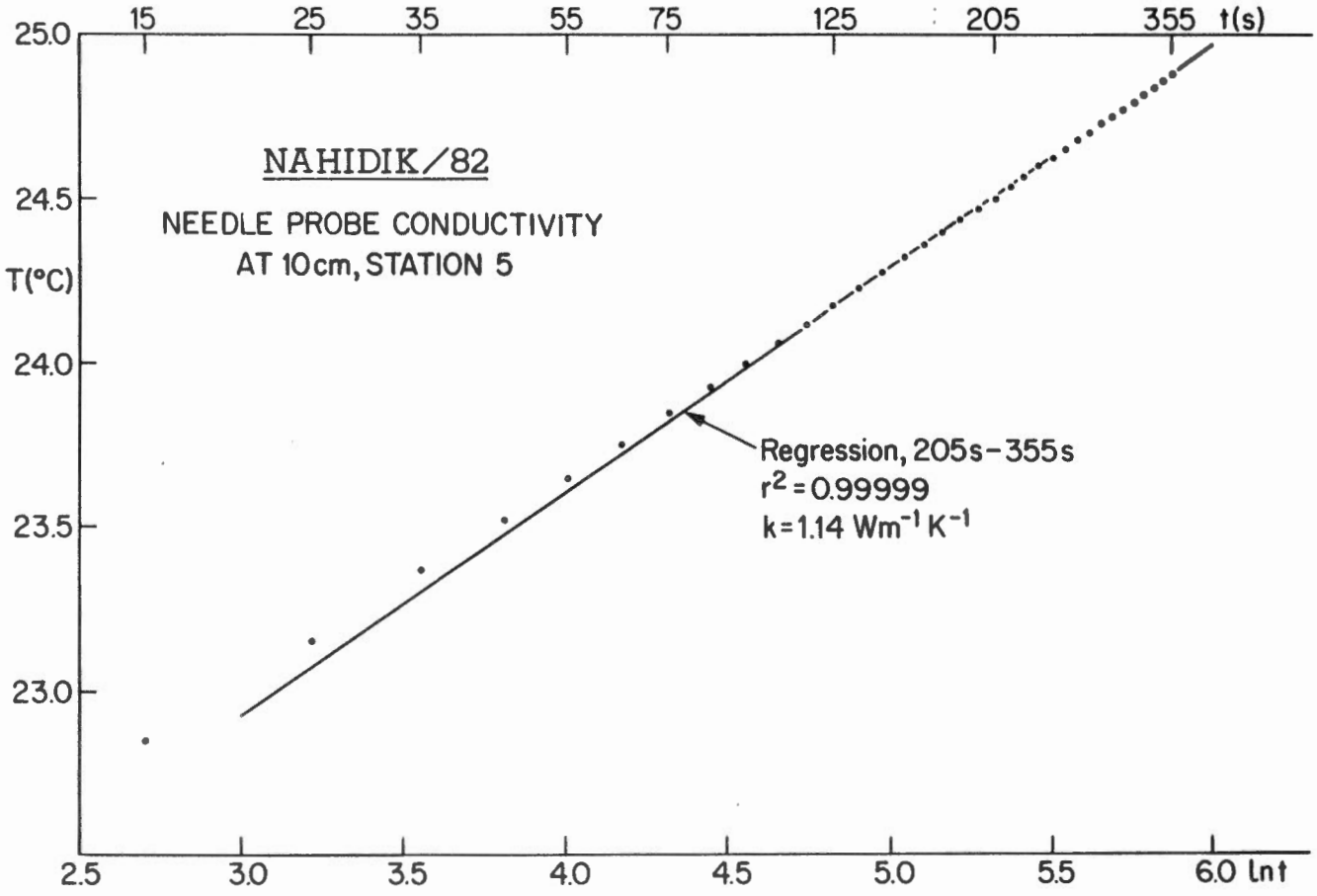
15
25
35
55
75
125
205
355
t(s)
25.0
24.5
24.0
23.5
23.0
T(°C)
NAHIDIK/82
NEEDLE PROBE CONDUCTIVITY
AT 10cm, STATION 5
Regression, 205s-355s
r² = 0.99999
k = 1.14 Wm⁻¹ K⁻¹
2.5
3.0
3.5
4.0
4.5
5.0
5.5
6.0 lnt

FIGURE 4.2

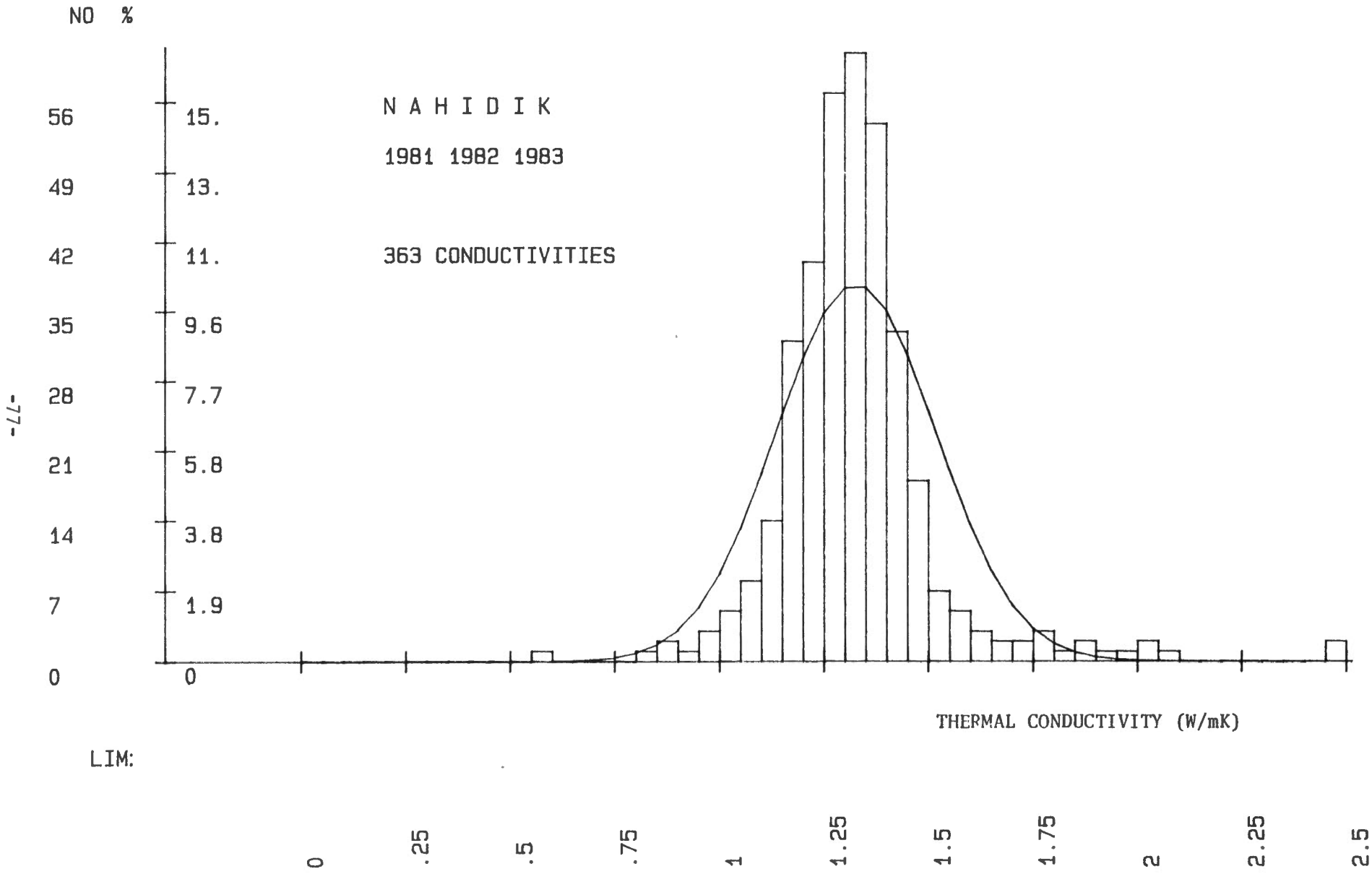
NO %
56
49
42
35
28
21
14
7
0
15.
13.
11.
9.6
7.7
5.8
3.8
1.9
0
N A H I D I K
1981 1982 1983
363 CONDUCTIVITIES
THERMAL CONDUCTIVITY (W/mK)
LIM:
0
.25
.5
.75
1
1.25
1.5
1.75
2
2.25
2.5

FIGURE 4.3

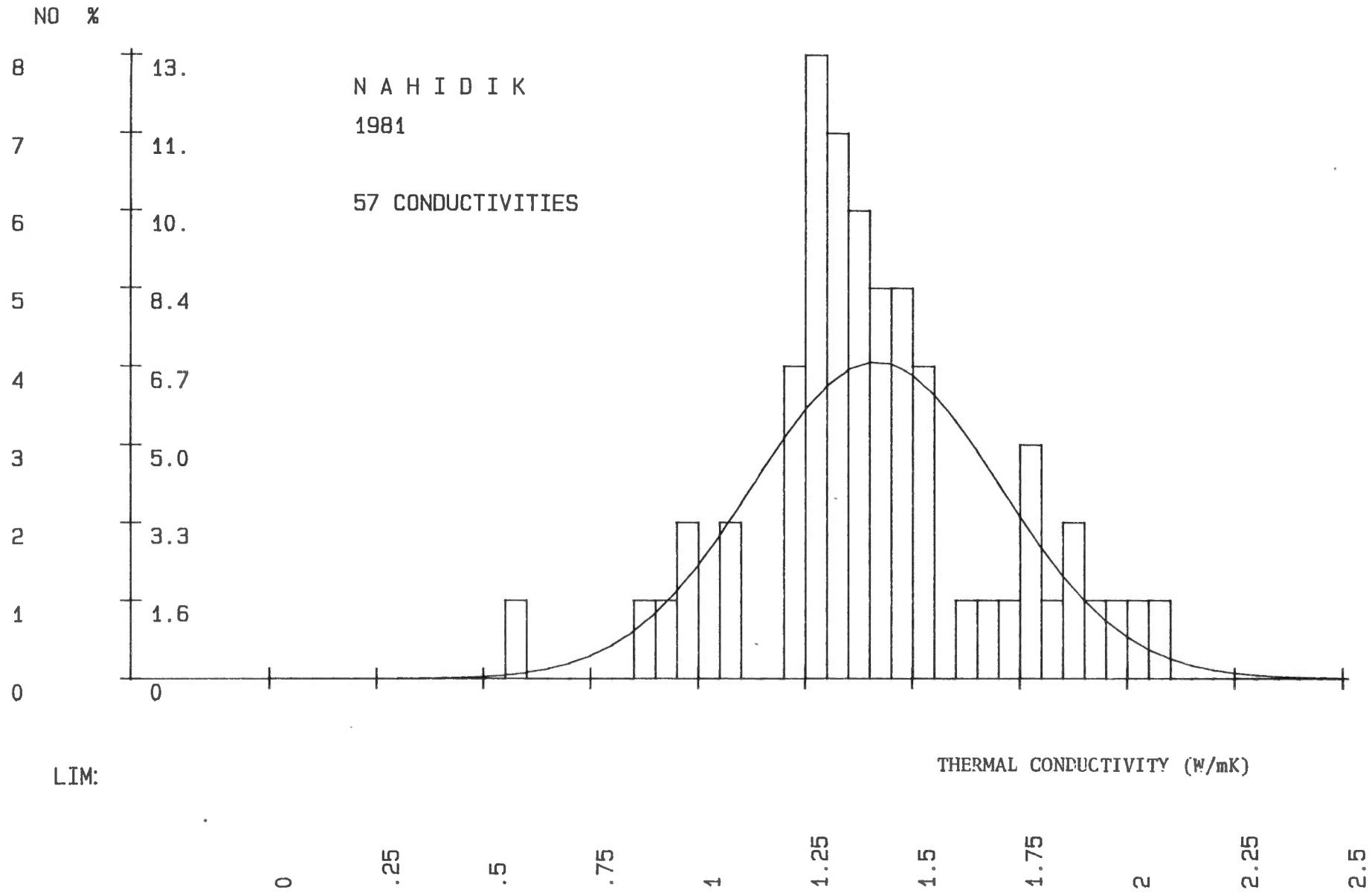
NO %
8
7
6
5
4
3
2
1
0
13.
11.
10.
8.4
6.7
5.0
3.3
1.6
0
N A H I D I K
1981
57 CONDUCTIVITIES
LIM:
0
.25
.5
.75
1
1.25
1.5
1.75
2
2.25
2.5
THERMAL CONDUCTIVITY (W/mK)

FIGURE 4.1

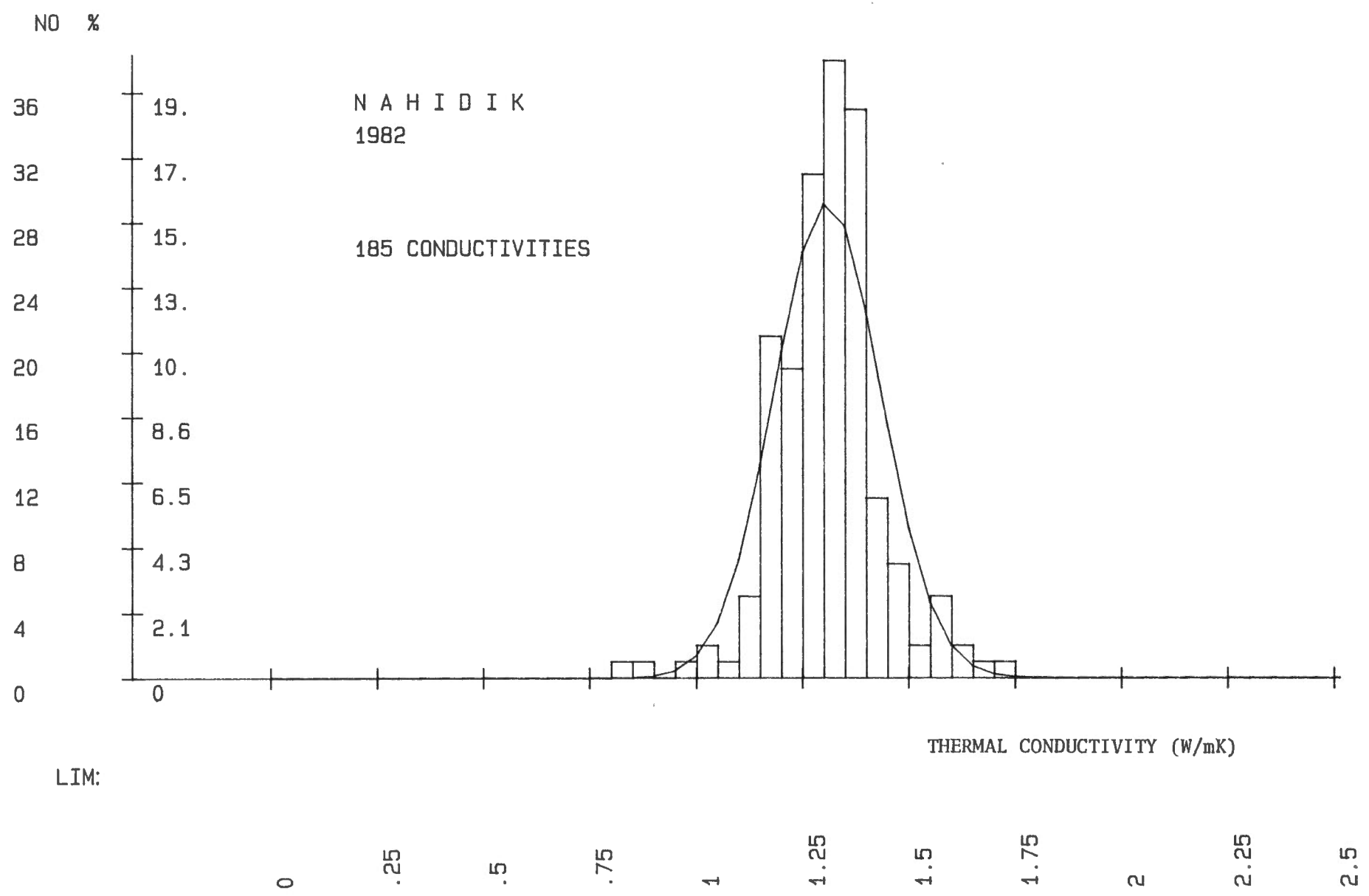
NO %
36
32
28
24
20
16
12
8
4
0
19.
17.
15.
13.
10.
8.6
6.5
4.3
2.1
0
N A H I D I K
1982
185 CONDUCTIVITIES
THERMAL CONDUCTIVITY (W/mK)
LIM:
0
.25
.5
.75
1
1.25
1.5
1.75
2
2.25
2.5

FIGURE 4.5

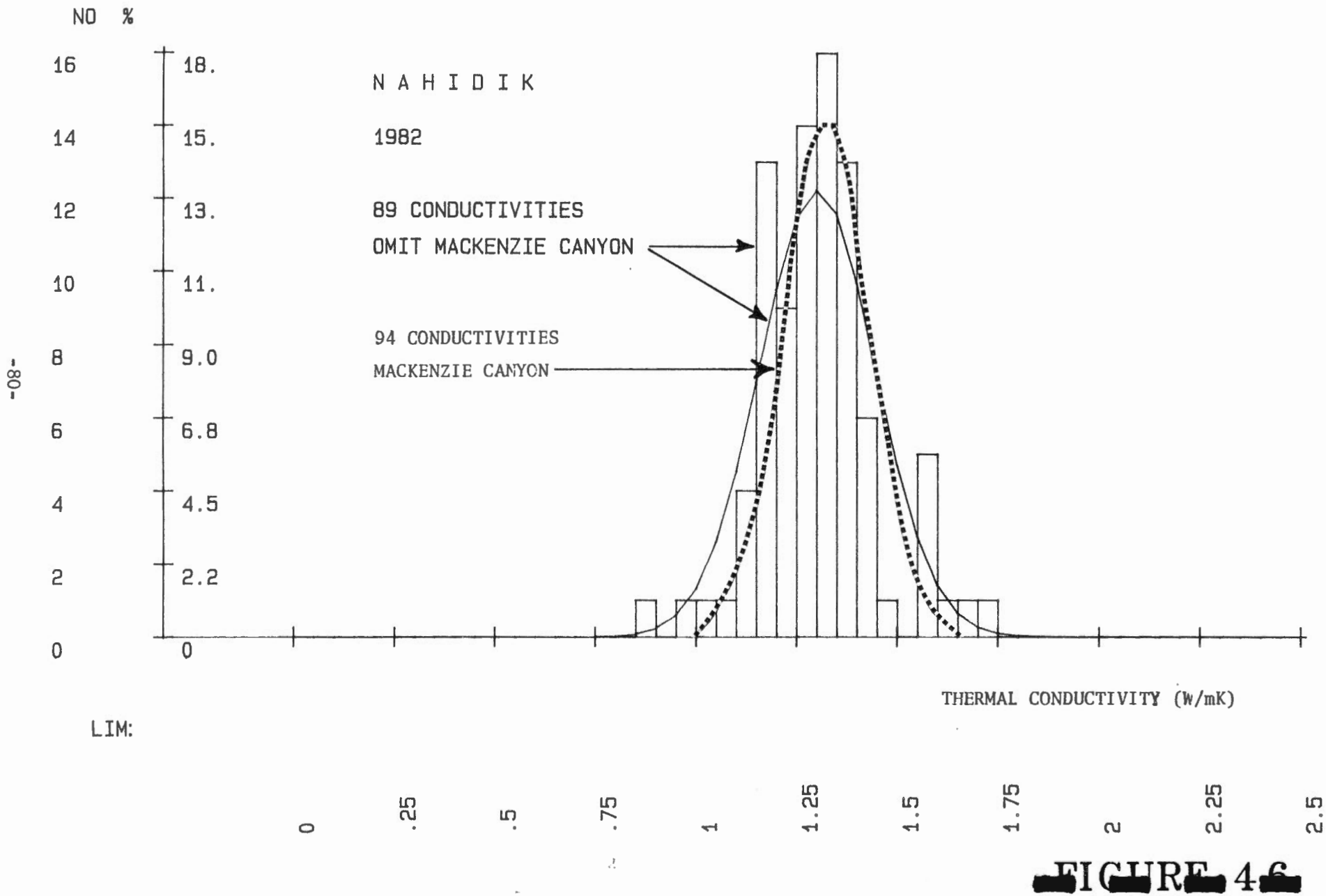
NO %
16
14
12
10
8
6
4
2
0
18.
15.
13.
11.
9.0
6.8
4.5
2.2
0
N A H I D I K
1982
89 CONDUCTIVITIES
OMIT MACKENZIE CANYON
94 CONDUCTIVITIES
MACKENZIE CANYON
THERMAL CONDUCTIVITY (W/mK)
LIM:
0
.25
.5
.75
1
1.25
1.5
1.75
2
2.25
2.5

FIGURE 46

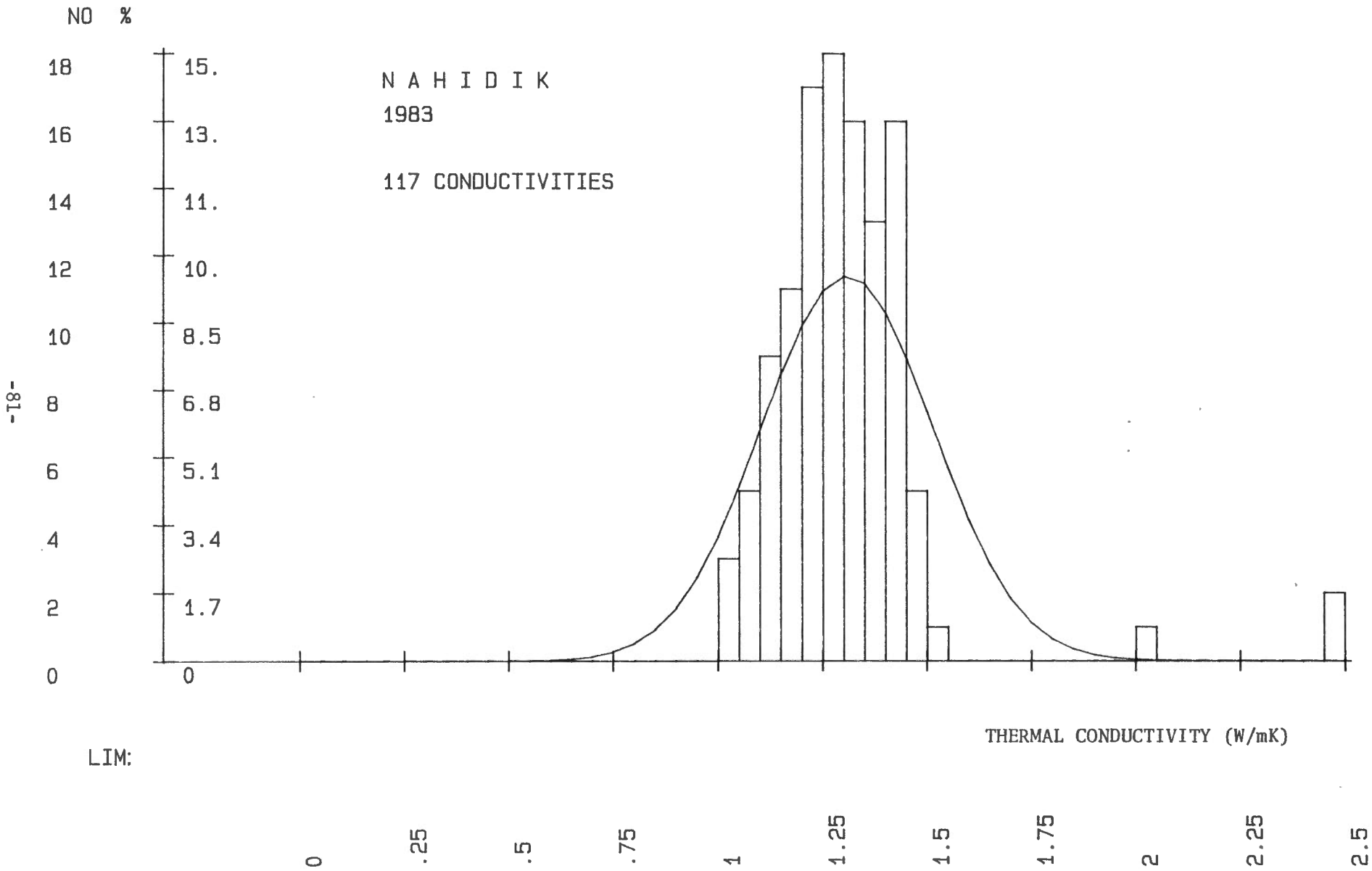
HEWLETT PACKARD
NO %
18
16
14
12
10
8
6
4
2
0
15.
13.
11.
10.
8.5
6.8
5.1
3.4
1.7
0
N A H I D I K
1983
117 CONDUCTIVITIES
THERMAL CONDUCTIVITY (W/mK)
LIM:
0
.25
.5
.75
1
1.25
1.5
1.75
2
2.25
2.5

FIGURE 4.7

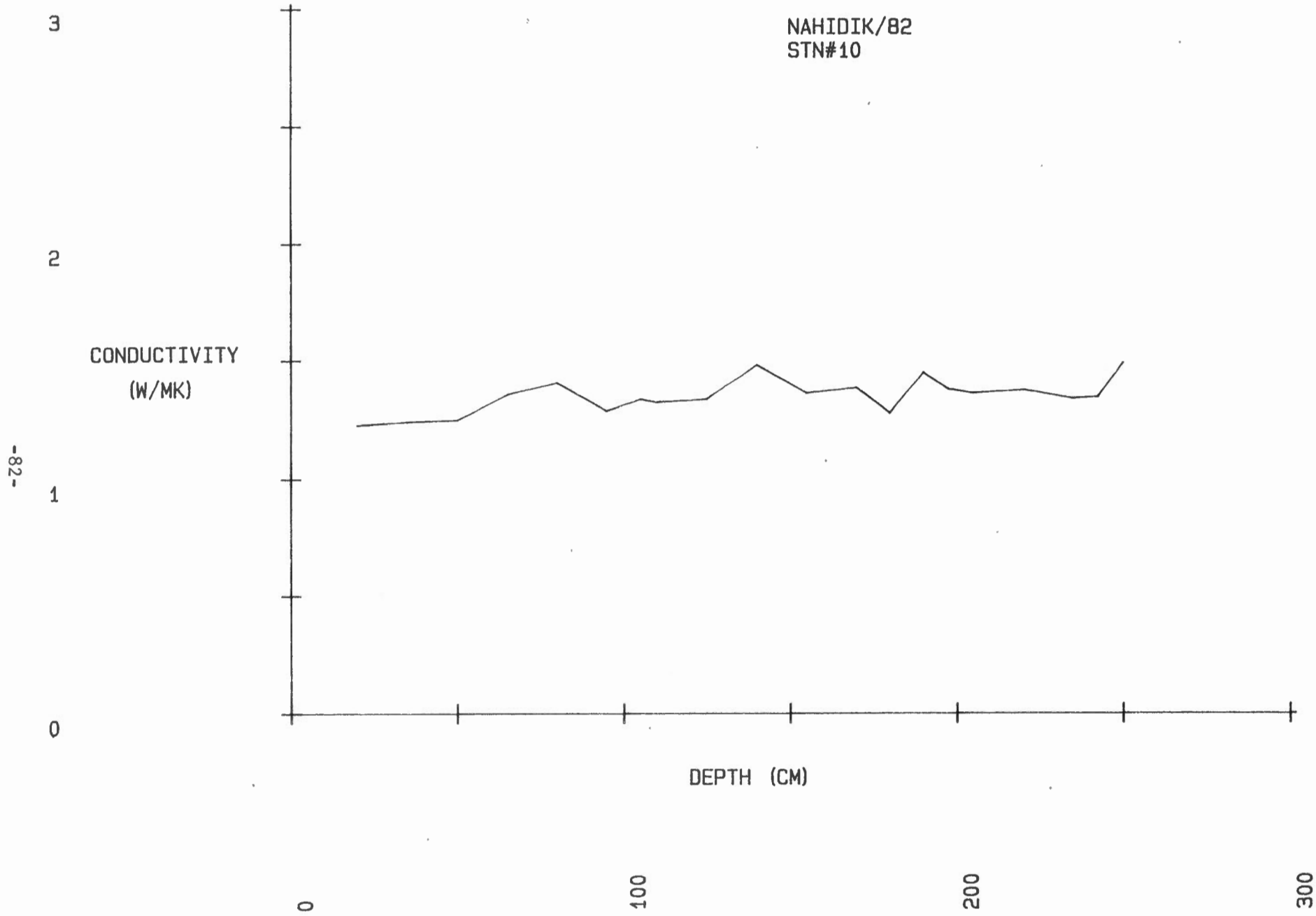
NAHIDIK/82
STN#10
CONDUCTIVITY
(W/MK)
3
2
1
0
DEPTH (CM)
0
100
200
300

FIGURE 4.8

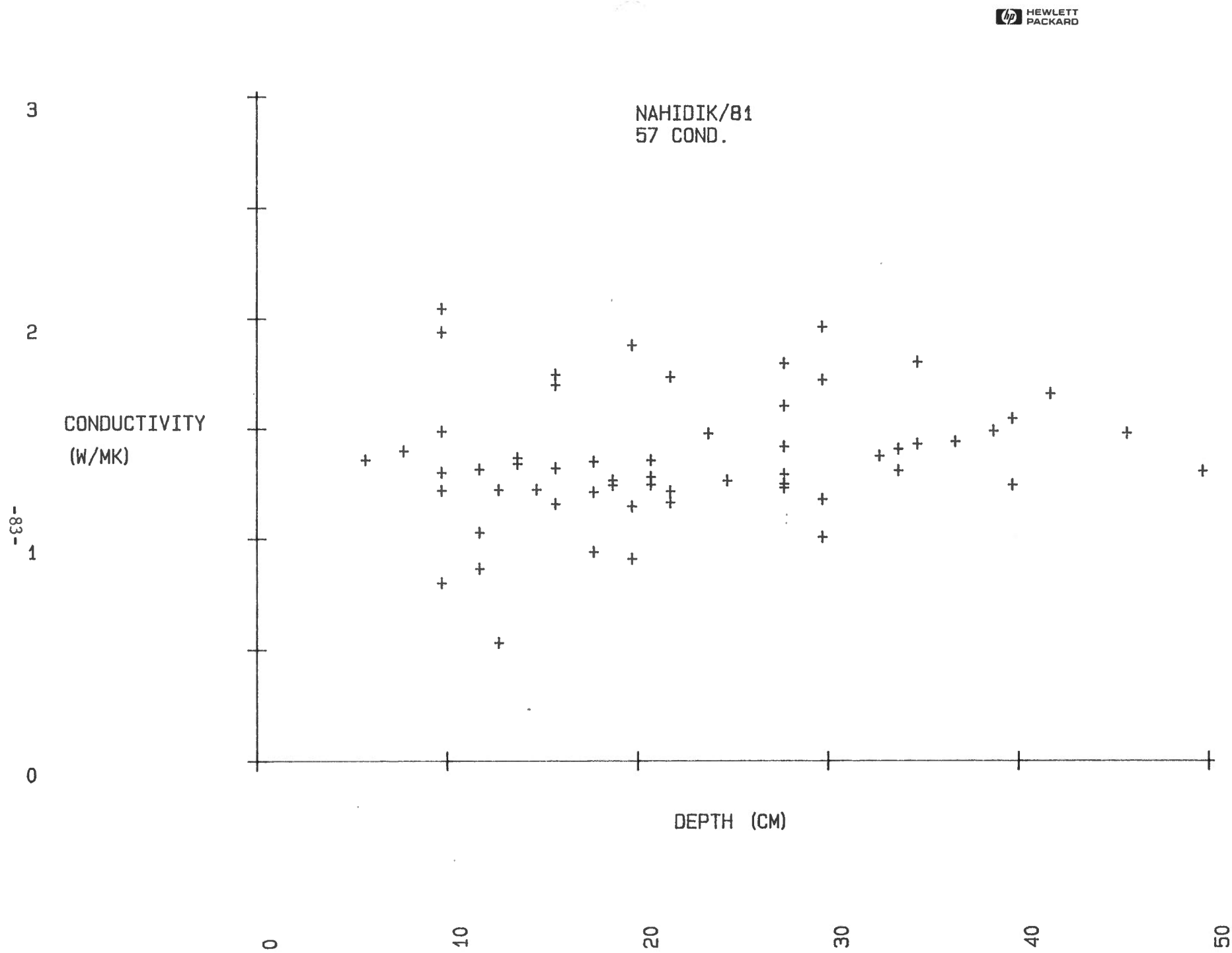
HEWLETT PACKARD
NAHIDIK/81
57 COND.
CONDUCTIVITY
(W/MK)
3
2
1
0
DEPTH (CM)
0
10
20
30
40
50

FIGURE 4.9

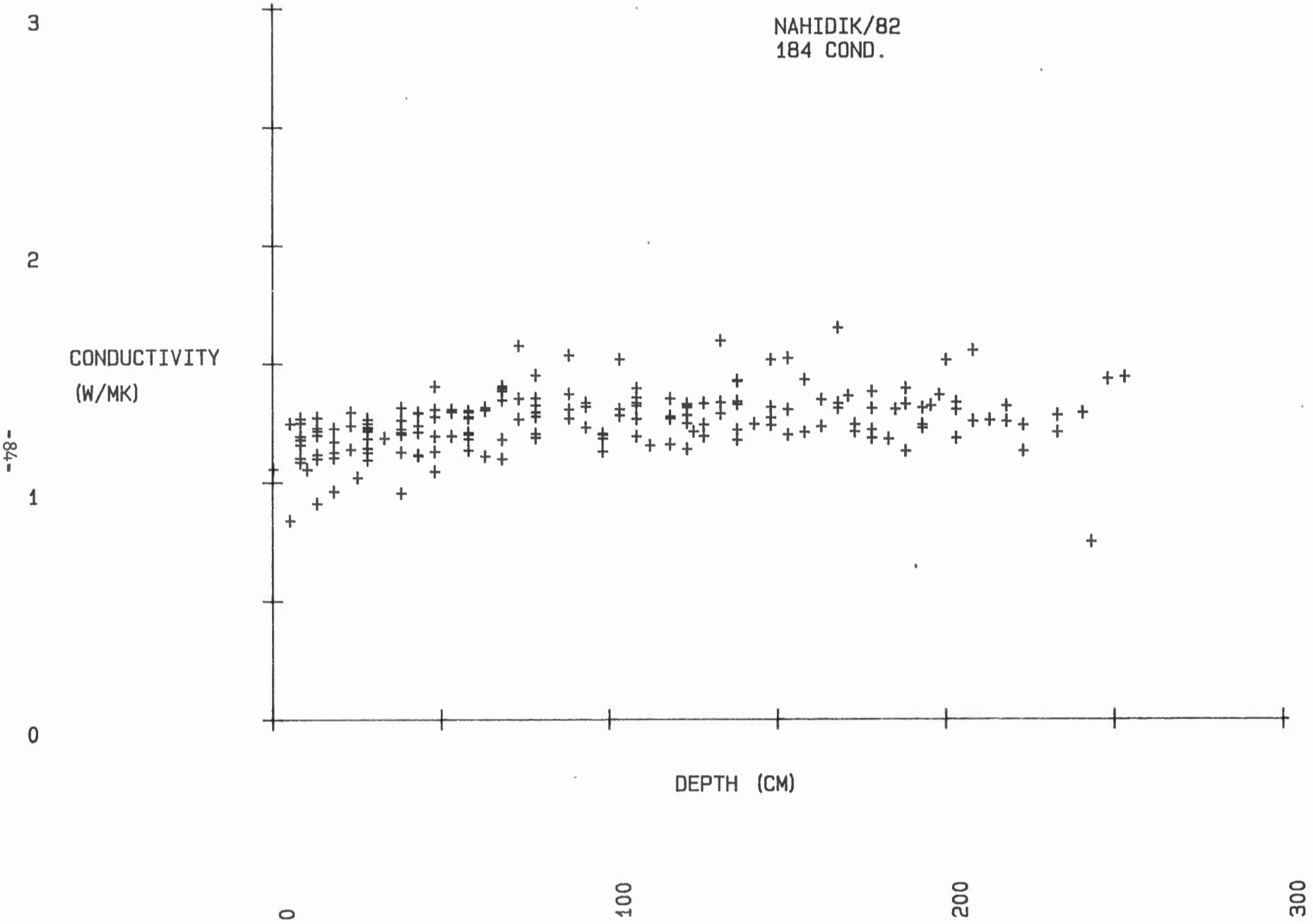
NAHIDIK/82
184 COND.
CONDUCTIVITY
(W/MK)
3
2
1
0
DEPTH (CM)
0
100
200
300

FIGURE 4.10

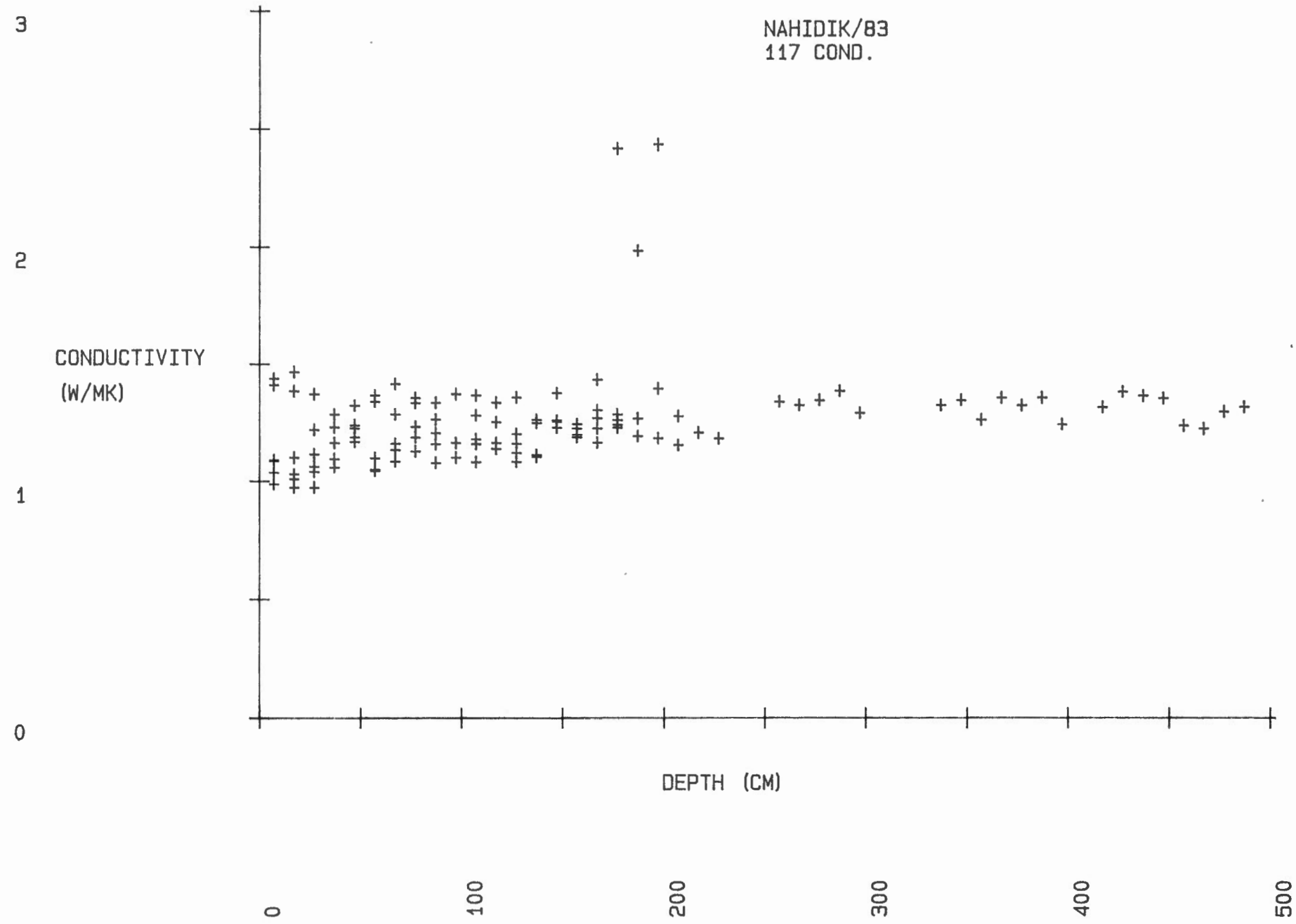
NAHIDIK/83
117 COND.
CONDUCTIVITY
(W/MK)
3
2
1
0
DEPTH (CM)
0
100
200
300
400
500

FIGURE 4.11

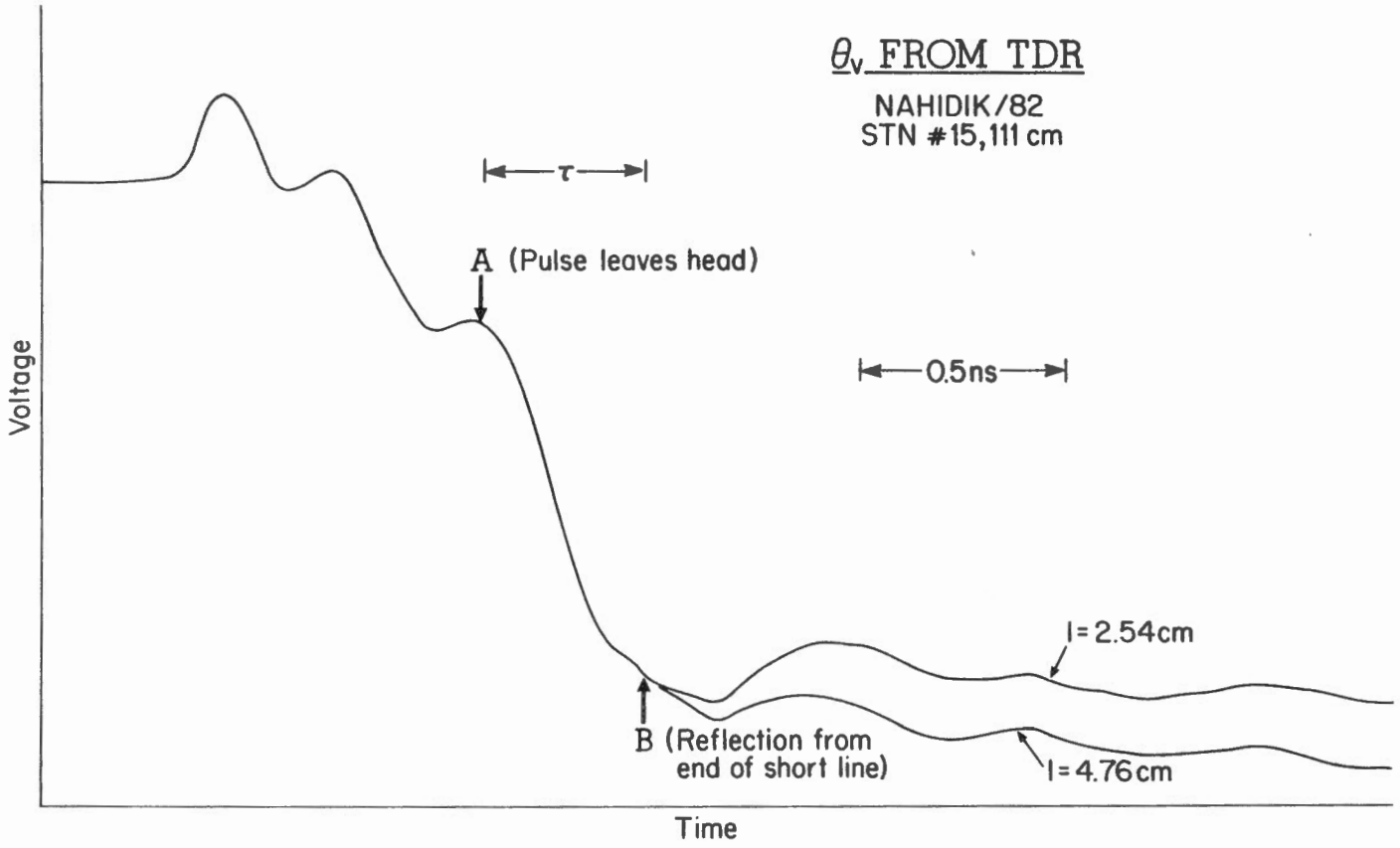
θ_v FROM TDR
NAHIDIK/82
STN #15,111 cm
τ
A (Pulse leaves head)
0.5ns
Voltage
l = 2.54cm
B (Reflection from end of short line)
l = 4.76cm
Time

FIGURE 5.1

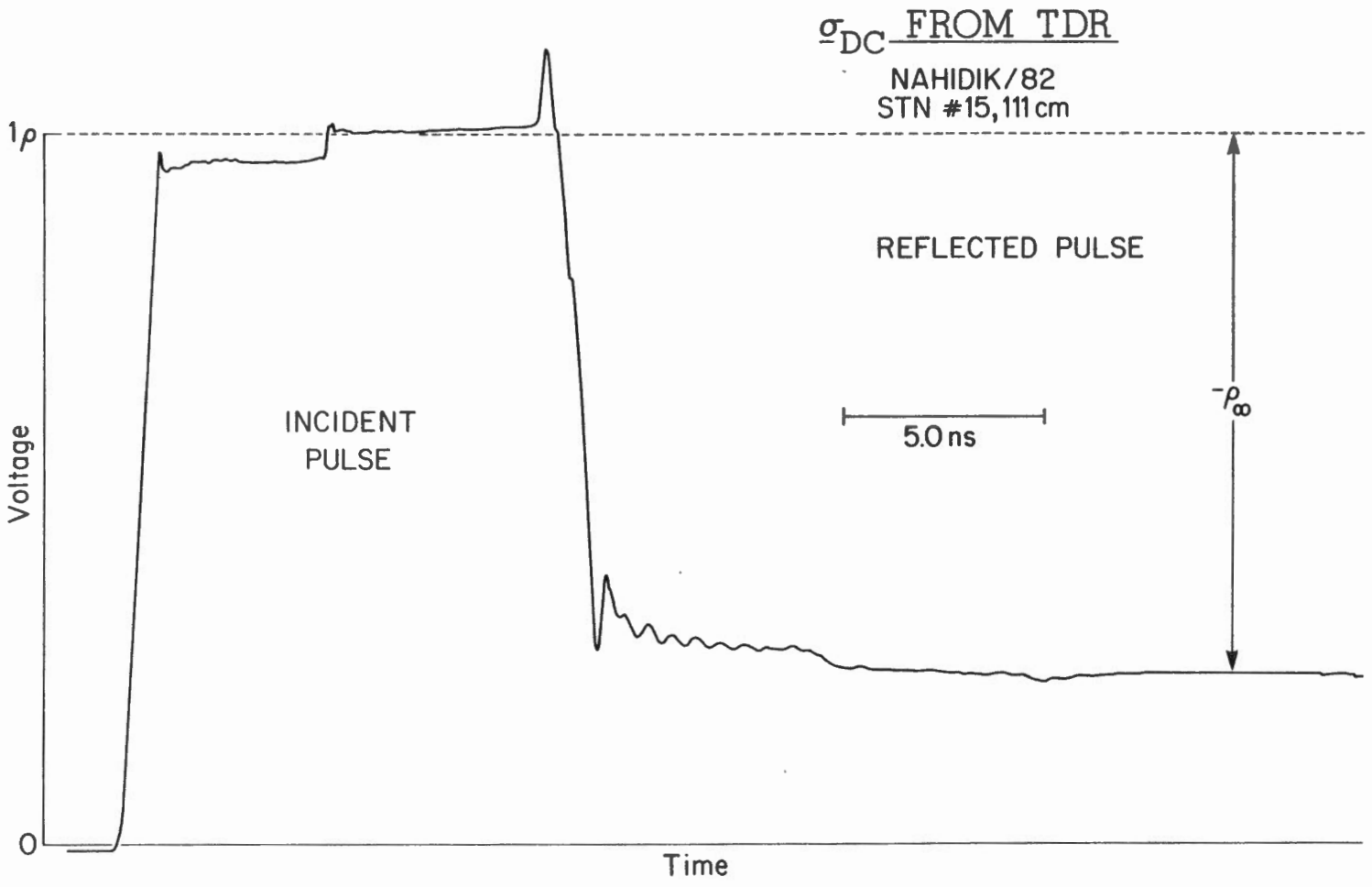
σ_{DC} FROM TDR
NAHIDIK/82
STN #15,111 cm
1ρ
0
Voltage
INCIDENT
PULSE
REFLECTED PULSE
5.0 ns
$-\rho_\infty$
Time

FIGURE 5.2

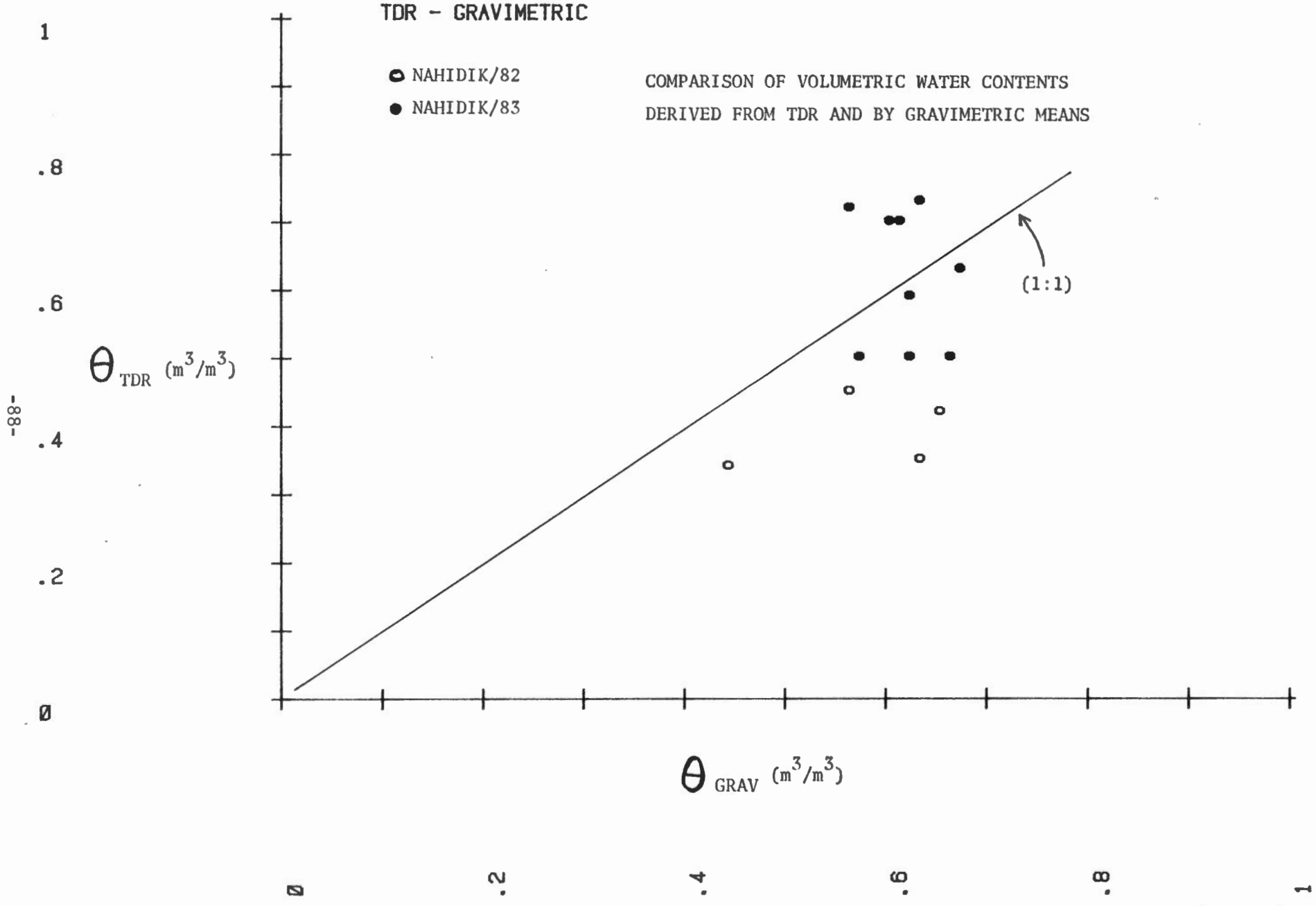
TDR - GRAVIMETRIC
NAHIDIK/82
NAHIDIK/83
COMPARISON OF VOLUMETRIC WATER CONTENTS
DERIVED FROM TDR AND BY GRAVIMETRIC MEANS
(1:1)
θ TDR (m3/m3)
θ GRAV (m3/m3)
1
.8
.6
.4
.2
Ø
Ø
.2
.4
.6
.8
1

FIGURE 5.3

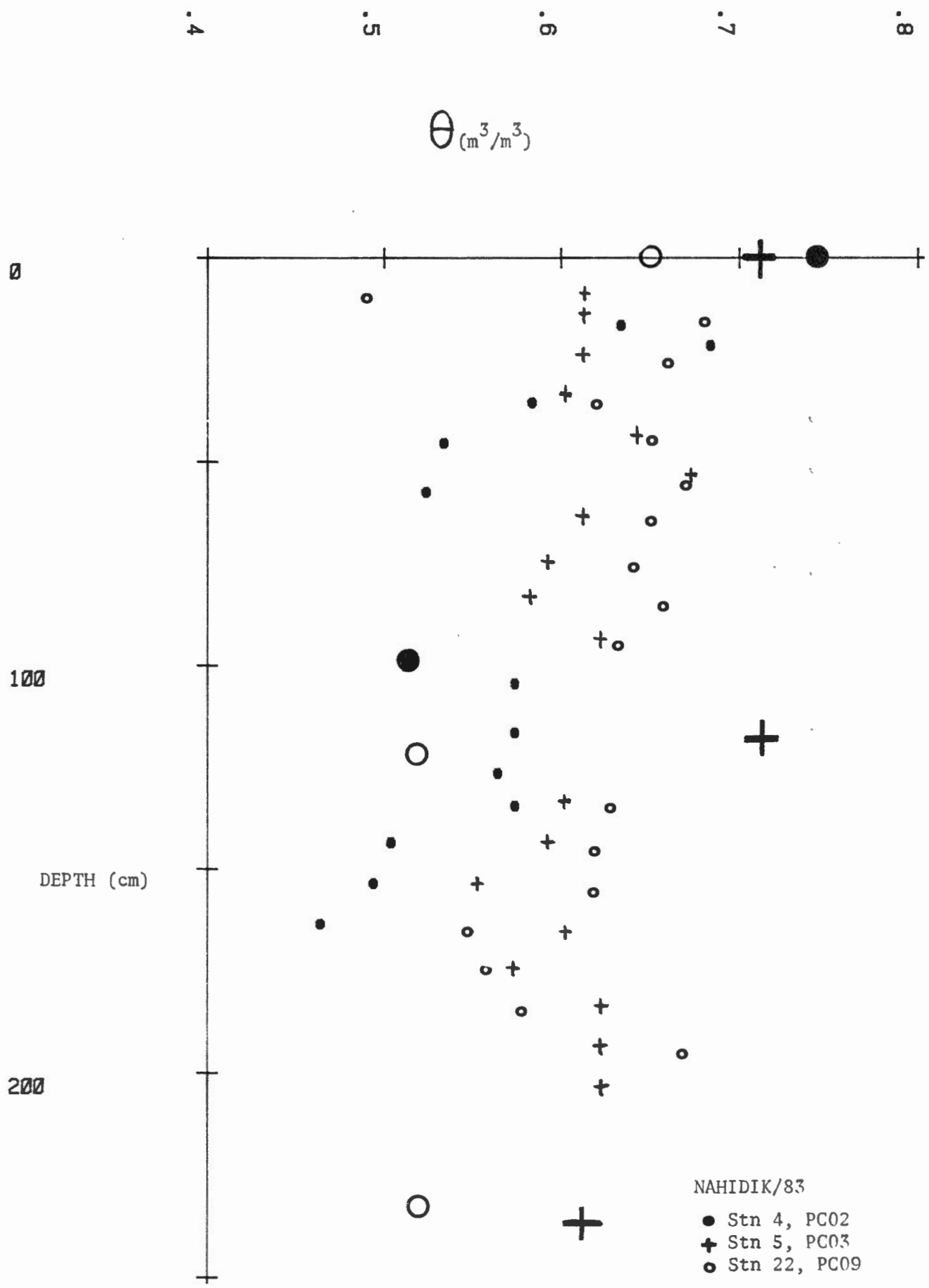
.4
.5
.6
.7
.8
θ (m³/m³)
0
100
200
DEPTH (cm)
NAHIDIK/83
Stn 4, PC02
Stn 5, PC03
Stn 22, PC09

FIGURE 5.4

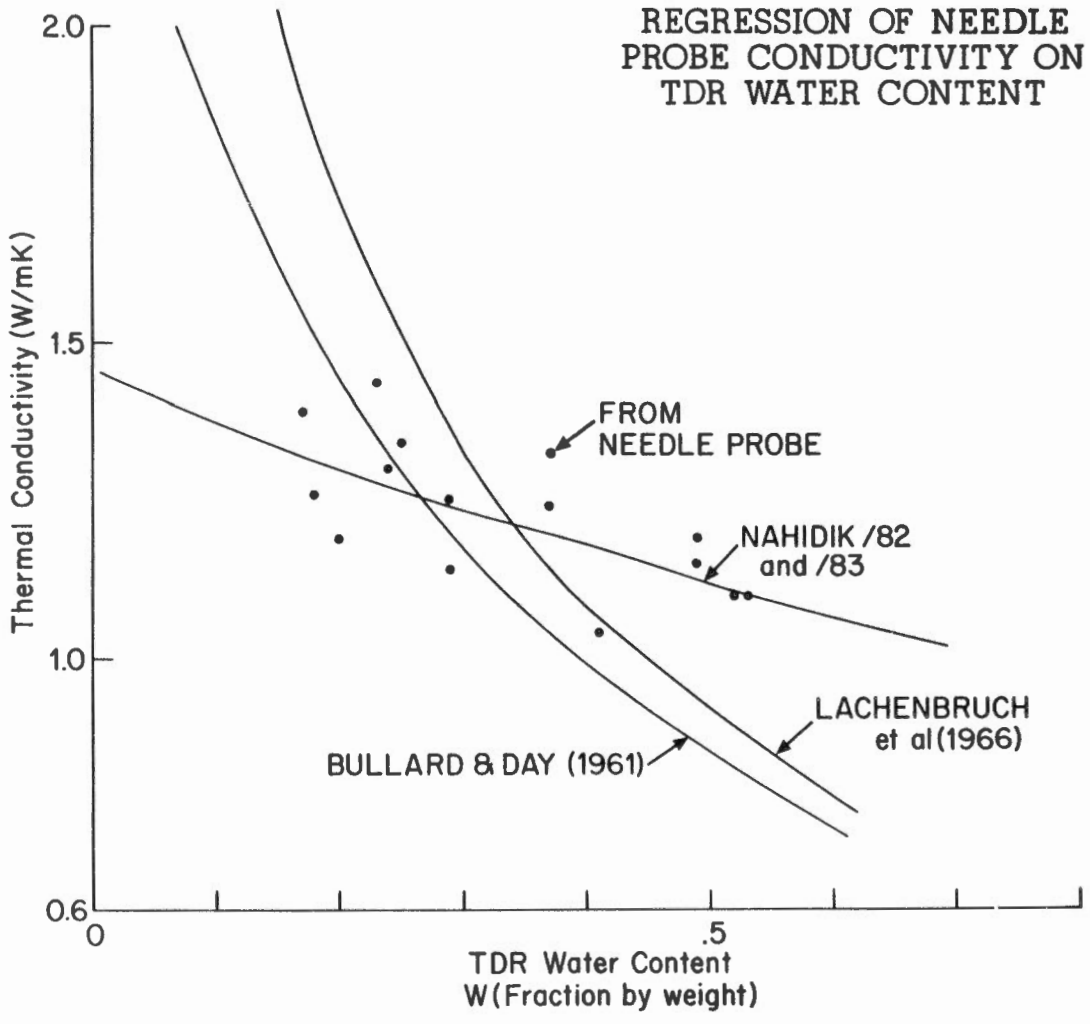
REGRESSION OF NEEDLE
PROBE CONDUCTIVITY ON
TDR WATER CONTENT
2.0
1.5
1.0
0.6
0
.5
Thermal Conductivity (W/mK)
TDR Water Content
W(Fraction by weight)
FROM
NEEDLE PROBE
NAHIDIK /82
and /83
LACHENBRUCH
et al(1966)
BULLARD & DAY (1961)

FIGURE 5.5

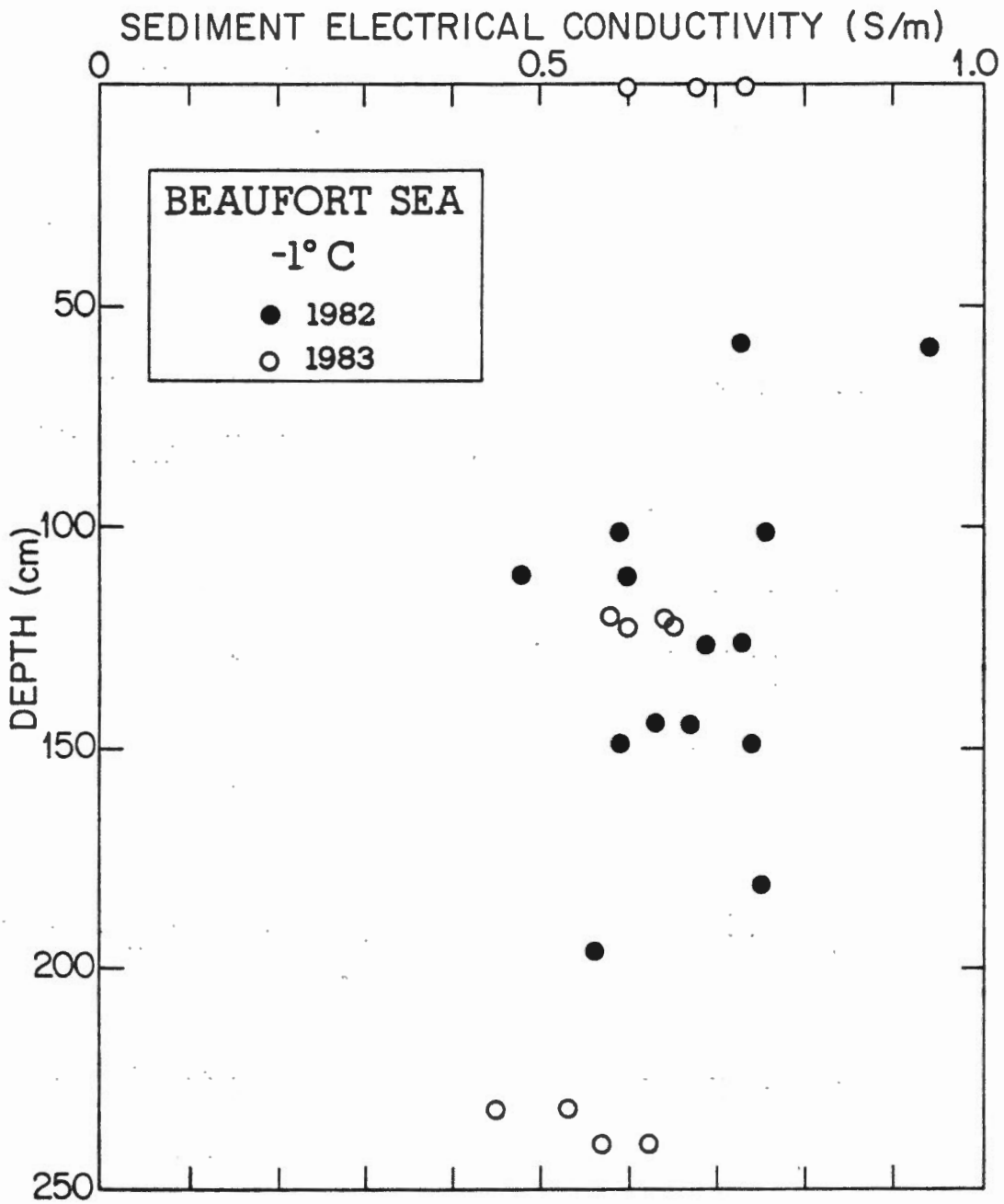
SEDIMENT ELECTRICAL CONDUCTIVITY (S/m)
0
0.5
1.0
BEAUFORT SEA
-1° C
1982
1983
DEPTH (cm)
50
100
150
200
250

FIGURE 5.6

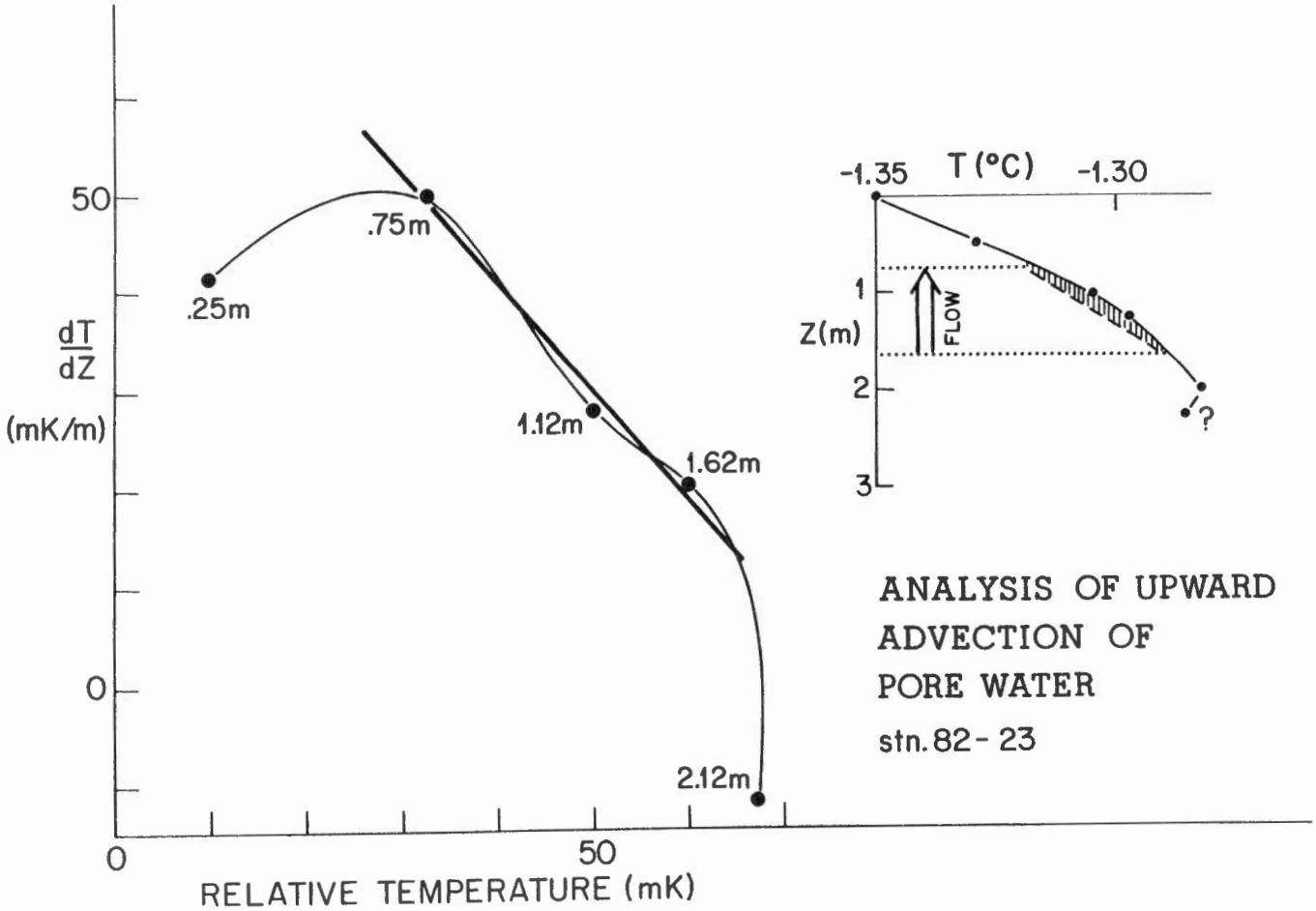
50
0
dT/dZ
(mK/m)
.25m
.75m
1.12m
1.62m
2.12m
0
50
RELATIVE TEMPERATURE (mK)
-1.35
T (°C)
-1.30
1
2
3
Z(m)
FLOW
?
ANALYSIS OF UPWARD
ADVECTION OF
PORE WATER
stn. 82 - 23

FIGURE 6.1

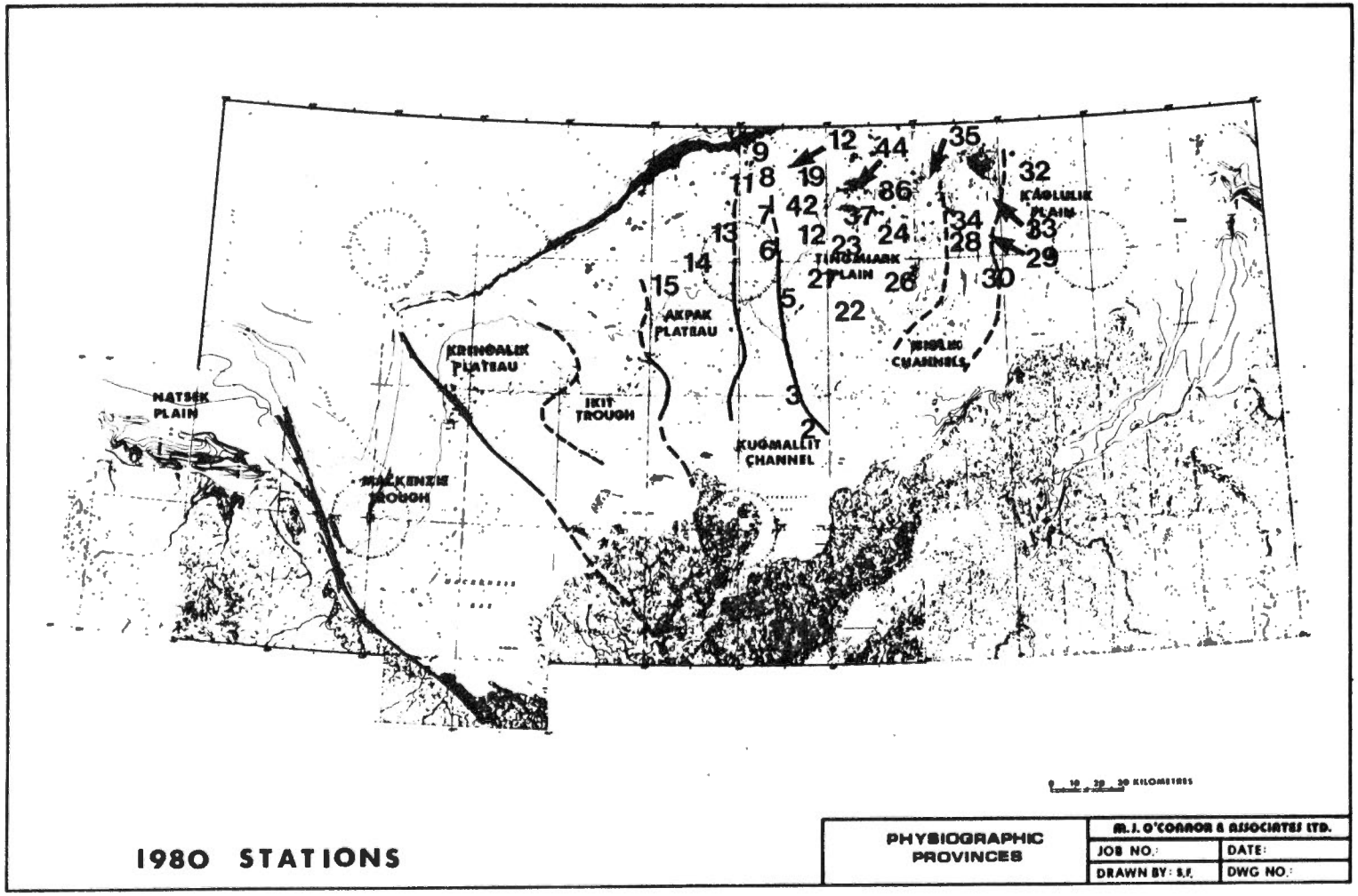
9
12
44
35
11
8
19
32
86
KÅGLULIK PLAIN
7
42
37
34
33
13
6
12
23
24
28
29
14
TUKTOYAKTUK PLAIN
27
26
30
15
5
22
AKPAK PLATEAU
KRINGALIK PLATEAU
NATSEK PLAIN
IKIT TROUGH
3
2
KUGMALLIT CHANNEL
MACKENZIE TROUGH
1980 STATIONS
PHYSIOGRAPHIC PROVINCES
M. J. O'CONNOR & ASSOCIATES LTD.
JOB NO.:
DATE:
DRAWN BY: S.F.
DWG NO.:

FIGURE 7.1

APPENDIX A

Gradiometer depth -

temperature profiles, 1981-83

The conversion from processor "bits" to temperature

is explained in the text, section 3.1.

NAHIDIK/81 STN#1

Z(M)	BITS	OFFSET	BITS(CORR)	T(C)
.10	163	0	163	-1.821
.50	149	0	149	-1.748
.90	135	0	135	-1.747
1.30	142	0	142	-1.942

NAHIDIK/81 STN#2

Z(M)	BITS	OFFSET	BITS(CORR)	T(C)
.70	172	0	172	-1.811
1.10	150	0	150	-1.766
1.50	182	0	182	-1.788
1.90	176	0	176	-1.711
2.30	166	0	166	-1.699
2.70	166	0	166	-1.888

NAHIDIK/81 STN#3

Z(M)	BITS	OFFSET	BITS(CORR)	T(C)
.40	431	0	431	-1.309
.80	285	0	285	-1.508
1.20	260	0	260	-1.652
1.60	238	0	238	-1.624
2.00	220	0	220	-1.614
2.40	208	0	208	-1.794

NAHIDIK/81 STN#4

Z(M)	BITS	OFFSET	BITS(CORR)	T(C)
.20	152	0	152	-1.744
.60	132	0	132	-1.751
1.00	145	0	145	-1.935

NAHIDIK/81 STN#6

Z(M)	BITS	OFFSET	BITS(CORR)	T(C)
.70	201	0	201	-1.755
1.10	167	0	167	-1.734
1.50	197	0	197	-1.762
1.90	194	0	194	-1.687
2.30	182	0	182	-1.674
2.70	177	0	177	-1.863

NAHIDIK/81 STN#7

Z(M)	BITS	OFFSET	BITS(CORR)	T(C)
.20	208	0	208	-1.667
.60	181	0	181	-1.675
1.00	184	0	184	-1.848

NAHIDIK/81 STN#8

Z(M)	BITS	OFFSET	BITS(CORR)	T(C)
.40	413	0	413	-1.343
.80	401	0	401	-1.291
1.20	426	0	426	-1.360
1.60	400	0	400	-1.381
2.00	297	0	297	-1.490
2.40	244	0	244	-1.714

NAHIDIK/81 STN#9

Z(M)	BITS	OFFSET	BITS(CORR)	T(C)
.40	167	20	187	-1.772
.80	164	24	188	-1.711
1.20	159	31	190	-1.663
1.60	158	29	187	-1.616
2.00	170	20	190	-1.651
2.40	187	0	187	-1.891

NAHIDIK/81 STN#11

Z(M)	BITS	OFFSET	BITS(CORR)	T(C)
.40	162	20	182	-1.782
.80	168	24	192	-1.704
1.20	163	31	194	-1.655
1.60	156	29	185	-1.619
2.00	165	20	185	-1.659
2.40	180	0	180	-1.906

NAHIDIK/81 STN#12

Z(M)	BITS	OFFSET	BITS(CORR)	T(C)
.40	223	20	243	-1.663
.80	210	24	234	-1.623
1.20	195	31	226	-1.588
1.60	195	29	224	-1.564
2.00	190	20	210	-1.620
2.40	199	0	199	-1.864

NAHIDIK/81 STN#13

Z(M)	BITS	OFFSET	BITS(CORR)	T(C)
.30	230	20	250	-1.649
.70	222	24	246	-1.600
1.10	207	31	238	-1.562
1.50	203	29	232	-1.553
1.90	206	20	226	-1.594
2.30	217	0	217	-1.824

NAHIDIK/81 STN#15

Z(M)	BITS	OFFSET	BITS(CORR)	T(C)
.70	151	20	171	-1.803
1.10	150	24	174	-1.738
1.50	148	31	179	-1.686
1.90	151	29	180	-1.626
2.30	162	20	182	-1.664
2.70	188	0	188	-1.889

NAHIDIK/81 STN#16

Z(M)	BITS	OFFSET	BITS(CORR)	T(C)
.30	437	24	461	-1.195
.70	365	31	396	-1.199
1.10	292	29	321	-1.423
1.50	260	20	280	-1.508
1.90	251	0	251	-1.749

NAHIDIK/81 STN#17

Z(M)	BITS	OFFSET	BITS(CORR)	T(C)
0.00	320	31	351	-1.307
.40	370	29	399	-1.303
.60	414	20	434	-1.252
1.00	405	0	405	-1.416

NAHIDIK/82 STN#5

Z(M)	BITS	OFFSET	BITS(CORR)	T(C)
1.10	483	-17	466	-1.307
1.60	473	-47	426	-1.432
2.10	425	-17	408	-1.488
2.60	430	-27	403	-1.503
2.85	425	-21	404	-1.500
3.60	420	-16	404	-1.500
3.85	402	0	402	-1.507

NAHIDIK/82 STN#6

Z(M)	BITS	OFFSET	BITS(CORR)	T(C)
.25	441	-17	424	-1.438
.75	455	-47	408	-1.488
1.25	416	-17	399	-1.516
1.75	423	-27	396	-1.525
2.00	418	-21	397	-1.522
2.75	414	-16	398	-1.519
3.00	402	0	402	-1.507

NAHIDIK/82 STN#8

Z(M)	BITS	OFFSET	BITS(CORR)	T(C)
.77	494	-17	477	-1.272
1.27	529	-47	482	-1.257
1.77	496	-17	479	-1.266
2.02	498	-27	471	-1.291
2.27	491	-21	470	-1.294
3.02	477	-16	461	-1.322
3.27	459	0	459	-1.329

NAHIDIK/82 STN#9

Z(M)	BITS	OFFSET	BITS(CORR)	T(C)
.77	539	-17	522	-1.132
1.27	563	-47	516	-1.151
1.77	513	-17	496	-1.213
2.02	511	-27	484	-1.251
2.27	499	-21	478	-1.269
3.02	491	-16	475	-1.279
3.27	475	0	475	-1.279

NAHIDIK/82 STN#10

Z(M)	BITS	OFFSET	BITS(CORR)	T(C)
.77	568	-17	551	-1.042
1.27	597	-47	550	-1.045
1.77	538	-17	521	-1.135
2.02	522	-27	495	-1.216
2.27	503	-21	482	-1.257
3.02	482	-16	466	-1.307
3.27	457	0	457	-1.335

NAHIDIK/82 STN#11

Z(M)	BITS	OFFSET	BITS(CORR)	T(C)
.77	819	-17	802	-.263
1.27	806	-47	759	-.396
1.77	686	-17	669	-.675
2.02	614	-27	587	-.930
2.27	579	-21	558	-1.020
3.02	518	-16	502	-1.194
3.27	498	0	498	-1.207

NAHIDIK/82 STN#12

Z(M)	BITS	OFFSET	BITS(CORR)	T(C)
.77	732	-17	715	-.532
1.27	696	-47	649	-.737
1.77	589	-17	572	-.976
2.02	551	-27	524	-1.126
2.27	524	-21	503	-1.191
3.02	505	-16	489	-1.235
3.27	485	0	485	-1.247

NAHIDIK/82 STN#13

Z(M)	BITS	OFFSET	BITS(CORR)	T(C)
.20	492	-17	475	-1.279
.70	527	-47	480	-1.263
1.20	496	-17	479	-1.266
1.70	502	-27	475	-1.279
1.95	495	-21	474	-1.282
2.70	489	-16	473	-1.285
2.95	471	0	471	-1.291

NAHIDIK/82 STN#15

Z(M)	BITS	OFFSET	BITS(CORR)	T(C)
0.00	735	-47	688	-.616
.50	625	-17	608	-.865
1.00	573	-27	546	-1.057
1.25	548	-21	527	-1.117
2.00	510	-16	494	-1.219
2.25	491	0	491	-1.229

NAHIDIK/82 STN#23

Z(M)	BITS	OFFSET	BITS(CORR)	T(C)
0.00	499	-47	452	-1.350
.50	476	-17	459	-1.329
1.00	494	-27	467	-1.304
1.25	490	-21	469	-1.297
2.00	490	-16	474	-1.282
2.25	473	0	473	-1.285

NAHIDIK/82 STN#26

Z(M)	BITS	OFFSET	BITS(CORR)	T(C)
0.00	596	-47	549	-1.048
.50	501	-17	484	-1.251
1.00	489	-27	462	-1.319
1.25	474	-21	453	-1.347
2.00	450	-16	434	-1.407
2.25	425	0	425	-1.435

NAHIDIK/82 STN#28

Z(M)	BITS	OFFSET	BITS(CORR)	T(C)
.20	508	-17	491	-1.229
.70	515	-47	468	-1.300
1.20	452	-17	435	-1.403
1.70	450	-27	423	-1.441
1.95	439	-21	418	-1.457
2.70	431	-16	415	-1.466
2.95	411	0	411	-1.478

NAHIDIK/82 STN#29

Z(M)	BITS	OFFSET	BITS(CORR)	T(C)
.77	516	-17	499	-1.204
1.27	517	-47	470	-1.294
1.77	453	-17	436	-1.400
2.02	441	-27	414	-1.469
2.27	429	-21	408	-1.488
3.02	421	-16	405	-1.497
3.27	403	0	403	-1.503

NAHIDIK/83 STN#3

Z(M)	BITS	OFFSET	BITS(CORR)	T(C)
.20	443	10	453	-1.423
.70	431	5	436	-1.475
1.20	431	-3	428	-1.500
1.45	408	24	432	-1.488
1.70	419	1	420	-1.525
1.95	423	12	435	-1.478
2.20	454	-13	441	-1.460
2.45	628	-167	461	-1.398
2.70	423	0	423	-1.516

NAHIDIK/83 STN#4

Z(M)	BITS	OFFSET	BITS(CORR)	T(C)
.60	441	10	451	-1.429
1.10	435	5	440	-1.463
1.60	443	-3	440	-1.463
1.85	424	24	448	-1.438
2.10	375	1	376	-1.661
2.35	433	12	445	-1.447
2.60	458	-13	445	-1.447
2.85	633	-167	466	-1.382
3.10	431	0	431	-1.491

NAHIDIK/83 STN#5

Z(M)	BITS	OFFSET	BITS(CORR)	T(C)
.70	440	10	450	-1.432
1.20	451	5	456	-1.413
1.70	470	-3	467	-1.379
1.95	455	24	479	-1.342
2.20	462	1	463	-1.392
2.45	477	12	489	-1.311
2.70	512	-13	499	-1.280
2.95	683	-167	516	-1.227
3.20	493	0	493	-1.299

NAHIDIK/83 STN#22

Z(M)	BITS	OFFSET	BITS(CORR)	T(C)
1.00	400	10	410	-1.556
1.50	403	5	408	-1.562
2.00	414	-3	411	-1.553
2.25	388	24	412	-1.550
2.50	417	1	418	-1.531
2.75	407	12	419	-1.528
3.00	437	-13	424	-1.512
3.25	577	-167	410	-1.556
3.50	415	0	415	-1.540

NAHIDIK/83 STN#23

Z(M)	BITS	OFFSET	BITS(CORR)	T(C)
.70	411	10	421	-1.522
1.20	403	5	408	-1.562
1.70	407	-3	404	-1.574
1.95	381	24	405	-1.571
2.20	408	1	409	-1.559
2.45	396	12	408	-1.562
2.70	429	-13	416	-1.537
2.95	564	-167	397	-1.596
3.20	404	0	404	-1.574

NAHIDIK/83 STN#25

Z(M)	BITS	OFFSET	BITS(CORR)	T(C)
.50	447	10	457	-1.410
1.00	474	5	479	-1.342
1.50	502	-3	499	-1.280
1.75	499	24	523	-1.206
2.00	530	1	531	-1.181
2.25	527	12	539	-1.156
2.50	562	-13	549	-1.125
2.75	724	-167	557	-1.100
3.00	558	0	558	-1.097

APPENDIX B

Temperature gradients over
selected intervals

NAHIDIK/81

****

	Z	DT/DZ (MK/M)	+ -	T(Z=0) (C)
8101	NAHIDIK/81 -1			
	.10 M - .50 M	200.0	.0	-1.84
	.10 M - .90 M	100.0	33.3	
8102	NAHIDIK/81 -2			
	.70 M -1.10 M	125.0	.0	-1.90
	.70 M -1.50 M	37.5	29.2	
8103	NAHIDIK/81 -3			
	.40 M -1.20 M	-437.5	20.8	-1.13
	.40 M -1.20 M	-437.5	20.8	
8104	NAHIDIK/81 -4			
	.20 M - .60 M	-25.0	.0	-1.74
	.20 M -1.00 M	-237.5	70.8	
8106	NAHIDIK/81 -6			
	.70 M -1.10 M	50.0	.0	-1.79
	.70 M -1.50 M	-12.5	20.8	
8107	NAHIDIK/81 -7			
	.20 M - .60 M	-25.0	.0	-1.66
	.20 M -1.00 M	-225.0	66.7	
8108	NAHIDIK/81 -8			
	.40 M - .80 M	125.0	.0	-1.39
	.40 M -1.60 M	-47.5	28.9	

8109	NAHIDIK/81 -9			
	.40 M -1.20 M	112.5	12.5	-1.85
	.40 M -1.60 M	127.5	9.2	
8111	NAHIDIK/81 -11			
	.40 M -1.20 M	137.5	20.8	-1.87
	.40 M -1.60 M	135.0	11.5	
8112	NAHIDIK/81 -12			
	.40 M -1.20 M	62.5	12.5	-1.72
	.40 M -1.60 M	77.5	9.2	
8113	NAHIDIK/81 -13			
	.30 M -1.10 M	75.0	8.3	-1.70
	.30 M -1.50 M	72.5	4.7	
8115	NAHIDIK/81 -15			
	.70 M -1.50 M	125.0	8.3	-1.92
	.70 M -1.90 M	145.0	9.4	
8116	NAHIDIK/81 -16			
	.30 M - .70 M	-100.0	.0	-1.20
	.30 M -1.50 M	-272.5	34.8	
8117	NAHIDIK/81 -17			
	.00 M - .60 M	139.3	32.1	-1.38
	.00 M - .60 M	139.3	32.1	

NAHIDIK/82

****

	Z	DT/DZ (MK/M)	+ -	T(Z=0) (C)
8205	NAHIDIK/82 -5			
	1.10 M -1.60 M	-260.0	.0	-1.01
	2.10 M -3.85 M	-8.7	4.0	
8206	NAHIDIK/82 -6			
	.25 M -1.25 M	-80.0	6.7	-1.41
	1.25 M -3.00 M	6.7	4.2	
8208	NAHIDIK/82 -8			
	.77 M -1.77 M	10.0	10.0	-1.27
	1.77 M -3.27 M	-36.7	5.6	
8209	NAHIDIK/82 -9			
	.77 M -1.77 M	-80.0	13.3	-1.06
	2.02 M -3.27 M	-15.3	2.5	
8210	NAHIDIK/82 -10			
	.77 M -1.77 M	-90.0	30.0	-.96
	2.02 M -3.27 M	-88.2	6.9	
8211	NAHIDIK/82 -11			
	.77 M -1.77 M	-410.0	50.0	.08
	2.02 M -3.27 M	-224.7	21.8	
8212	NAHIDIK/82 -12			
	.77 M -1.77 M	-440.0	13.3	-.18
	2.02 M -3.27 M	-84.7	17.3	
8213	NAHIDIK/82 -13			
	.20 M -1.20 M	10.0	3.3	-1.27
	1.20 M -2.95 M	-13.7	3.2	

8215	NAHIDIK/82 -15				
	.00 M	-1.25 M	-403.4	23.7	-.63
	1.25 M	-2.25 M	-115.4	10.8	
8223	NAHIDIK/82 -23				
	.00 M	-1.00 M	50.0	3.3	-1.35
	.00 M	-2.25 M	29.9	4.3	
8226	NAHIDIK/82 -26				
	.00 M	-1.00 M	-270.0	50.0	-1.07
	1.00 M	-2.25 M	-91.8	3.5	
8228	NAHIDIK/82 -28				
	.20 M	-1.20 M	-180.0	6.7	-1.18
	1.20 M	-2.95 M	-34.7	6.4	
8229	NAHIDIK/82 -29				
	.77 M	-1.77 M	-200.0	6.7	-1.04
	1.77 M	-3.27 M	-51.6	14.9	

NAHIDIK/83

****

	Z	DT/DZ (MK/M)	+ -	T(Z=0) (C)
8303	NAHIDIK/83 -3			
	.20 M -1.45 M	-53.6	15.0	-1.42
	1.70 M -2.45 M	164.0	14.7	
	2.45 M -2.70 M	-480.0	.0	
8304	NAHIDIK/83 -4			
	.60 M -1.85 M	-11.5	17.7	-1.43
	2.10 M -2.85 M	336.0	90.9	
	2.85 M -3.10 M	-440.0	.0	
8305	NAHIDIK/83 -5			
	.70 M -1.95 M	71.2	7.4	-1.49
	2.20 M -2.95 M	216.0	18.3	
	2.95 M -3.20 M	-280.0	.0	
8322	NAHIDIK/83 -22			
	1.00 M -1.50 M	-20.0	.0	-1.53
	1.00 M -3.00 M	22.5	4.5	
	2.50 M -3.00 M	40.0	.0	
8323	NAHIDIK/83 -23			
	.70 M -1.20 M	-80.0	.0	-1.46
	1.70 M -2.45 M	20.0	11.0	
	2.70 M -3.20 M	-80.0	53.3	
8325	NAHIDIK/83 -25			
	.50 M -1.50 M	130.0	3.3	-1.47
	.50 M -3.00 M	136.7	7.5	
	1.75 M -3.00 M	97.1	7.4	

APPENDIX C

Thermal conductivity data file giving:

station

depth (cm)

k (W/mK)

R, correlation coefficient

ambient temperature of measurement (°C)

DT, temperature rise over measurement internal (K)

T1, T2, measurement interval in seconds from beginning of heating

P, heating power (W)

L, length of needle probe in sample (mm)

NEEDLE PROBE CONDUCTIVITY FOR FILE NAHIDIKCN1

STN	DEPTH (CM)	K (W/M.K)	R	AMBIENT (C)	DT (K)	T1 (S)	T2 (S)	P (W)	L (MM)	RECORD
NR1	13	1.28	1.00000	22.83	0.28	205	345	0.53	60.0	1
	19	1.30	0.99999	22.38	0.28	205	345	0.53	60.0	2
	25	1.32	0.99999	23.22	0.27	205	345	0.52	60.0	3
NR2	10	1.27	0.99999	23.46	0.29	205	345	0.53	60.0	4
	16	1.21	0.99999	23.06	0.30	205	345	0.53	60.0	5
	22	1.22	0.99999	24.17	0.30	205	345	0.52	60.0	6
	28	1.29	1.00000	22.77	0.28	205	345	0.53	60.0	7
	34	1.36	0.99998	22.95	0.27	205	345	0.53	60.0	8
NR3	16	1.38	0.99983	23.74	0.26	205	345	0.52	60.0	9
	22	1.27	0.99999	23.38	0.29	205	345	0.53	60.0	10
	28	1.35	0.99999	24.42	0.27	205	345	0.52	60.0	11
	34	1.46	1.00000	23.00	0.25	205	345	0.53	60.0	12
	40	1.60	0.99998	23.29	0.23	205	345	0.53	60.0	13
NR 4	10	1.54	0.99999	23.08	0.24	205	345	0.53	60.0	14
	16	1.75	0.99990	23.65	0.21	205	345	0.53	60.0	15
NR5	13	.59	0.99969	22.74	0.61	215	355	0.54	60.0	16
	20	1.20	1.00000	22.77	0.30	215	355	0.53	60.0	17
	30	1.23	1.00000	23.79	0.28	215	355	0.53	60.0	18
	40	1.30	0.99984	22.55	0.28	215	355	0.53	60.0	19
	50	1.36	0.99997	22.89	0.26	215	355	0.53	60.0	20
NR6	10	1.99	0.99991	23.16	0.18	205	345	0.53	60.0	21
	20	1.93	0.99995	22.80	0.19	205	345	0.53	60.0	22
	30	2.02	0.99998	23.78	0.18	205	345	0.53	60.0	23
NR7	6	1.41	0.99996	20.97	0.25	215	355	0.53	60.0	24
	12	1.37	0.99995	20.45	0.26	215	355	0.53	60.0	25
	18	1.41	0.99994	21.46	0.25	215	355	0.52	60.0	26
	24	1.53	0.99994	20.27	0.23	215	355	0.53	60.0	27
	30	1.78	0.99991	20.53	0.20	215	355	0.53	60.0	28
NR9	15	1.28	1.00000	23.31	0.28	205	345	0.52	60.0	29
	21	1.30	1.00000	22.98	0.28	205	345	0.53	60.0	30
	28	1.30	0.99999	24.06	0.27	205	345	0.52	60.0	1
	33	1.43	0.99998	22.68	0.25	205	345	0.53	60.0	32
	39	1.54	0.99995	22.89	0.24	205	345	0.53	60.0	33
NR10	12	1.08	0.99996	22.87	0.34	205	345	0.53	60.0	4
	18	1.27	1.00000	23.43	0.29	205	345	0.53	60.0	5
NR11	10	1.35	0.99996	23.20	0.27	205	345	0.52	60.0	36
	19	1.32	0.99998	22.96	0.28	205	345	0.53	60.0	37
	28	1.66	0.99998	24.00	0.22	205	345	0.52	60.0	8
	37	1.50	0.99997	22.64	0.24	205	345	0.53	60.0	39
	46	1.54	0.99996	22.71	0.24	205	345	0.52	60.0	40
NR12	10	.85	0.83056	21.97	0.26	205	345	0.53	60.0	1
	20	.96	0.87207	22.10	0.25	205	345	0.53	60.0	2
	30	1.06	0.89869	23.32	0.23	205	345	0.53	60.0	43
NR13	8	1.45	0.99998	23.18	0.25	205	345	0.52	60.0	44
	14	1.42	0.99998	22.86	0.26	205	345	0.52	60.0	5
	21	1.34	0.99999	23.86	0.27	205	345	0.52	60.0	46
	28	1.47	0.99998	22.60	0.25	205	345	0.53	60.0	47
	35	1.86	0.99993	22.71	0.20	205	345	0.52	60.0	8

NEEDLE PROBE CONDUCTIVITY FOR FILE NAHIDIKCN1

STN	DEPTH (CM)	K (W/M.K)	R	AMBIENT (C)	DT (K)	T1 (S)	T2 (S)	P (W)	L (MM)	RECORD
NR15	12	.92	0.93049	22.30	0.29	205	345	0.54	60.0	49
	18	.99	0.94004	22.78	0.27	205	345	0.53	60.0	50
NR16	14	1.39	0.99999	22.68	0.26	205	345	0.52	60.0	51
	21	1.41	0.99999	22.45	0.26	205	345	0.52	60.0	52
	28	1.30	0.99999	23.58	0.27	205	345	0.52	60.0	53
	35	1.49	0.99998	22.27	0.24	205	345	0.52	60.0	54
	42	1.71	0.99997	22.54	0.21	205	345	0.52	60.0	55
NR17	10	2.10	0.99996	23.45	0.17	205	345	0.53	60.0	56
	16	1.80	0.99999	23.07	0.20	205	345	0.53	60.0	57
	22	1.79	0.99996	24.33	0.20	205	345	0.52	60.0	58
	28	1.85	0.99985	23.16	0.20	205	345	0.53	60.0	59
	1	1.41	0.99993	23.86	0.26	205	345	0.53	60.0	60

NEEDLE PROBE CONDUCTIVITY FOR FILE NAHIDIKCND

STN	DEPTH (CM)	K (W/M.K)	R	AMBIENT (C)	DT (K)	T1 (S)	T2 (S)	P (W)	L (MM)	RECO D
NP5	2	1.11	0.99995	19.09	0.34	205	355	0.52	60.0	1
	10	1.14	0.99999	18.72	0.33	205	355	0.52	60.0	2
	20	1.16	0.99999	20.32	0.32	205	355	0.52	60.0	3
	30	1.20	0.99999	19.39	0.32	205	355	0.52	60.0	4
	40	1.32	0.99999	20.01	0.29	205	355	0.52	60.0	5
	50	1.18	0.99999	19.86	0.32	205	355	0.52	60.0	6
	60	1.19	0.99999	19.42	0.32	205	355	0.52	60.0	7
	70	1.15	1.00000	20.36	0.33	205	355	0.52	60.0	8
	80	1.24	1.00000	19.06	0.31	205	355	0.52	60.0	9
	90	1.36	0.99999	19.32	0.28	205	355	0.52	60.0	0
	100	1.24	1.00000	19.31	0.30	205	355	0.52	60.0	11
	110	1.25	1.00000	18.79	0.30	205	355	0.52	60.0	12
	120	1.22	0.99999	19.71	0.31	205	355	0.52	60.0	3
	130	1.25	1.00000	18.36	0.30	205	355	0.52	60.0	4
	140	1.38	0.99999	18.70	0.27	205	355	0.52	60.0	15
NP6	12	1.11	0.99994	17.83	0.34	205	355	0.52	60.0	6
	27	1.07	0.99999	17.61	0.35	205	355	0.52	60.0	7
	50	1.10	0.99999	18.00	0.34	205	355	0.51	60.0	18
	65	1.16	0.99999	16.72	0.32	205	355	0.52	60.0	19
	80	1.35	1.00000	17.24	0.28	205	355	0.52	60.0	0
	80	1.26	0.99999	17.41	0.31	195	345	0.51	60.0	1
	100	1.19	0.99999	16.58	0.33	195	345	0.52	60.0	22
	114	1.21	0.99999	17.24	0.32	195	345	0.51	60.0	3
	127	1.27	0.99999	16.22	0.31	195	345	0.52	60.0	4
	150	1.30	0.99999	15.96	0.30	195	345	0.52	60.0	25
NP8	15	1.28	0.99999	18.26	0.29	205	355	0.51	60.0	26
	30	1.29	1.00000	17.20	0.29	205	355	0.52	60.0	7
	45	1.17	1.00000	17.50	0.32	205	355	0.51	60.0	8
	65	1.37	0.99999	19.12	0.28	205	355	0.52	60.0	29
	80	1.50	0.99999	19.27	0.25	205	355	0.52	60.0	0
	95	1.37	0.99999	18.74	0.28	195	345	0.52	60.0	1
	110	1.38	0.99999	17.98	0.28	195	345	0.52	60.0	32
	125	1.31	1.00000	18.45	0.30	195	345	0.51	60.0	33
	135	1.35	1.00000	17.02	0.29	195	345	0.52	60.0	4
	145	1.30	0.99999	17.13	0.30	195	345	0.52	60.0	35
	165	1.29	0.99999	19.78	0.29	205	355	0.52	60.0	36
	180	1.24	0.99999	19.10	0.31	205	355	0.52	60.0	7
	195	1.29	0.99999	19.62	0.29	205	355	0.52	60.0	8
	210	1.31	0.99998	18.03	0.29	205	355	0.52	60.0	39
	225	1.19	0.99996	17.73	0.32	205	355	0.53	60.0	0
NP9	15	1.17	0.99999	18.74	0.31	205	345	0.52	60.0	1
	30	1.18	0.99999	17.89	0.31	205	345	0.52	60.0	42
	45	1.17	0.99998	18.21	0.31	205	345	0.52	60.0	43
	60	1.26	0.99998	16.55	0.29	205	345	0.52	60.0	4
	75	1.32	0.99999	16.34	0.27	205	345	0.52	60.0	5
	100	1.26	0.99999	16.23	0.28	205	345	0.52	60.0	46
	125	1.20	0.99996	20.01	0.30	205	345	0.53	60.0	7
	140	1.23	0.99998	19.52	0.29	205	345	0.52	60.0	8
	155	1.26	0.99998	17.52	0.29	205	345	0.52	60.0	49
	170	1.37	0.99999	17.24	0.26	205	345	0.52	60.0	50
	160	1.27	0.99999	17.24	0.28	205	345	0.52	60.0	51
	175	1.27	1.00000	16.23	0.28	205	345	0.52	60.0	52
	190	1.19	0.99999	19.47	0.30	205	345	0.52	60.0	53
	205	1.24	0.99997	17.25	0.29	205	345	0.52	60.0	54
	220	1.31	0.99999	17.06	0.27	205	345	0.52	60.0	55

NEEDLE PROBE CONDUCTIVITY FOR FILE NAHIDIKCND

STN	DEPTH (CM)	K (W/M.K)	R	AMBIENT (C)	DT (K)	T1 (S)	T2 (S)	P (W)	L (MM)	RECORD
NP10	20	1.23	1.00000	19.52	0.28	215	355	0.52	60.0	56
	35	1.24	1.00000	19.05	0.28	215	355	0.52	60.0	57
	50	1.25	0.99999	19.83	0.27	215	355	0.51	60.0	58
	65	1.36	0.99999	18.36	0.26	215	355	0.52	60.0	59
	80	1.41	0.99999	18.57	0.25	215	355	0.52	60.0	60
	95	1.29	0.99999	18.10	0.28	205	345	0.52	60.0	61
	105	1.34	0.99998	17.75	0.27	205	345	0.52	60.0	62
	110	1.32	1.00000	20.12	0.27	205	345	0.52	60.0	63
	125	1.34	1.00000	18.86	0.27	205	345	0.52	60.0	64
	140	1.48	1.00000	18.92	0.24	205	345	0.52	60.0	65
	155	1.36	0.99999	18.54	0.26	205	345	0.52	60.0	66
	170	1.39	0.99999	17.92	0.26	205	345	0.52	60.0	67
	180	1.28	1.00000	18.77	0.28	205	345	0.52	60.0	68
	190	1.45	0.99999	18.99	0.25	205	345	0.52	60.0	69
	198	1.38	1.00000	19.36	0.26	205	345	0.52	60.0	70
	205	1.36	0.99999	19.28	0.26	205	345	0.52	60.0	71
	220	1.38	1.00000	18.57	0.26	205	345	0.52	60.0	72
	235	1.34	0.99999	19.25	0.27	205	345	0.52	60.0	73
	243	1.35	0.99999	17.88	0.27	205	345	0.52	60.0	74
	250	1.49	0.99999	18.28	0.24	205	345	0.52	60.0	75
NP11	10	1.23	1.00000	18.04	0.28	215	355	0.51	60.0	76
	20	1.18	0.99999	16.88	0.29	215	355	0.52	60.0	77
	30	1.15	0.99998	17.56	0.30	215	355	0.51	60.0	78
	40	1.26	0.99998	16.24	0.27	215	355	0.52	60.0	79
	50	1.36	0.99998	16.51	0.25	215	355	0.52	60.0	80
	60	1.33	0.99999	16.74	0.26	215	355	0.52	60.0	81
	70	1.40	1.00000	16.24	0.25	215	355	0.52	60.0	82
	80	1.35	0.99999	17.02	0.25	215	355	0.51	60.0	83
	100	1.26	0.99999	17.46	0.28	215	355	0.52	60.0	84
	110	1.41	0.99998	17.62	0.25	215	355	0.52	60.0	85
	120	1.33	0.99999	18.22	0.27	205	345	0.52	60.0	86
	130	1.30	0.99999	17.42	0.28	205	345	0.52	60.0	87
	140	1.28	0.99998	18.21	0.28	205	345	0.51	60.0	88
	150	1.33	0.99998	16.86	0.27	205	345	0.52	60.0	89
	160	1.49	0.99999	17.16	0.24	205	345	0.52	60.0	90
	173	1.42	0.99999	19.64	0.25	205	345	0.52	60.0	91
	180	1.44	0.99999	19.18	0.25	205	345	0.52	60.0	92
	190	1.38	1.00000	20.02	0.26	205	345	0.52	60.0	93
	200	1.42	0.99999	18.71	0.25	205	345	0.52	60.0	94
	210	1.61	0.99999	19.10	0.22	205	345	0.52	60.0	95

NEEDLE PROBE CONDUCTIVITY FOR FILE NAHIDIKCN1

STN	DEPTH (CM)	K (W/M.K)	R	AMBIENT (C)	DT (K)	T1 (S)	T2 (S)	P (W)	L (MM)	RECO)
NP12	10	1.32	1.00000	19.26	0.27	205	345	0.52	60.0	156
	25	1.35	0.99999	18.64	0.27	205	345	0.52	60.0	1 7
	40	1.37	0.99999	19.35	0.26	205	345	0.51	60.0	1 3
	55	1.35	1.00000	17.92	0.27	205	345	0.52	60.0	159
	70	1.46	0.99999	18.11	0.25	205	345	0.52	60.0	1 9
	80	1.38	0.99998	19.98	0.26	205	345	0.52	60.0	1 1
	95	1.39	0.99999	18.99	0.26	205	345	0.52	60.0	162
	110	1.32	0.99999	19.78	0.27	205	345	0.51	60.0	163
	125	1.38	0.99999	18.28	0.26	205	345	0.52	60.0	1 4
	140	1.48	0.99999	18.54	0.24	205	345	0.52	60.0	1 5
	150	1.37	0.99999	18.30	0.26	205	345	0.52	60.0	166
	175	1.30	0.99993	19.23	0.28	205	345	0.52	60.0	1 7
	185	1.24	0.99999	19.96	0.29	205	345	0.52	60.0	1 3
	195	1.30	0.99998	18.53	0.28	205	345	0.52	60.0	169
	205	1.39	0.99999	18.77	0.26	205	345	0.52	60.0	170
	215	1.32	1.00000	18.74	0.27	205	345	0.52	60.0	1 1
	225	1.30	0.99999	18.14	0.28	205	345	0.52	60.0	1.2
	235	1.27	0.99999	18.77	0.28	205	345	0.52	60.0	173
	245	.81	0.99999	16.23	0.45	205	345	0.52	60.0	1 4
	255	1.50	0.99999	19.45	0.24	205	345	0.52	60.0	1 5
NP13	10	1.21	0.99998	17.69	0.28	215	355	0.52	60.0	176
	20	1.28	0.99999	17.30	0.27	215	355	0.52	60.0	177
	30	1.24	0.99999	18.36	0.28	215	355	0.51	60.0	1 3
	40	1.01	0.99999	16.48	0.35	215	355	0.53	60.0	1.9
	50	1.46	0.99999	17.60	0.24	215	355	0.52	60.0	180
NP15	10	1.25	0.99999	19.63	0.29	205	345	0.52	60.0	1 1
	20	1.02	1.00000	18.55	0.36	205	345	0.53	60.0	1 2
	30	1.27	0.99999	19.70	0.28	205	345	0.52	60.0	183
	40	1.26	0.99999	18.30	0.29	205	345	0.52	60.0	184
	50	1.33	0.99999	18.54	0.27	205	345	0.52	60.0	1 5
	60	1.26	0.99999	18.50	0.28	205	345	0.52	60.0	186
	70	1.24	1.00000	17.91	0.29	205	345	0.52	60.0	187
	80	1.33	0.99999	18.69	0.27	205	345	0.51	60.0	1 3
	90	1.43	0.99997	17.33	0.25	205	345	0.52	60.0	1 9
	105	1.57	0.99998	20.60	0.23	205	345	0.52	60.0	190
	110	1.39	0.99999	20.26	0.26	205	345	0.52	60.0	191
	120	1.41	0.99999	19.69	0.26	205	345	0.52	60.0	1 2
	125	1.38	0.99999	20.67	0.26	205	345	0.52	60.0	193
	130	1.39	0.99999	19.37	0.26	205	345	0.52	60.0	194
	135	1.65	0.99999	19.72	0.22	205	345	0.52	60.0	1 5
	110	1.45	1.00000	19.84	0.25	205	345	0.52	60.0	1 5
	125	1.37	1.00000	18.77	0.26	205	345	0.52	60.0	197
	140	1.40	0.99999	19.00	0.26	205	345	0.52	60.0	198
	155	1.58	0.99997	17.16	0.23	205	345	0.52	60.0	1 9
	170	1.71	0.99999	17.18	0.21	205	345	0.52	60.0	200

NEEDLE PROBE CONDUCTIVITY FOR FILE NAHIDIKCN1

STN	DEPTH (CM)	K (W/M.K)	R	AMBIENT (C)	DT (K)	T1 (S)	T2 (S)	P (W)	L (MM)	RECORD
NP23	15	1.15	0.99998	17.26	0.30	215	355	0.51	60.0	201
	30	1.20	0.99997	16.94	0.29	215	355	0.52	60.0	202
	45	1.17	0.99998	17.98	0.29	215	355	0.51	60.0	203
	60	1.24	0.99998	16.78	0.28	215	355	0.52	60.0	204
	75	1.41	0.99999	17.25	0.24	215	355	0.52	60.0	205
	90	1.32	1.00000	17.55	0.26	215	355	0.51	60.0	206
	105	1.36	1.00000	16.85	0.25	215	355	0.51	60.0	207
	120	1.33	0.99999	17.52	0.25	215	355	0.51	60.0	208
	135	1.39	0.99999	16.34	0.25	215	355	0.51	60.0	209
	150	1.57	0.99998	16.87	0.22	215	355	0.51	60.0	210
	165	1.40	1.00000	16.20	0.25	205	345	0.51	60.0	211
	180	1.37	0.99999	15.44	0.26	205	345	0.51	60.0	212
	187	1.36	0.99999	16.29	0.26	205	345	0.51	60.0	213
	195	1.37	0.99998	14.95	0.26	205	345	0.51	60.0	214
	202	1.57	0.99999	15.38	0.23	205	345	0.51	60.0	215
NP26	15	1.27	0.99999	19.83	0.27	215	355	0.52	60.0	216
	30	1.30	1.00000	19.13	0.27	215	355	0.52	60.0	217
	45	1.29	0.99999	20.33	0.27	215	355	0.52	60.0	218
	60	1.36	0.99998	18.94	0.26	215	355	0.52	60.0	219
	75	1.63	0.99999	18.84	0.21	215	355	0.52	60.0	220
	15	1.25	0.99999	20.24	0.29	205	345	0.52	60.0	221
	30	1.28	0.99999	19.50	0.28	205	345	0.53	60.0	222
	45	1.27	0.99998	20.70	0.28	205	345	0.52	60.0	223
	60	1.35	0.99998	19.39	0.27	205	345	0.53	60.0	224
	90	1.59	0.99998	18.74	0.23	205	345	0.53	60.0	225
NP28	7	.89	0.99998	21.75	0.41	205	345	0.53	60.0	226
	15	.96	1.00000	20.53	0.38	205	345	0.54	60.0	227
	30	1.32	1.00000	22.01	0.27	205	345	0.52	60.0	228
	45	1.35	0.99999	20.47	0.27	205	345	0.53	60.0	229
	60	1.33	0.99997	20.43	0.28	205	345	0.53	60.0	230
	7	1.30	1.00000	22.28	0.28	205	345	0.53	60.0	231
	15	1.33	1.00000	21.71	0.28	205	345	0.53	60.0	232
	30	1.32	1.00000	22.32	0.27	205	345	0.52	60.0	233
	45	1.35	0.99999	20.83	0.27	205	345	0.53	60.0	234
	70	1.44	0.99998	20.74	0.25	205	345	0.53	60.0	235
NP25	10	1.16	0.99996	21.83	0.31	215	355	0.53	60.0	236
	25	1.19	0.99999	21.16	0.30	215	355	0.53	60.0	237
	40	1.18	0.99998	22.02	0.30	215	355	0.53	60.0	238
	55	1.25	0.99993	20.52	0.28	215	355	0.53	60.0	239
	70	1.45	0.99990	20.84	0.24	215	355	0.53	60.0	240
	10	1.31	0.99999	22.47	0.28	205	345	0.52	60.0	241
	25	1.29	0.99999	21.67	0.28	205	345	0.53	60.0	242
	40	1.28	0.99999	22.53	0.28	205	345	0.52	60.0	243
	55	1.36	0.99999	21.05	0.27	205	345	0.53	60.0	244
	83	1.34	0.99999	20.71	0.27	205	345	0.53	60.0	245

NEEDLE PROBE CONDUCTIVITY FOR FILE NAHIDIKCND

STN	DEPTH (CM)	K (W/M.K)	R	AMBIENT (C)	DT (K)	T1 (S)	T2 (S)	P (W)	L (MM)	RECO)
NKNP03	10	1.14	1.00000	20.44	0.32	202	342	0.52	60.0	196
	20	1.03	0.99907	20.60	0.36	202	342	0.52	60.0	1 7
	30	1.12	1.00000	19.63	0.32	202	342	0.52	60.0	1[illegible]8
NKNP04	10	1.09	1.00000	19.17	0.32	207	347	0.52	60.0	189
	20	1.06	1.00000	18.22	0.33	207	347	0.52	60.0	1 8
	30	1.03	0.99992	17.82	0.34	207	347	0.52	60.0	1 1
	40	1.11	0.99992	17.74	0.32	207	347	0.52	60.0	192
	50	1.29	0.99993	18.30	0.27	207	347	0.52	60.0	193
	60	1.15	0.99993	17.49	0.30	207	347	0.52	60.0	1 4
	70	1.21	0.99992	17.02	0.28	207	347	0.50	60.0	1[illegible]5
	80	1.24	0.99996	16.64	0.28	207	347	0.52	60.0	196
	90	1.26	0.99998	16.92	0.28	207	347	0.51	60.0	1 7
	110	1.23	0.99999	19.43	0.29	206	346	0.52	60.0	1 3
	120	1.22	0.99999	18.78	0.29	206	346	0.52	60.0	199
	130	1.18	1.00000	18.47	0.30	206	346	0.52	60.0	2[illegible]0
	140	1.17	0.99999	18.10	0.31	206	346	0.52	60.0	2 1
	150	1.43	0.99999	18.66	0.25	206	346	0.52	60.0	2[illegible]2
	160	1.30	0.99998	17.96	0.27	206	346	0.52	60.0	203
	170	1.32	0.99999	17.69	0.26	206	346	0.50	60.0	2 4
	180	1.30	0.99998	17.16	0.28	206	346	0.52	60.0	2 5
	190	1.32	0.99997	17.37	0.27	206	346	0.51	60.0	206
NKNP05	10	1.15	1.00000	20.49	0.31	207	347	0.52	60.0	2[illegible]7
	20	1.16	1.00000	19.66	0.31	207	347	0.52	60.0	2 9
	30	1.17	0.99999	19.23	0.30	207	347	0.52	60.0	209
	40	1.22	0.99999	18.86	0.29	207	347	0.52	60.0	210
	50	1.24	1.00000	19.19	0.29	207	347	0.52	60.0	2 1
	60	1.10	0.99999	18.45	0.32	207	347	0.52	60.0	2[illegible]2
	70	1.19	0.99999	18.07	0.29	207	347	0.50	60.0	213
	80	1.29	0.99998	17.41	0.28	207	347	0.52	60.0	2 4
	90	1.21	0.99999	17.64	0.29	207	347	0.51	60.0	2 5
	100	1.22	1.00000	18.64	0.29	206	346	0.51	60.0	216
	110	1.21	1.00000	18.13	0.29	206	346	0.51	60.0	217
	120	1.19	1.00000	17.90	0.29	206	346	0.51	60.0	2 8
	130	1.21	1.00000	19.05	0.29	206	346	0.51	60.0	2[illegible]9
	140	1.32	0.99999	19.71	0.27	206	346	0.51	60.0	220
	150	1.28	1.00000	19.20	0.27	206	346	0.51	60.0	2 1
	160	1.25	0.99999	19.02	0.27	206	346	0.50	60.0	2 2
	170	1.22	1.00000	18.59	0.29	206	346	0.51	60.0	223
	180	1.28	1.00000	18.97	0.27	206	346	0.51	60.0	2[illegible]4
	200	1.24	1.00000	19.07	0.29	203	343	0.51	60.0	2 5
	210	1.21	1.00000	18.54	0.30	203	343	0.52	60.0	2[illegible]6
	220	1.26	1.00000	18.36	0.28	203	343	0.51	60.0	227
	230	1.24	1.00000	18.19	0.29	203	343	0.52	60.0	2 8

NEEDLE PROBE CONDUCTIVITY FOR FILE NAHIDIKCND

STN	DEPTH (CM)	K (W/M.K)	R	AMBIENT (C)	DT (K)	T1 (S)	T2 (S)	P (W)	L (MM)	RECORD
NKNP22	10	1.04	0.99999	19.67	0.34	207	347	0.52	60.0	229
	20	1.08	0.99997	19.20	0.33	207	347	0.52	60.0	230
	30	1.09	0.99998	18.95	0.33	207	347	0.52	60.0	231
	40	1.15	0.99998	18.80	0.31	207	347	0.52	60.0	232
	50	1.22	0.99998	19.35	0.29	207	347	0.52	60.0	233
	60	1.10	0.99998	18.68	0.32	207	347	0.52	60.0	234
	70	1.14	0.99998	18.45	0.30	207	347	0.50	60.0	235
	80	1.18	0.99998	18.06	0.30	207	347	0.52	60.0	236
	90	1.13	0.99998	18.36	0.31	207	347	0.51	60.0	237
	100	1.16	0.99999	18.74	0.31	207	347	0.52	60.0	238
	110	1.14	0.99998	18.18	0.31	207	347	0.52	60.0	239
	130	1.14	0.99998	19.17	0.31	207	347	0.52	60.0	240
	140	1.16	0.99998	18.78	0.31	207	347	0.52	60.0	241
	150	1.31	0.99999	19.42	0.27	207	347	0.52	60.0	242
	160	1.24	0.99999	18.54	0.29	207	347	0.52	60.0	243
	170	1.28	0.99998	18.27	0.27	207	347	0.50	60.0	244
	180	1.32	0.99997	17.84	0.27	207	347	0.52	60.0	245
	190	1.25	0.99998	18.20	0.28	207	347	0.52	60.0	246
	200	1.45	0.99999	18.44	0.25	202	342	0.52	60.0	247
	210	1.33	1.00000	18.13	0.27	202	342	0.52	60.0	248
NKNP23	10	1.46	0.99946	19.66	0.34	225	435	0.55	60.0	249
	20	1.52	0.99948	19.52	0.32	225	435	0.55	60.0	250
	30	1.43	0.99942	19.30	0.34	225	435	0.55	60.0	251
	40	1.34	0.99958	18.83	0.37	225	435	0.55	60.0	252
	50	1.38	0.99932	18.87	0.35	225	435	0.55	60.0	253
	60	1.39	0.99963	18.59	0.35	225	435	0.55	60.0	254
	70	1.34	0.99967	18.31	0.36	225	435	0.55	60.0	255
	80	1.39	0.99951	18.26	0.34	225	435	0.55	60.0	256
	90	1.32	0.99955	17.78	0.36	225	435	0.55	60.0	257
	110	1.34	0.99963	19.60	0.36	225	435	0.55	60.0	258
	120	1.31	0.99928	19.55	0.37	225	435	0.55	60.0	259
	130	1.41	0.99925	19.14	0.34	225	435	0.55	60.0	260
	140	1.30	0.99949	19.21	0.37	225	435	0.56	60.0	261
	150	1.31	0.99968	18.95	0.37	225	435	0.55	60.0	262
	160	1.28	0.99956	18.76	0.38	225	435	0.55	60.0	263
	170	1.49	0.99935	18.47	0.33	225	435	0.56	60.0	264
	180	2.47	0.99893	18.40	0.20	225	435	0.55	60.0	265
	190	2.04	0.99869	19.18	0.24	225	435	0.55	60.0	266
	200	2.49	0.99893	18.20	0.20	225	435	0.55	60.0	267

NEEDLE PROBE CONDUCTIVITY FOR FILE NAHIDIKCND

STN	DEPTH (CM)	K (W/M.K)	R	AMBIENT (C)	DT (K)	T1 (S)	T2 (S)	P (W)	L (MM)	RECO)
NKNP25	10	1.49	0.99878	23.21	0.33	225	435	0.56	60.0	2 9
	20	1.44	0.99944	22.70	0.34	225	435	0.56	60.0	2 9
	30	1.27	0.99942	22.18	0.40	225	435	0.56	60.0	2.0
	40	1.28	0.99919	22.11	0.38	225	435	0.56	60.0	271
	50	1.28	0.99955	21.97	0.38	225	435	0.56	60.0	2 2
	60	1.42	0.99917	21.83	0.34	225	435	0.56	60.0	2 3
	70	1.47	0.99934	21.39	0.33	225	435	0.56	60.0	274
	80	1.41	0.99948	20.96	0.34	225	435	0.56	60.0	275
	90	1.39	0.99952	20.65	0.35	225	435	0.56	60.0	2 6
	100	1.43	0.99904	20.52	0.35	225	435	0.56	60.0	2.7
	110	1.42	0.99924	20.31	0.35	225	435	0.56	60.0	278
	120	1.39	0.99942	20.08	0.36	225	435	0.56	60.0	2 9
	130	1.26	0.99948	19.85	0.39	225	435	0.56	60.0	2 9
	170	1.36	0.99953	19.03	0.36	225	435	0.56	60.0	281
	180	1.34	0.99958	18.94	0.37	225	435	0.56	60.0	2 2
	260	1.39	0.99929	21.02	0.34	225	435	0.55	60.0	2 3
	270	1.38	0.99924	20.77	0.35	225	435	0.56	60.0	284
	280	1.40	0.99912	20.64	0.35	225	435	0.56	60.0	285
	290	1.44	0.99919	20.65	0.34	225	435	0.56	60.0	2 6
	300	1.35	0.99959	20.30	0.36	225	435	0.56	60.0	2.7
	340	1.38	0.99948	19.55	0.35	225	435	0.56	60.0	288
	350	1.40	0.99953	19.50	0.35	225	435	0.56	60.0	2 9
	360	1.32	0.99949	19.16	0.36	225	435	0.56	60.0	2 9
	370	1.41	0.99959	19.20	0.34	225	435	0.56	60.0	291
	380	1.38	0.99963	19.00	0.35	225	435	0.56	60.0	292
	390	1.41	0.99925	18.94	0.34	225	435	0.56	60.0	2 3
	400	1.30	0.99962	18.68	0.38	225	435	0.56	60.0	2.4
	420	1.37	0.99946	21.26	0.36	225	435	0.56	60.0	295
	430	1.44	0.99935	20.97	0.34	225	435	0.56	60.0	2 6
	440	1.42	0.99923	20.58	0.35	225	435	0.56	60.0	2 7
	450	1.41	0.99927	20.26	0.35	225	435	0.56	60.0	298
	460	1.29	0.99941	19.95	0.39	225	435	0.56	60.0	299
	470	1.28	0.99957	19.31	0.38	225	435	0.56	60.0	3 3
	480	1.35	0.99935	19.27	0.36	225	435	0.56	60.0	3.1
	490	1.37	0.99960	19.27	0.36	225	435	0.56	60.0	302
	500	1.40	0.99942	18.99	0.34	225	435	0.56	60.0	3 3

APPENDIX D

Thermal conductivity plots
for selected core

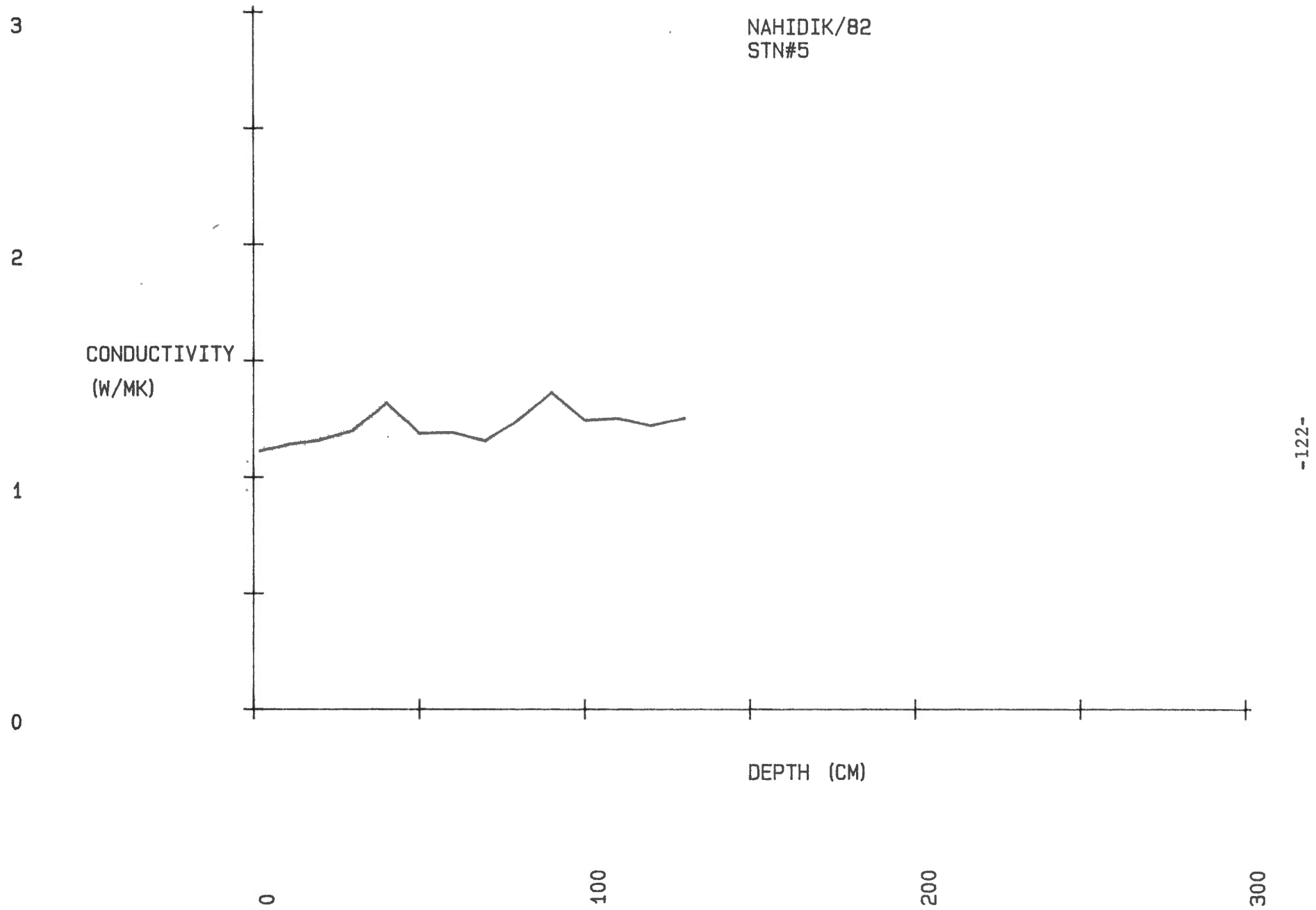
NAHIDIK/82
STN#5
CONDUCTIVITY
(W/MK)
3
2
1
0
0
100
200
300
DEPTH (CM)

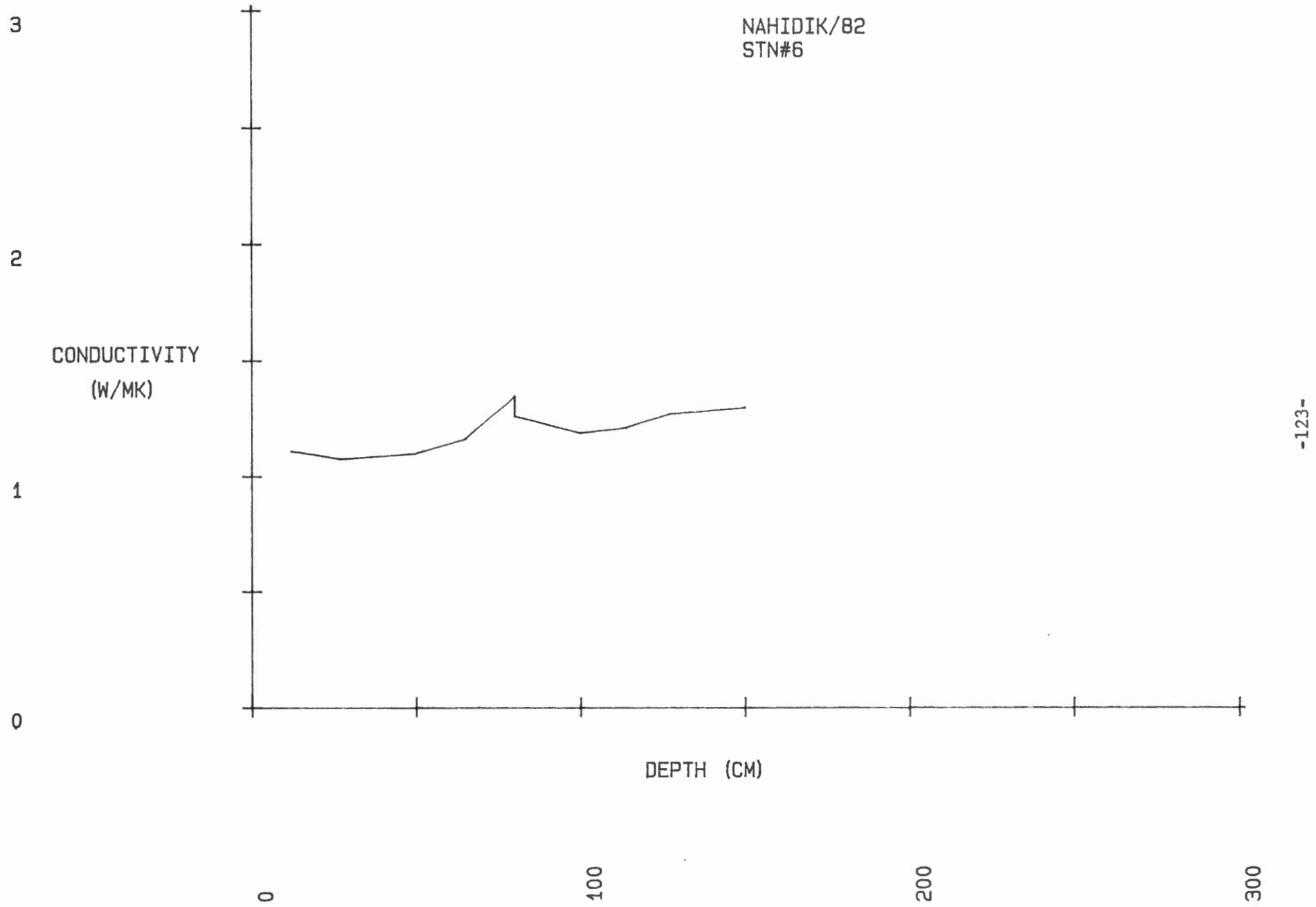
NAHIDIK/82
STN#6
CONDUCTIVITY
(W/MK)
3
2
1
0
DEPTH (CM)
0
100
200
300

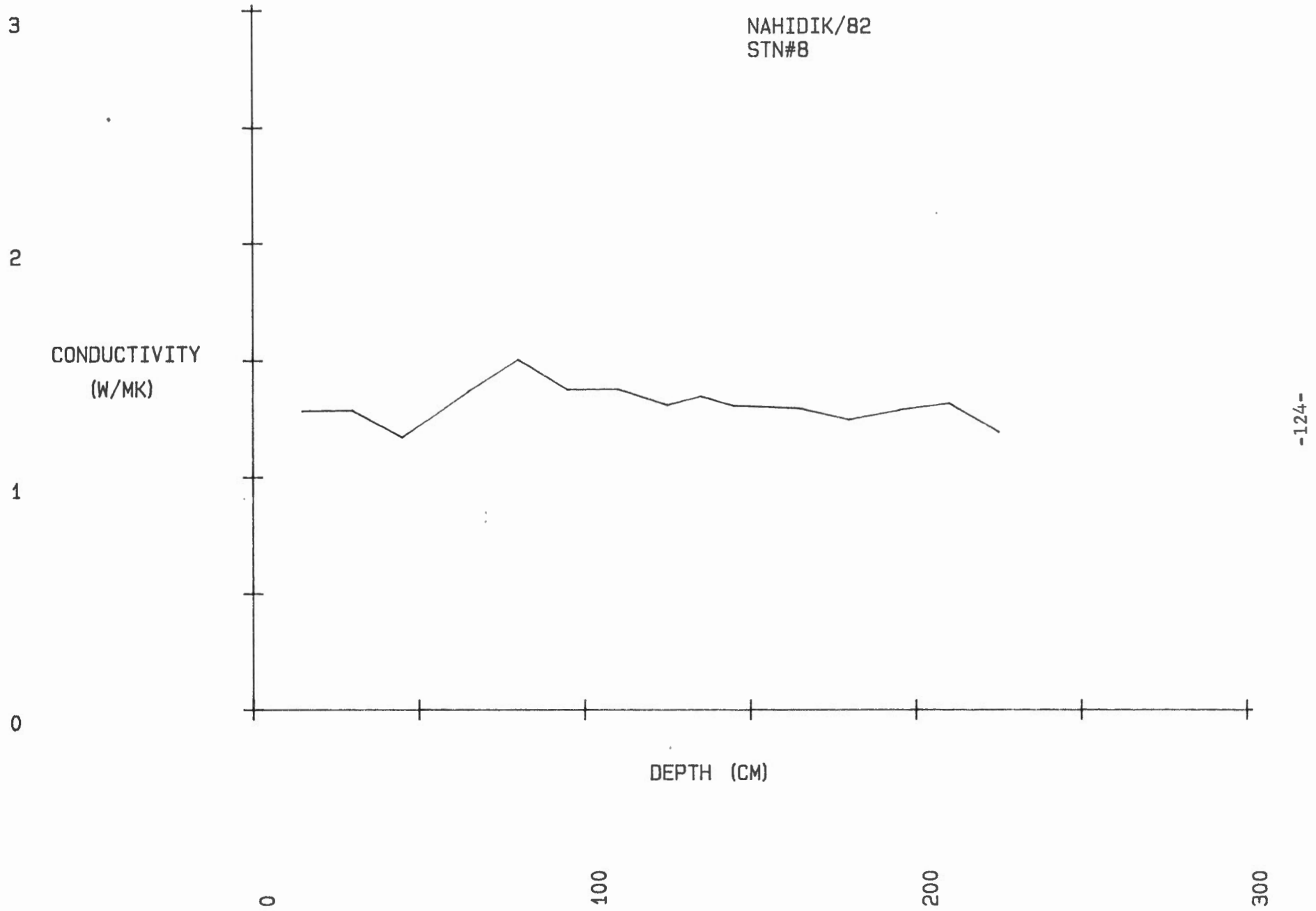
NAHIDIK/82
STN#8
3
2
1
0
CONDUCTIVITY
(W/MK)
DEPTH (CM)
0
100
200
300

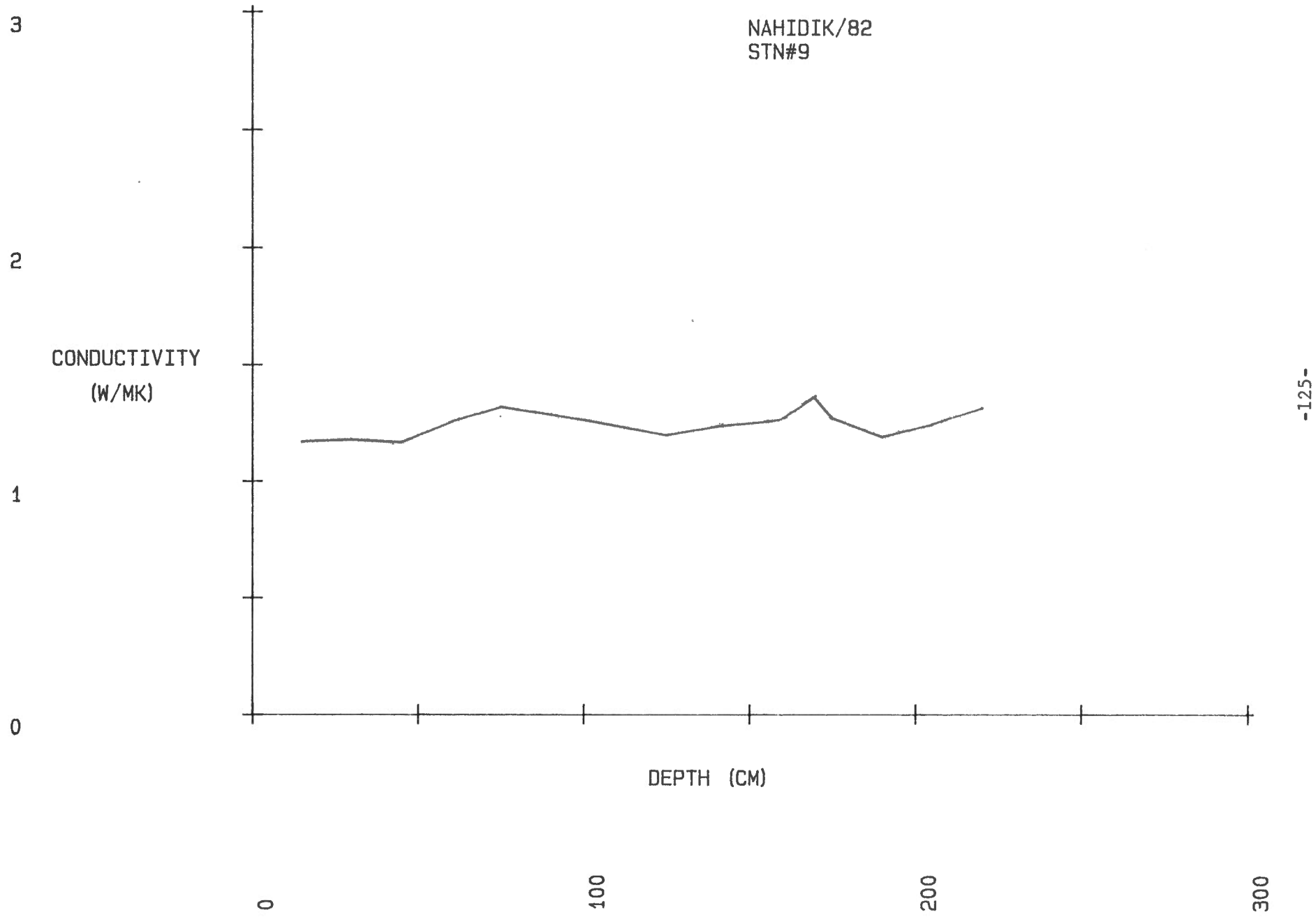
NAHIDIK/82
STN#9
3
2
1
0
CONDUCTIVITY
(W/MK)
0
100
200
300
DEPTH (CM)

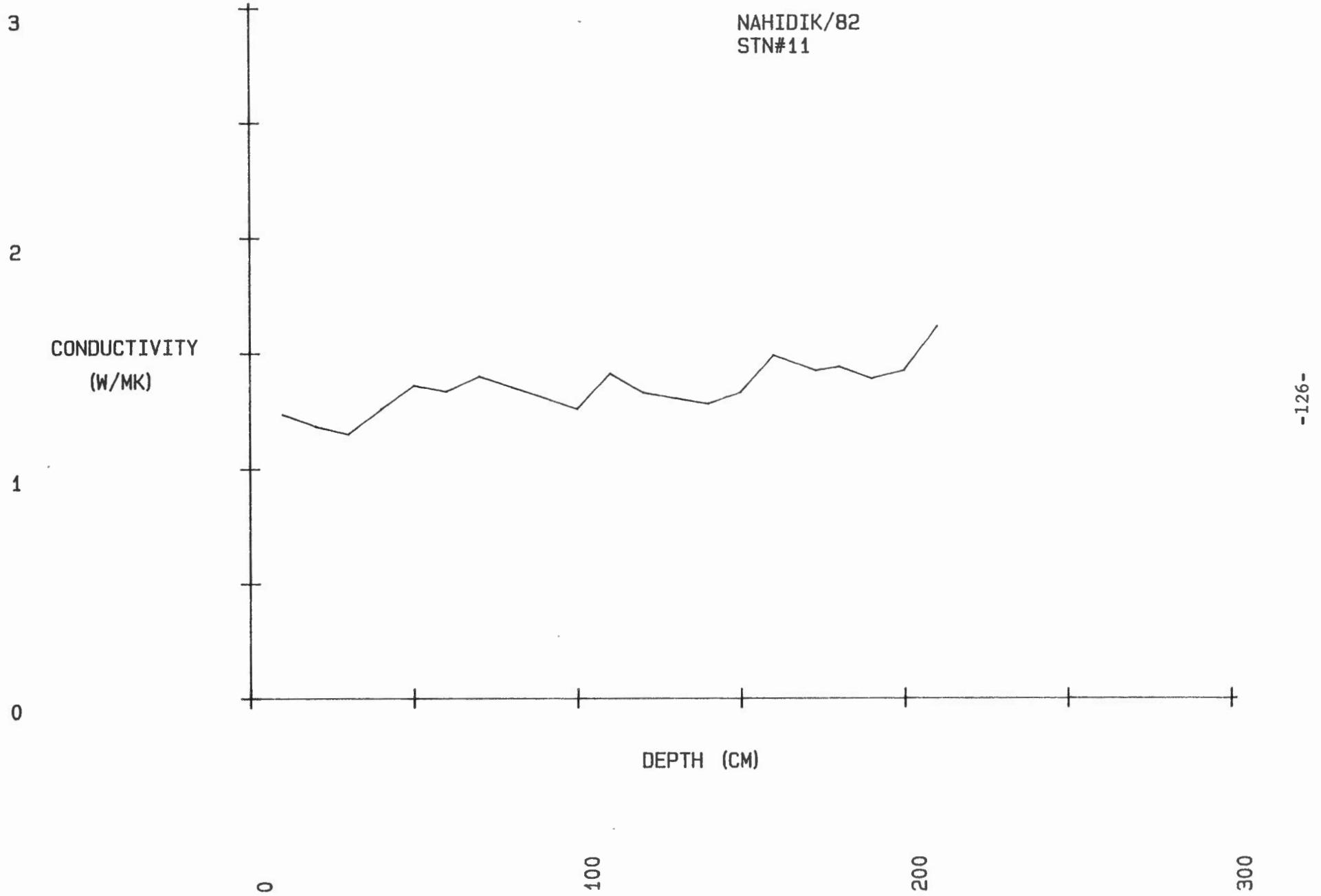
NAHIDIK/82
STN#11
3
2
1
0
CONDUCTIVITY
(W/MK)
0
100
200
300
DEPTH (CM)

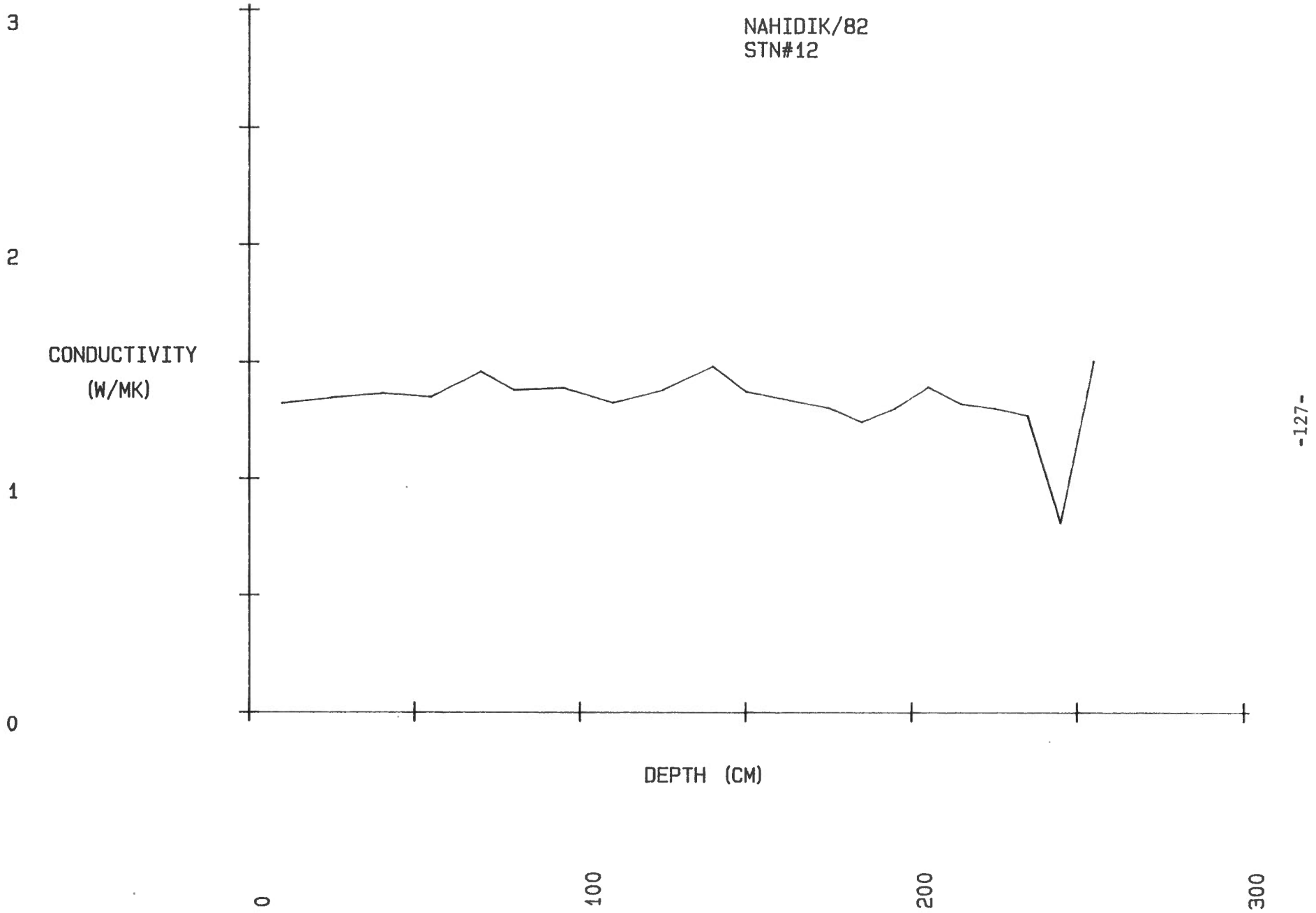
NAHIDIK/82
STN#12
CONDUCTIVITY
(W/MK)
3
2
1
0
DEPTH (CM)
0
100
200
300

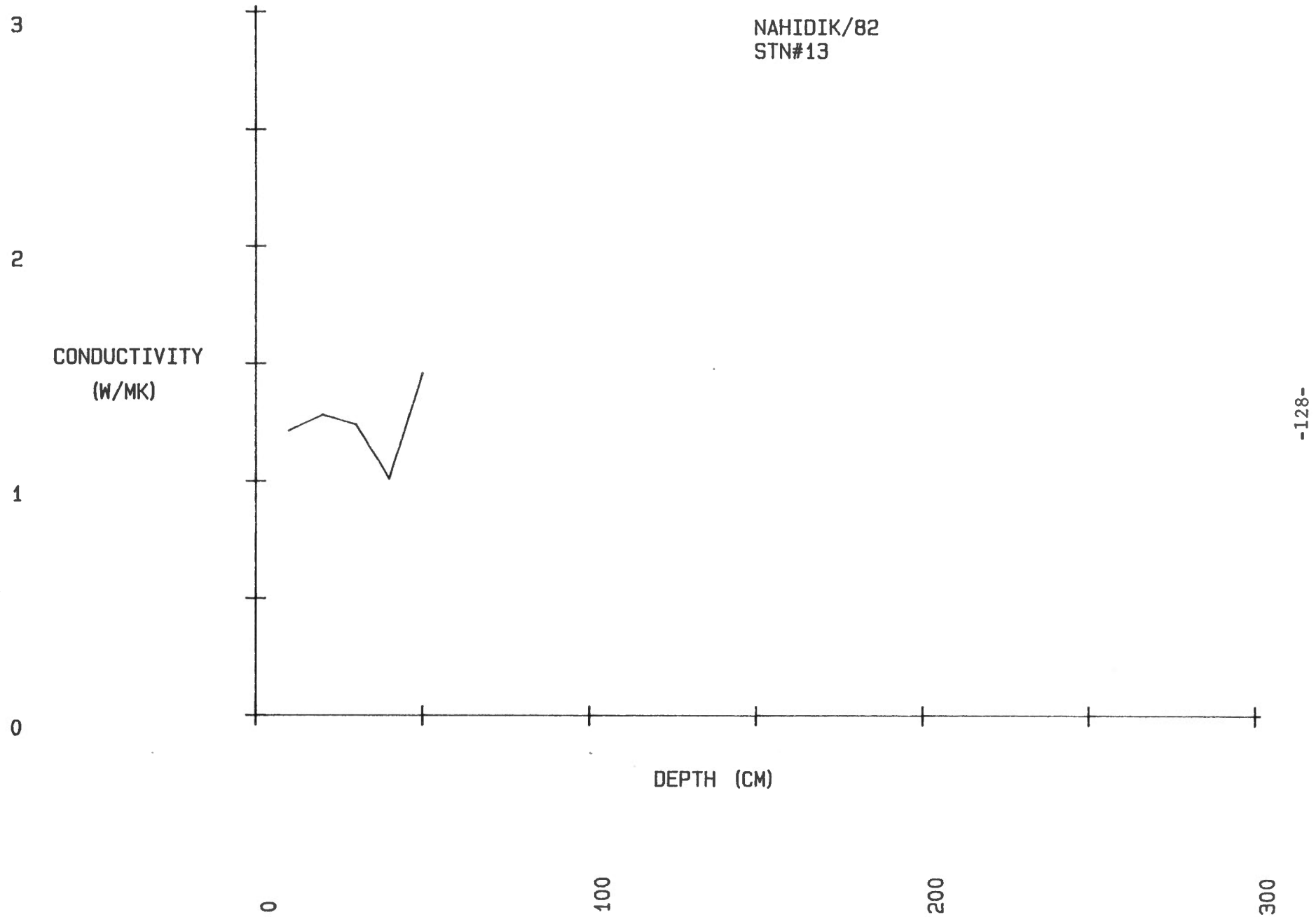
NAHIDIK/82
STN#13
CONDUCTIVITY
(W/MK)
3
2
1
0
DEPTH (CM)
0
100
200
300

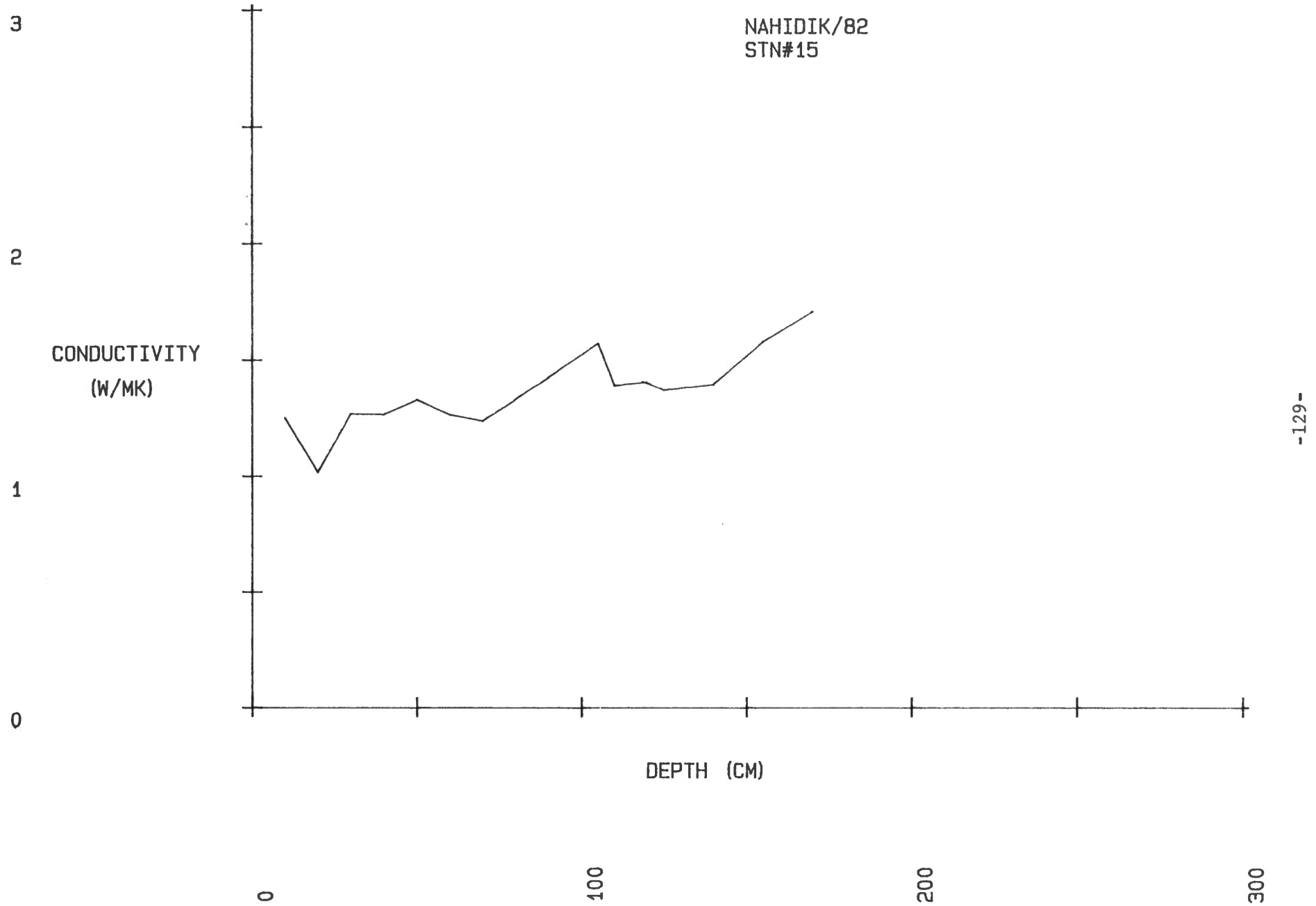
NAHIDIK/82
STN#15
3
2
1
0
CONDUCTIVITY
(W/MK)
DEPTH (CM)
0
100
200
300

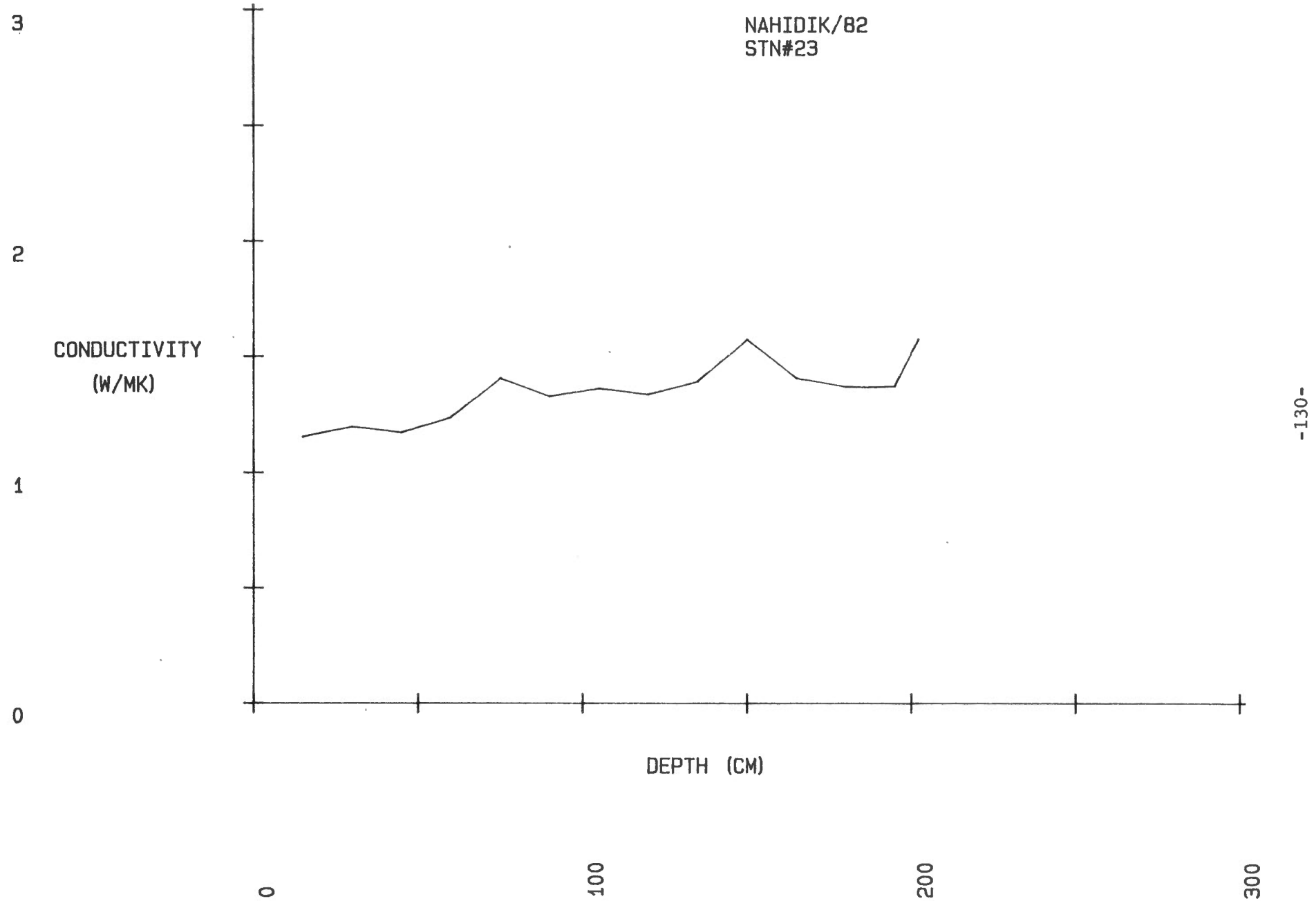
NAHIDIK/82
STN#23
3
2
1
0
CONDUCTIVITY
(W/MK)
DEPTH (CM)
0
100
200
300

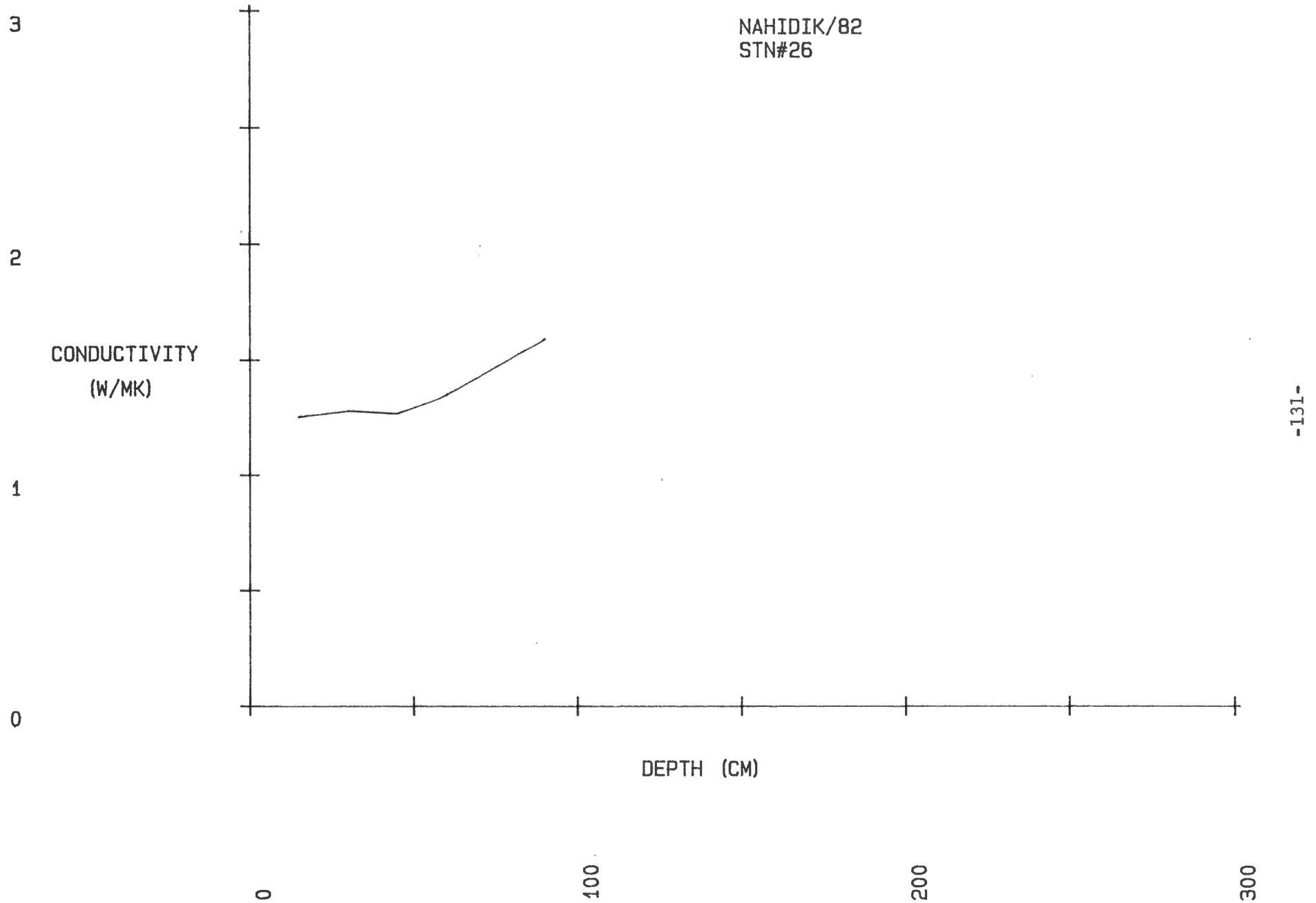
NAHIDIK/82
STN#26
CONDUCTIVITY
(W/MK)
3
2
1
0
DEPTH (CM)
0
100
200
300

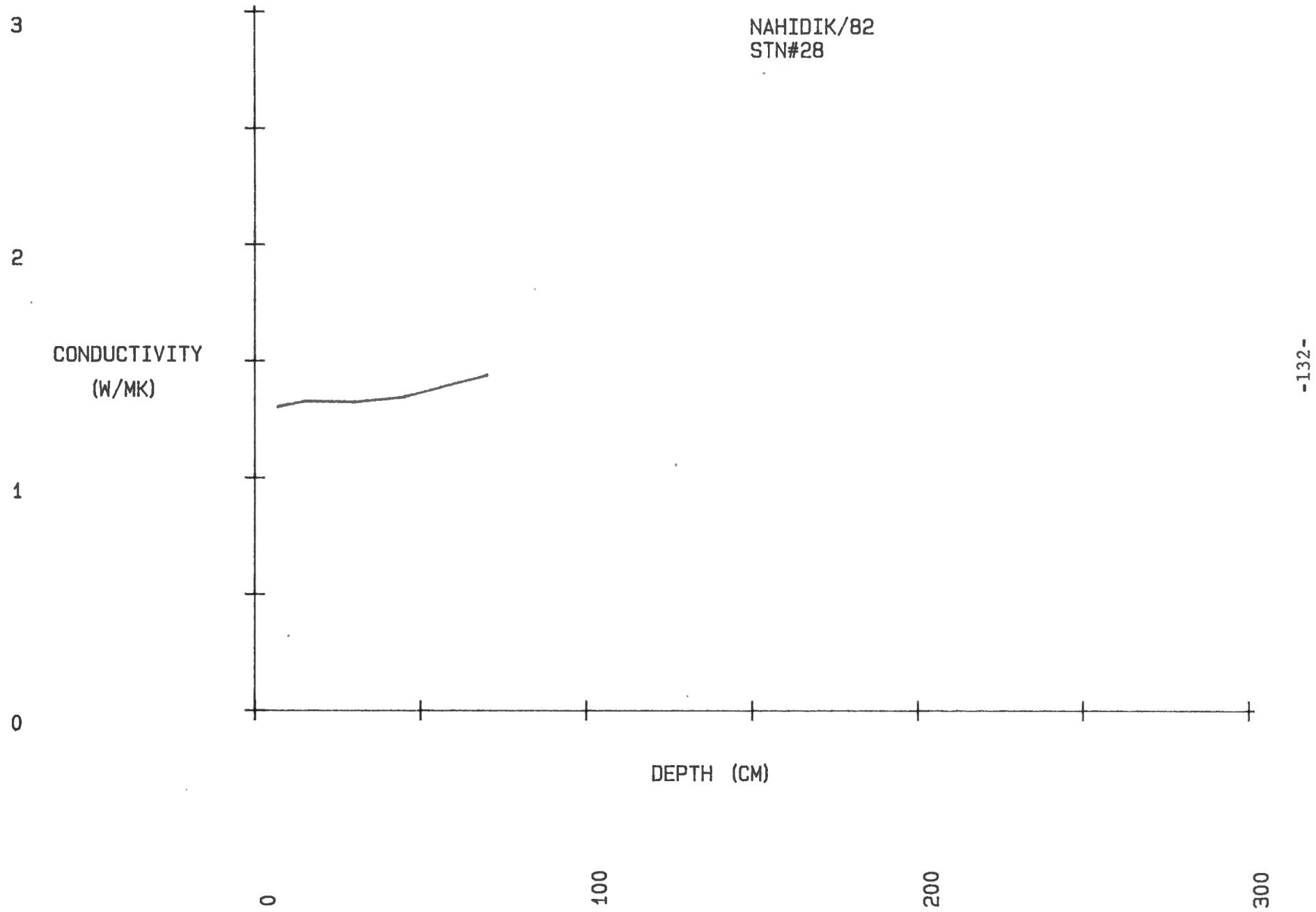
NAHIDIK/82
STN#28
CONDUCTIVITY
(W/MK)
3
2
1
0
DEPTH (CM)
0
100
200
300

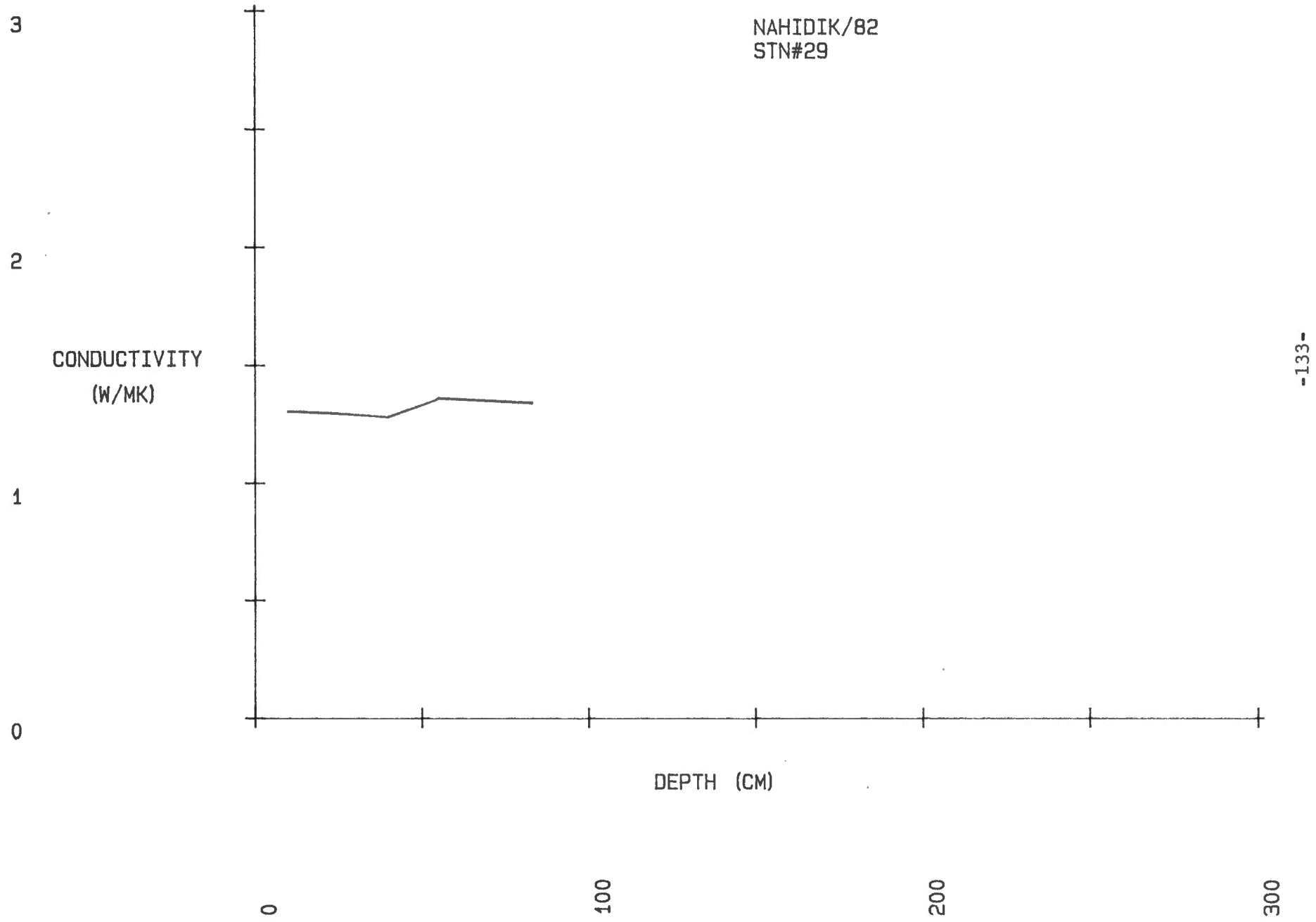
NAHIDIK/82
STN#29
CONDUCTIVITY
(W/MK)
3
2
1
0
DEPTH (CM)
0
100
200
300

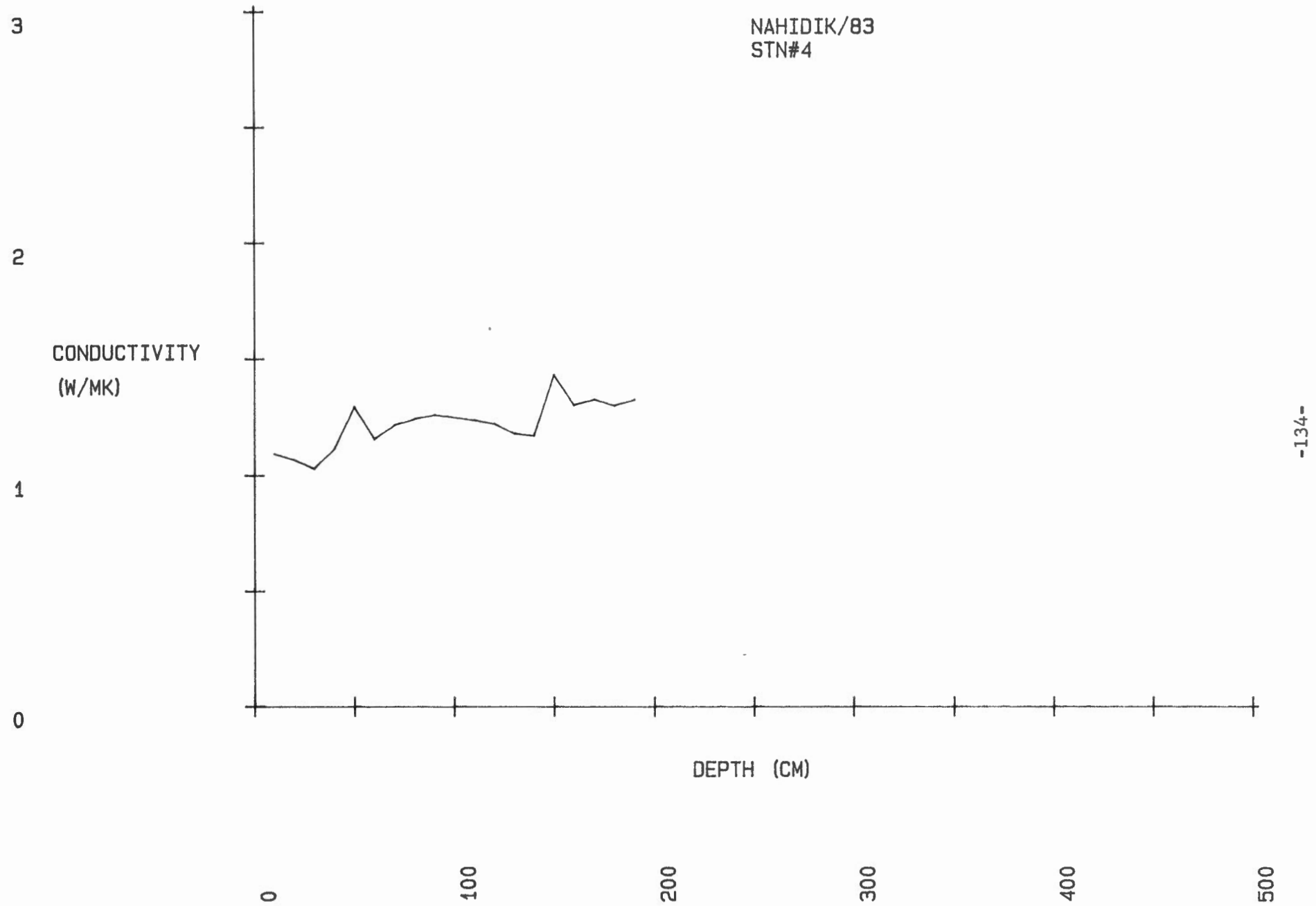
NAHIDIK/83
STN#4
CONDUCTIVITY
(W/MK)
3
2
1
0
DEPTH (CM)
0
100
200
300
400
500

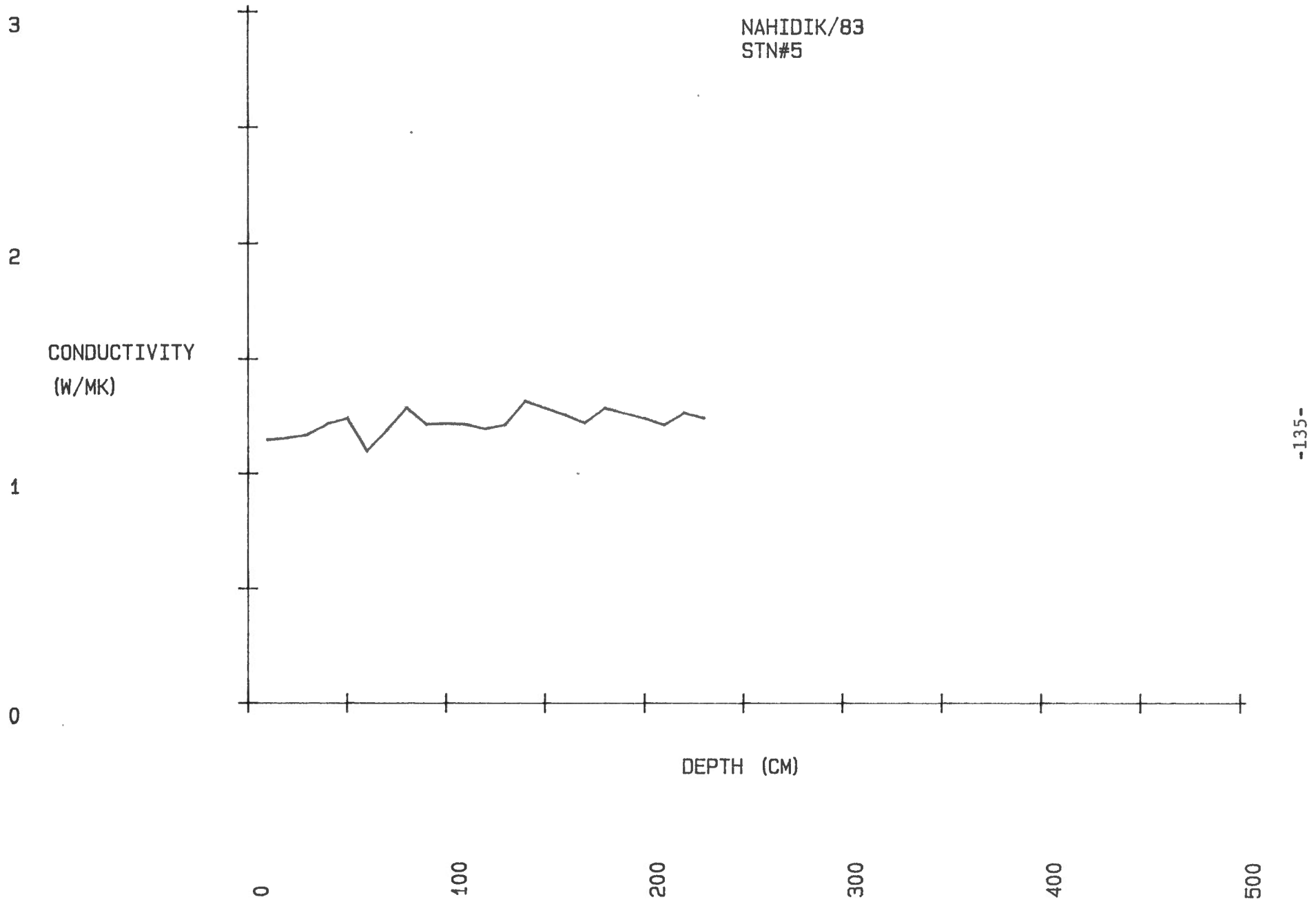
NAHIDIK/83
STN#5
CONDUCTIVITY
(W/MK)
3
2
1
0
DEPTH (CM)
0
100
200
300
400
500

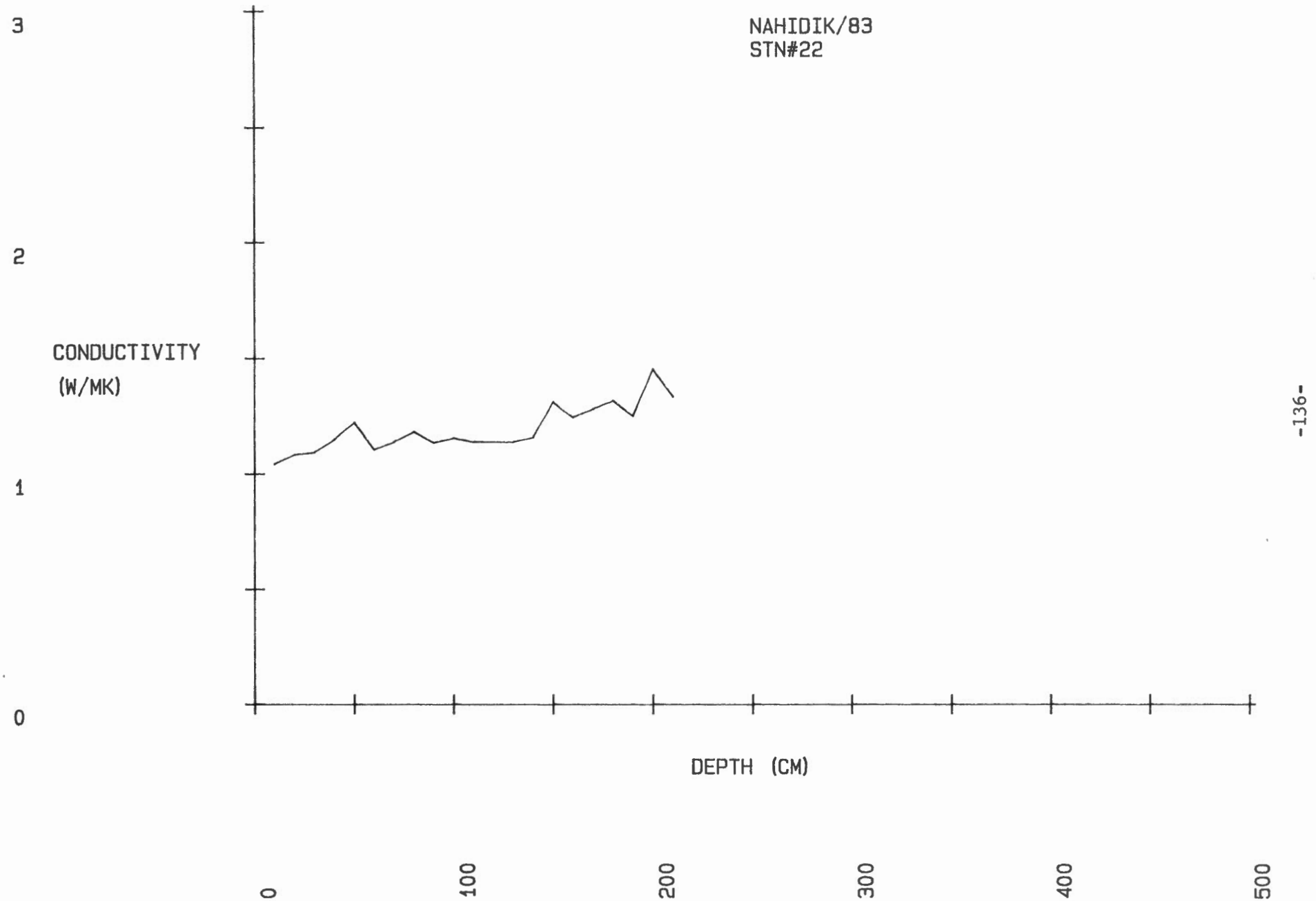
NAHIDIK/83
STN#22
3
2
1
0
CONDUCTIVITY
(W/MK)
DEPTH (CM)
0
100
200
300
400
500

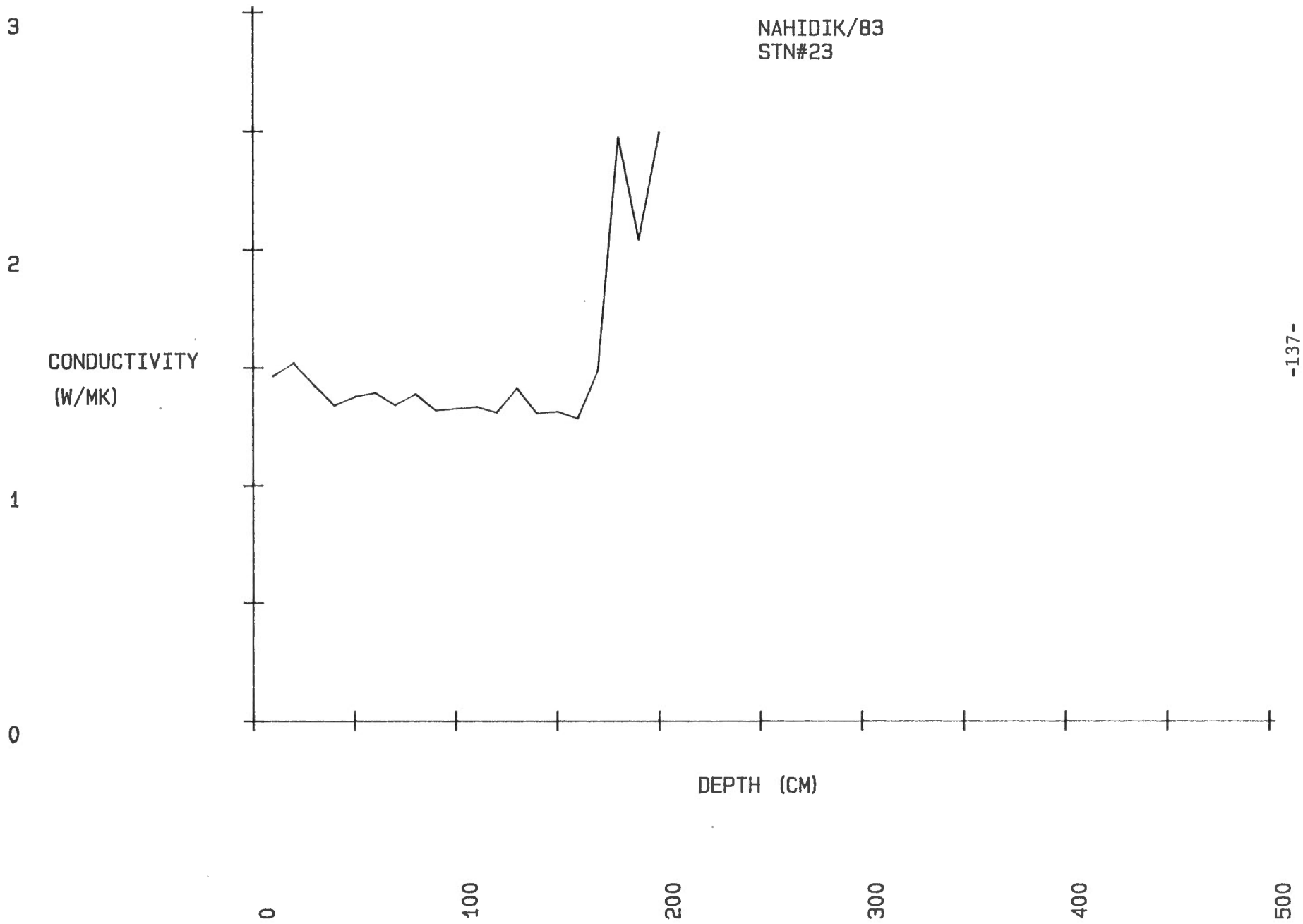
NAHIDIK/83
STN#23
CONDUCTIVITY
(W/MK)
3
2
1
0
DEPTH (CM)
0
100
200
300
400
500

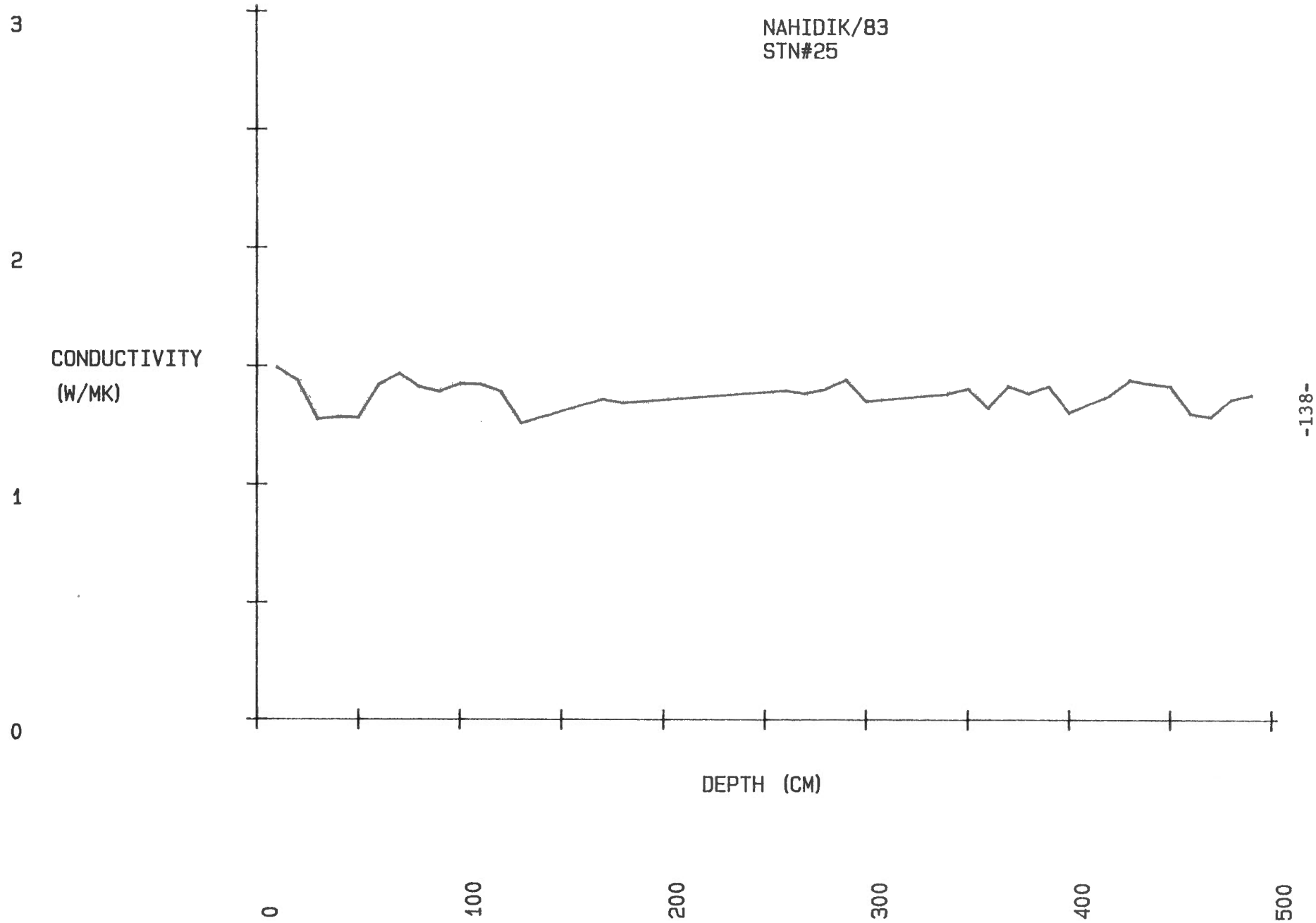
NAHIDIK/83
STN#25
3
2
1
0
CONDUCTIVITY
(W/MK)
-138-
DEPTH (CM)
0
100
200
300
400
500